

# Towards Jetography

GAVIN P. SALAM

LPTHE, UPMC Univ. Paris 6,  
CNRS UMR 7589, 75252 Paris 05, France

## Abstract

As the LHC prepares to start taking data, this review is intended to provide a QCD theorist's understanding and views on jet finding at hadron colliders, including recent developments. My hope is that it will serve both as a primer for the newcomer to jets and as a quick reference for those with some experience of the subject. It is devoted to the questions of how one defines jets, how jets relate to partons, and to the emerging subject of how best to use jets at the LHC.

# Contents

<b>1</b>	<b>Introduction</b>	<b>4</b>
<b>2</b>	<b>Jet algorithms</b>	<b>5</b>
2.1	Cone algorithms . . . . .	6
2.1.1	Iteration . . . . .	7
2.1.2	Overlapping cones: the progressive removal approach . . . . .	8
2.1.3	Overlapping cones: the split–merge approach . . . . .	8
2.1.4	Infrared and collinear safety, midpoint cones . . . . .	9
2.1.5	Exact seedless cones . . . . .	14
2.1.6	Dark towers . . . . .	15
2.2	Sequential recombination jet algorithms . . . . .	16
2.2.1	Jade algorithm . . . . .	16
2.2.2	The $k_t$ algorithm in $e^+e^-$ . . . . .	17
2.2.3	The $k_t$ algorithm with incoming hadrons . . . . .	18
2.2.4	The Cambridge and Aachen algorithms . . . . .	20
2.2.5	The anti- $k_t$ algorithm . . . . .	21
2.2.6	Other sequential recombination ideas . . . . .	22
2.3	Jet finding as a minimisation problem . . . . .	23
2.4	Recombination schemes . . . . .	25
2.5	Summary . . . . .	25
<b>3</b>	<b>Computational geometry and jet-finding</b>	<b>26</b>
3.1	Sequential recombination algorithms . . . . .	29
3.1.1	$k_t$ algorithm . . . . .	29
3.1.2	Special cases . . . . .	31
3.2	A polynomial-time seedless cone . . . . .	32
3.3	Speed summaries . . . . .	34
<b>4</b>	<b>Understanding jets</b>	<b>36</b>
4.1	Reach . . . . .	36
4.1.1	Two-particle case . . . . .	36
4.1.2	General case . . . . .	38
4.2	Perturbative properties, $p_t$ and mass . . . . .	39
4.2.1	Jet $p_t$ . . . . .	39

4.2.2	Jet mass . . . . .	42
4.2.3	Other properties . . . . .	43
4.3	Hadronisation . . . . .	43
4.4	UE, pileup, jet areas . . . . .	47
4.4.1	Jet areas . . . . .	48
4.4.2	Back reaction . . . . .	53
4.5	Summary . . . . .	54
<b>5</b>	<b>Using jets</b>	<b>55</b>
5.1	Choosing an algorithm and a radius . . . . .	56
5.1.1	Analytical study . . . . .	56
5.1.2	Numerical studies . . . . .	58
5.2	Pileup subtraction . . . . .	64
5.3	Substructure . . . . .	68
5.3.1	Two-pronged decays . . . . .	68
5.3.2	Three-pronged decays . . . . .	71
5.4	Summary . . . . .	74
<b>6</b>	<b>Conclusions</b>	<b>75</b>
	<b>Acknowledgements</b>	<b>76</b>
	<b>Bibliography</b>	<b>76</b>

# 1 Introduction

It is common to discuss high-energy phenomena in quantum chromodynamics (QCD) in terms of quarks and gluons. Yet quarks and gluons are never visible in their own right. Almost immediately after being produced, a quark or gluon fragments and hadronises, leading to a collimated spray of energetic hadrons — a jet. Jets are obvious structures when one looks at an event display, and by measuring their energy and direction one can get close to the idea of the original “parton”. The concept of a parton is, however, ambiguous: the fact that partons have divergent branching probabilities in perturbative QCD means that one must introduce a prescription for defining what exactly one means by the term. Similarly, jets also need to be defined — this is generally done through a jet definition, a set of rules for how to group particles into jets and how to assign a momentum to the resulting jet. A good jet definition can be applied to experimental measurements, to the output of parton-showering Monte Carlos and to partonic calculations, and the resulting jets provide a common representation of all these different kinds of events.

There is no single optimal way of defining jets, and over the 30 years that have passed since the first detailed proposal for measuring jets [1], many jet definitions have been developed and used. The ideas behind jet definitions are rather varied. One of the aims of this review (section 2) is to provide an overview of the different kinds of jet definition that exist. Given that the main use of jets in the coming years will be at the Large Hadron Collider at CERN (LHC), the emphasis here and throughout the review will be on hadron-collider jets, though a number of the ideas in jet-finding actually have their origins in studies of  $e^+e^-$  collisions.

One of the characteristics of the LHC is that its particle multiplicity is expected to be much higher than in preceding colliders. Some part of the increase is due to the LHC’s higher energy, but most of it will be a consequence of the multiple minimum-bias interactions (pileup) that will occur in each bunch crossing. High multiplicities pose practical challenges for the computer codes that carry out jet-finding, because the computing time that is required usually scales as some power of the multiplicity,  $N$ . Until a few years ago, this was often a limiting factor in experimental choices of jet finding methodology. Recent years’ work (described in section 3) has shown how these practical issues can be resolved by exploiting their relation to problems in computational geometry. This makes it easier for LHC’s jet-finding choices to be based on physics considerations rather than practical ones.

Given a set of practical jet algorithms, the next question is to establish their similarities and differences. Any jet algorithm will form a jet from a single hard isolated particle. However, different jet definitions may do different things when two hard particles are close by, when a parton radiates a soft gluon, or when the jet is immersed in noise from pileup. Section 4 examines standard and recent results on these issues, for the most important of the current jet algorithms.

Once one has understood how jets behave, the final question that needs to be addressed

is that of determining the jet definitions and methods that are optimal for specific physics analysis tasks. One might call this subject “jetography”, in analogy with photography, where an understanding of optics, of one’s light sensor, and of properties of the subject help guide the choice of focus, aperture and length of exposure. In the context of the LHC, it is probably fair to say that jetography is still in its infancy, hence the title of the review. Nevertheless some first results have emerged in the past year and a half, notably (as discussed in section 5) with respect to simple dijet mass reconstructions, hadronic decays of boosted heavy particles, and the question of limiting the effect of pileup.

One thing that this review does not do is examine the wide range of uses of jets in LHC and other experiments’ analyses. This is a vast subject, and to obtain a full overview probably requires that one consult the main ATLAS and CMS physics analysis programme documents [2, 3] as well as recent work by the Tevatron and HERA. A summary of the situation is to be found in [4]. Other reviews of jets in recent years include [5, 6]. Finally a topic that is barely touched upon here is the nascent field of jet-finding in heavy-ion collisions, for which the reader is referred to [7, 8].

## 2 Jet algorithms

Jet algorithms provide a set of rules for grouping particles into jets. They usually involve one or more parameters that indicate how close two particles must be for them to belong to the same jet. Additionally they are always associated with a recombination scheme, which indicates what momentum to assign to the combination of two particles (the simplest is the 4-vector sum). Taken together, a jet algorithm with its parameters and a recombination scheme form a “jet definition”.

An accord as to some general properties of jet definitions, the “Snowmass accord”, was set out in 1990 [9] by a group of influential theorists and experimenters, and reads as follows

Several important properties that should be met by a jet definition are [3]:

1. Simple to implement in an experimental analysis;
2. Simple to implement in the theoretical calculation;
3. Defined at any order of perturbation theory;
4. Yields finite cross sections at any order of perturbation theory;
5. Yields a cross section that is relatively insensitive to hadronisation.

where ref. [3] is given below as [10]. It is revelatory that ref. [9] is entitled “*Toward a standardization of jet definitions*” (my italics). If one reads the rest of the article, one realises that it wasn’t evident at the time what the standard jet definition should actually be, nor was there a clear path towards satisfying the Snowmass accords, at least for hadron colliders.

When the next major community-wide discussion on jets took place, in 2000, in preparation for Run II of the Tevatron [5], new jet algorithms had been invented [11, 12, 13, 14, 15], old algorithms had been patched [16] and it is probably fair to say that the community had *almost* satisfied the Snowmass requirements. Nevertheless, the recommendations of the Run II workshop were followed in only part of subsequent Tevatron work and, until recently, had also been ignored in much of the preparatory work towards LHC.

This means that there are currently very many hadron-collider jet algorithms in use — some dating from the 80’s, others from the 90’s. The situation is further confused by the fact that different algorithms share the same name (notably “iterative cone”), and that there is no single source of information on all the different algorithms. Additionally, it has not always been clear how any given algorithm fared on the Snowmass requirements.

The purpose of this section is to give an overview of all the main different algorithms, including some of the most recently developed ones, so as to provide the background for anyone reading current jet work from both the theory and experimental communities.

The section’s organisation reflects the split of jet algorithms into two broad categories. Firstly those based in one form or another on “cones”. They can be thought of as “top-down” algorithms, relying on the idea that QCD branching and hadronisation leaves the bulk features of an event’s energy flow unchanged (specifically, energy flow into a cone). Secondly, sequential recombination algorithms, “bottom-up” algorithms that repeatedly recombine the closest pair of particles according to some distance measure, usually related to the divergent structure of QCD matrix elements.

The nomenclature used to distinguish the types of jet algorithm (notably cones) is currently not always uniform across the field. That used here follows the lines set out in [17, 18].

Before continuing, a note is due concerning the completeness of this section. Its aim is to communicate the essential ideas about many of the main jet algorithms (a more concise overview is given in [18]). It will not describe every detail of every single jet algorithm. Where possible, references will be supplied to more complete descriptions. In some cases, no such reference exists, and the interested reader is then advised to consult computer code for the given jet algorithm.

## 2.1 Cone algorithms

The first-ever jet algorithm was developed by Sterman and Weinberg in the 1970’s [1]. It was intended for  $e^+e^-$  collisions and classified an event as having two jets if at least a fraction  $1 - \epsilon$  of the event’s energy was contained in two cones of opening half-angle  $\delta$  (and hence is known as a “cone” algorithm). This definition made it possible to have a fully consistent perturbative QCD calculation of the probability of having two jets in an event.

The two parameters  $\delta$  and  $\epsilon$  reflect the arbitrariness in deciding whether an event has two or more jets. Typically one would avoid taking extreme values ( $\epsilon$  too close to 0 or 1,  $\delta$  too close to zero), but apart from that the optimal choice of  $\delta$  and  $\epsilon$  would depend on the

specific physics analysis being carried out. The presence of separate angular and energy parameters to dictate the characteristics of the jet-finding is typical of cone algorithms, as we shall see below.

Cone algorithms have evolved substantially since [1] and are today mostly used at hadron colliders. The changes reflect the fact that in hadron collisions it doesn't make sense to discuss the total energy (since most of it is not involved in the hard reaction, and goes down the beam pipe), that it isn't always obvious, physically or computationally, *where* to place the cones, and that issues arise when trying to define events with more than two jets (with the associated problem of “overlapping” cones).

### 2.1.1 Iteration

Let us first examine the question of where to place the cones. Most of today's widely used cone algorithms are “iterative cones” (IC). In such algorithms, a seed particle  $i$  sets some initial direction, and one sums the momenta of all particles  $j$  within a circle (“cone”) of radius  $R$  around  $i$  in azimuthal angle  $\phi$  and rapidity  $y$  (or pseudorapidity  $\eta$ ),<sup>1</sup> i.e. taking all  $j$  such that

$$\Delta R_{ij}^2 = (y_i - y_j)^2 + (\phi_i - \phi_j)^2 < R^2, \quad (1)$$

where  $y_i$  and  $\phi_i$  are respectively the rapidity and azimuth of particle  $i$ . The direction of the resulting sum is then used as a new seed direction, and one iterates the procedure until the direction of the resulting cone is stable. The dimensionless parameter  $R$  here, known as the jet radius, replaces the angular scale  $\delta$  that was present in the original Serman-Weinberg proposal. The Serman-Weinberg  $\epsilon$  parameter is less-directly mirrored in hadron-collider cone algorithms. Rather, most physics analyses will use a cone algorithm to obtain jets without any specific energy cut, but then will consider only those jets that are above a certain transverse-momentum threshold.

To be fully specified, seeded iterative jet algorithms must deal with two issues:

- What should one take as the seeds?
- What should one do when the cones obtained by iterating two distinct seeds “overlap” (i.e. share particles)?

Different approaches to these issues lead to two broad classes of cone algorithm.

---

<sup>1</sup>These are standard hadron-collider variables. Given a beam along the  $z$ -direction, a particle with longitudinal momentum  $p_z$ , energy  $E$  and angle  $\theta$  with respect to the beam (longitudinal) direction has rapidity  $y \equiv \ln \frac{E+p_z}{E-p_z}$  and pseudorapidity  $\eta \equiv -\ln \tan \theta/2$ . Massless particles have  $y = \eta$ . Differences in rapidity are invariant under longitudinal boosts, whereas differences in pseudorapidity are invariant only for massless particles. Where an analysis in  $e^+e^-$  will use particles' energies and the angles between the particles, an analysis in a  $pp$  collider will often use  $p_t$  (or  $E_t$ ) and  $\Delta R_{ij}^2$  (defined either with rapidities or pseudorapidities).

### 2.1.2 Overlapping cones: the progressive removal approach

One approach is to take as one's first seed the particle (or calorimeter tower) with the largest transverse momentum. Once one has found the corresponding stable cone, one calls it a jet and removes from the event all particles contained in that jet. One then takes as a new seed the hardest particle/tower among those that remain, and uses that to find the next jet, repeating the procedure until no particles are left (above some optional threshold). This avoids any issue of overlapping cones. A possible name for such algorithms is iterative cone with progressive removal (IC-PR) of particles.

IC-PR algorithms' use of the hardest particle in an event gives them the drawback that they are collinear unsafe: the splitting of the hardest particle (say  $p_1$ ) into a nearly collinear pair  $(p_{1a}, p_{1b})$  can have the consequence that another, less hard particle,  $p_2$ , pointing in a different direction and with  $p_{t,1a}, p_{t,1b} < p_{t,2} < p_{t,1}$ , suddenly becomes the hardest particle in the event, thus leading to a different final set of jets. We will return to this in section 2.1.4.

**Fixed cones.** A widespread, simpler variant of IC-PR cone algorithms is one that does not iterate the cone direction, but rather identifies a fixed cone (FC)<sup>2</sup> around the seed direction and calls that a jet. It starts from the hardest seed and progressively removes particles as the jets are identified (thus FC-PR). It suffers from the same collinear unsafety issue as the IC-PR algorithms.

IC-PR and FC-PR algorithms are often referred to as UA1-type cone algorithms, even though the algorithm described in the original UA1 reference [19] is somewhat different.<sup>3</sup> This may be due to different versions of the UA1 algorithm having been presented at conferences prior to its final publication [19].<sup>4</sup>

### 2.1.3 Overlapping cones: the split–merge approach

Another approach to the issue of the same particle appearing in many cones applies if one chooses, as a first stage, to find all the stable cones obtained by iterating from all particles or calorimeter towers (or those for example above some seed threshold  $\sim 1 - 2\text{GeV}$ ).<sup>5</sup> One

---

<sup>2</sup>“Fixed cone” can be an ambiguous term. In particular, in some contexts it is used to refer to cones whose shape is fixed rather than cones whose position is fixed.

<sup>3</sup> The UA1 algorithm [19] proceeds as follows: the particle (or cell) with highest  $E_t$  starts a jet; working through the list of particles in decreasing  $E_t$ , each one is added to the jet to which it is closest, as long as it is within  $\Delta R < R$  ( $\Delta R^2 = \Delta\eta^2 + \Delta\phi^2$ ,  $R$  taken to be 1); otherwise, the particle initiates a new jet. Finally, once all remaining particles have  $E_t < 2.5\text{ GeV}$ , each particle is simply added to the jet nearest in  $\eta, \phi$  if its transverse momentum relative to the jet axis is less than 1 GeV and it is no further than  $45^\circ$  in direction from the jet axis.

<sup>4</sup>I am grateful to Torbjörn Sjöstrand for comments on this point.

<sup>5</sup>In one variant, CDF's JetClu [20], “ratcheting” is included, which means that during iteration of cone, all particles included in previous iterations are retained even if they are no longer within the geometrical cone, see also section 2.1.6.



may then run a split–merge (SM) procedure, which merges a pair of cones if more than a fraction  $f$  of the softer cone’s transverse momentum is in particles shared with the harder cone; otherwise the shared particles are assigned to the cone to which they are closer. A possible generic name for such algorithms is IC-SM. The exact behaviour of SM procedures depends on the precise ordering of split and merge steps and a fairly widespread procedure is described in detail in [5]. It essentially works as follows, acting on an initial list of “protojets”, which is just the full list of stable cones:

1. Take the protojet with the largest  $p_t$  (the ‘hardest’ protojet), label it  $a$ .
2. Find the next hardest protojet that shares particles with the  $a$  (i.e. overlaps), label it  $b$ . If no such protojet exists, then remove  $a$  from the list of protojets and add it to the list of final jets.
3. Determine the total  $p_t$  of the particles shared between the two protojets,  $p_{t,\text{shared}}$ .
  - If  $p_{t,\text{shared}}/p_{t,b} > f$ , where  $f$  is a free parameter known as the overlap threshold, replace protojets  $a$  and  $b$  with a single merged protojet.
  - Otherwise “split” the protojets, for example assigning the shared particles just to the protojet whose axis is closer (in angle).
4. Then repeat from step 1 as long as there are protojets left.

Generally the overlap threshold  $f$  is chosen to be 0.5 or 0.75 (the latter is probably to be preferred [21]). An alternative to SM is to have a “split-drop” (SD) procedure, where the non-shared particles that belong to the softer of two overlapping cones are simply dropped, i.e. are left out of jets altogether. The main example of an algorithm with a SD procedure is PxCone (described for example in [22]).

The outcome of split–merge and split–drop procedures depends on the initial set of stable cones. One of the main issues with IC-SM and IC-SD algorithms is that the addition of a new soft seed particle can lead to new stable cones being found, altering the final set of jets. This is infrared unsafety and we will discuss it in detail in the next section.

#### 2.1.4 Infrared and collinear safety, midpoint cones

Infrared and collinear (IRC) safety is the property that if one modifies an event by a collinear splitting or a soft emission, the set of hard jets should remain unchanged. It is a fundamental requirement for jet algorithms, related to points 4 and 5 of the Snowmass accord.

**The IC-PR case.** IC-PR algorithms suffer from collinear unsafety, as illustrated in fig. 1. With a collinear safe jet algorithm, if configuration (a) (with an optional virtual loop also drawn in) leads to one jet, then the same configuration with one particle split collinearly,

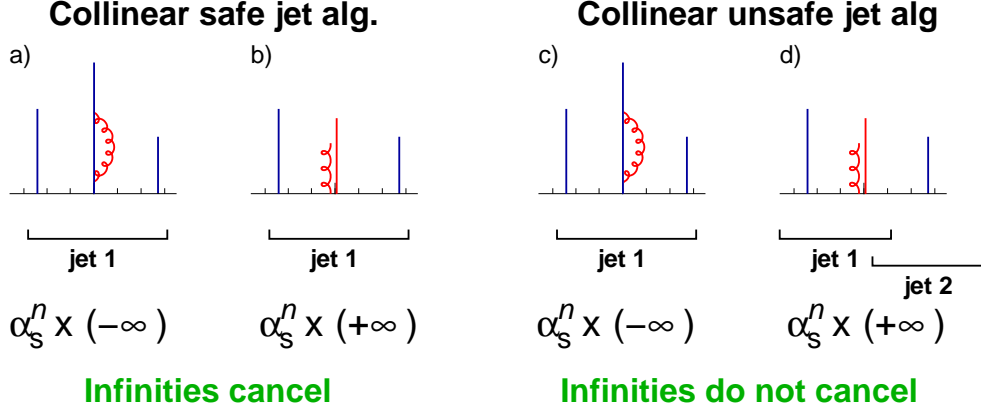


**Figure 1:** Illustration of collinear safety (left) and collinear unsafety in an IC-PR type algorithm (right) together with its implication for perturbative calculations (taken from the appendix of [17]). Partons are vertical lines, their height is proportional to their transverse momentum, and the horizontal axis indicates rapidity.

(b), also leads to a single jet. In perturbative QCD, after integrating over loop variables in (a) and the splitting angle in (b), both diagrams have infinite weights, but with opposite signs, so that the total weight for the 1-jet configuration is finite.

Diagrams (c) and (d) are similar, but for an IC-PR algorithm. In configuration (c), the central particle is hardest and provides the first seed. The stable cone obtained by iterating from this seed contains all the particles, and one obtains a single jet. In configuration (d), the fact that the central particle has split collinearly means that it is now the leftmost particle that is hardest and so provides the first seed. Iteration from that seed leads to a jet (jet 1) that does not contain the rightmost particle. That rightmost particle therefore remains, provides a new seed, and goes on to form a jet in its own right (for full details, see the appendix of [17]).

It is problematic for the result of the jet-finding to depend on a collinear splitting:

- Collinear splittings happen all the time in QCD, including through non-perturbative dynamics, making them hard to predict accurately.
- The formal perturbative QCD consequence of this is that the infinities in diagrams (c) and (d) contribute separately to the 1-jet and 2-jet cross sections. Thus both the 1-jet and 2-jet cross sections are divergent.
- Experimental detectors provide some regularisation of any collinear unsafety (because of their finite resolution), but the extent to which this happens depends on the particular combination of tracking, electromagnetic calorimetry and hadronic calorimetry that is used by the experiment. This is problematic: a jet cross section should not depend on the particular details of the detector.

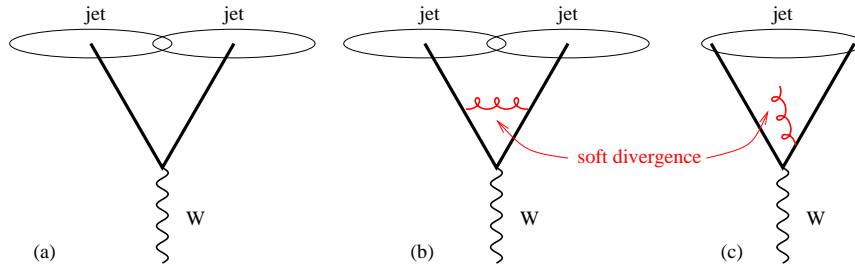


**Figure 2:** Configurations illustrating IR unsafety of IC-SM algorithms in events with a  $W$  and two hard partons. The addition of a soft gluon converts the event from having two jets to just one jet. In contrast to fig. 1, here the explicit angular structure is shown (rather than  $p_t$  as a function of rapidity).

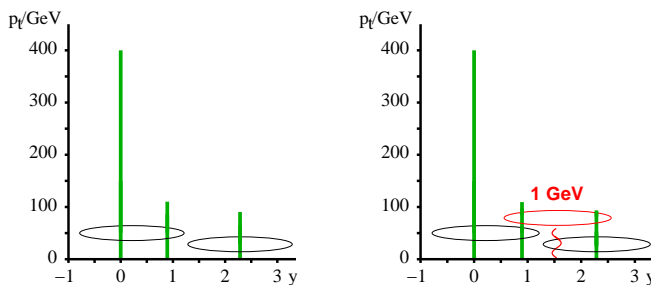


**Figure 3:** Configuration that is the source of IR unsafety in the midpoint (IC<sub>mp</sub>-SM) algorithm, with the diagram on the right illustrating the extra stable cone that can appear with the addition of a new soft seed. Taken from [24].

**The IC-SM case.** IC-SM (and IC-SD) type algorithms have the drawback that the addition of an extra soft particle, acting as a new seed, can cause the iterative process to find a new stable cone. Once passed through the split-merge step this can lead to the modification of the final jets, thus making the algorithm *infrared* unsafe. This is illustrated in fig. 2: in an event (a) with just two hard partons (and a  $W$ , which balances momentum), both partons act as seeds, there are two stable cones and two jets. The same occurs in the (negative) infinite loop diagram (b). However, in diagram (c) where an extra soft gluon has been emitted, the gluon provides a new seed and causes a new stable cone to be found containing both hard partons (as long as they have similar momenta and are separated by less than  $2R$ ). This stable cone overlaps with the two original ones and the result of the split-merge procedure is that only one jet is found. So the number of jets depends on the presence or absence of a soft gluon and after integration over the virtual/real soft-gluon momentum the two-jet and one-jet cross sections each get non-cancelling infinite contributions. This is a serious problem, just like collinear unsafety. A good discussion of it was given in [23].

**The midpoint “fix”.** A partial solution [16] (described also in [23]), which was recommended in [5], is to additionally search for new stable cones by iterating from midpoints

between each pair of stable cones found in the initial seeded iterations (IC<sub>mp</sub>-SM). This resolves the problem shown in fig. 2 and the resulting “midpoint” algorithm has often been presented as a cone algorithm that was free of IR safety issues. However, for configurations with three hard particles in a common neighbourhood (rather than two for the IC-SM algorithms) the IR safety reappears, as illustrated in fig. 3.

The “midpoint algorithm” has been widely used in Run II of the Tevatron within CDF (midpoint cone algorithm) and DØ (Run II Cone algorithm, or improved legacy cone algorithm). The two experiments have separate implementations, with slightly different treatment of seeds (CDF imposes a threshold, DØ does not) and cone iteration (DØ eliminates cones below a  $p_t$  threshold, CDF does not). In practice both algorithms incorporate a number of further technical subtleties (for example an upper limit on the number of iterations, or split-merge steps) and the best reference is probably the actual code (available both within FastJet [25] v2.4 and SpartyJet [26]).

**Impact of IRC unsafety.** The impact of infrared and collinear (IRC) unsafety depends on the observable in which one is interested. For example for the IC-SM type algorithms, the configuration on the right of fig. 2 is a NNLO contribution to the  $W + \text{jet}$  cross section, i.e. a contribution  $\alpha_s^3 \alpha_{EW} \times \infty$ . Physically, the infinity gets regularised by non-perturbative effects and so is replaced by a factor of order  $\ln p_t/\Lambda$ , giving an overall contribution  $\alpha_s^3 \alpha_{EW} \ln p_t/\Lambda$ . Since  $\alpha_s \sim 1/\ln(p_t/\Lambda)$ , this can be rewritten as  $\sim \alpha_s^2 \alpha_{EW}$ , i.e. the NNLO diagrams will give a contribution that is as large as the NLO diagrams. Thus the perturbative series looks like:

$$\underbrace{\alpha_s \alpha_{EW}}_{\text{LO}} + \underbrace{\alpha_s^2 \alpha_{EW}}_{\text{NLO}} + \underbrace{\alpha_s^3 \alpha_{EW} \ln \frac{p_t}{\Lambda}}_{\text{NNLO}} + \underbrace{\alpha_s^4 \alpha_{EW} \ln^2 \frac{p_t}{\Lambda}}_{\text{NNNLO}} + \dots, \\ \sim \underbrace{\alpha_s \alpha_{EW}}_{\text{LO}} + \underbrace{\alpha_s^2 \alpha_{EW}}_{\text{NLO}} + \underbrace{\alpha_s^2 \alpha_{EW}}_{\text{NNLO}} + \underbrace{\alpha_s^2 \alpha_{EW}}_{\text{NNNLO}} + \dots, \quad (2)$$

and it is meaningful to calculate the LO term, but no advantage is to be had by calculating terms beyond, because the neglected pieces will always be as large as the NLO term. If one instead examines the  $W + 2\text{-jet}$  cross section then the LO term is  $\alpha_s^2 \alpha_{EW}$ . The NLO term,  $\alpha_s^3 \alpha_{EW} \ln p_t/\Lambda \sim \alpha_s^2 \alpha_{EW}$  is of the same size, so even the LO prediction makes no sense.

The unsafety of the IC-SM algorithm can be labelled IR<sub>2+1</sub>: its IR unsafety is manifest for configurations with two hard particles in a common neighbourhood plus one soft one. The midpoint algorithm is IR<sub>3+1</sub>, while the IC-PR and FC-PR algorithms are Coll<sub>3+1</sub> (the collinear unsafety is manifest when there are 3 hard particles in a common neighbourhood, of which one splits collinearly).

For an algorithm labelled as IR <sub>$n+1$</sub>  or Coll <sub>$n+1$</sub> , the last meaningful order for the  $W + \text{jet}$  or the 2-jet cross section is N <sup>$n-2$</sup> LO. The last meaningful order for the  $W + 2\text{-jet}$  or the 3-jet cross section is N <sup>$n-3$</sup> LO. The situation is summarised for various process in table 1.

Observable	IR <sub>2+1</sub>	IR <sub>3+1</sub> , Coll <sub>3+1</sub>
Inclusive jet cross section	LO	NLO
$W/Z/H$ + 1-jet cross section	LO	NLO
3-jet cross section	none	LO
$W/Z/H$ + 2-jet cross section	none	LO
jet masses in 3-jet and $W/Z/H$ + 2-jet events	none	none

**Table 1:** Summary of the last meaningful order for various measurements with jet algorithms having different levels of IR and collinear unsafety. Adapted from [24].

One way of visualising infrared and collinear unsafety (especially for IR<sub>2+1</sub> algorithms) is that they lead to an ambiguity in the effective jet radius  $R$  — a soft emission or collinear splitting affects how far the jet algorithm will reach for particles. For the IR<sub>2+1</sub> algorithms that ambiguity is of  $\mathcal{O}(R)$  in the reach (i.e. the jet radius is devoid of meaning). For the IR<sub>3+1</sub> and Coll<sub>3+1</sub> algorithms this analogy is less useful.

**What to do with IRC unsafe measurements.** Many IRC-unsafe jet measurements exist in the experimental literature.<sup>6</sup> Some of these cases are like [27], where the measurement for the  $W+n$ -jet cross section is carried out with JetClu, an IR<sub>2+1</sub> unsafe algorithm for which no order of perturbation theory is meaningful when  $n > 1$ .

The question then arises of how one can compare NLO theory predictions like [28, 29, 30, 31, 32] with the experimental results. One approach to this is to carry out the NLO prediction with two somewhat different jet algorithms (for example SISCone and anti- $k_t$ , both discussed below), and use the difference between the NLO calculations with the two algorithms as a measure of the uncertainty in the prediction due to IR safety issues. This was done for example in ref. [32], which showed for the  $W + 3$  jets cross section at the Tevatron (measured with JetClu,  $R = 0.4$  for jets with  $|y| < 2$  [27]) that the difference between predictions with SISCone and anti- $k_t$  was  $\sim 20\%$  at LO (somewhat less at NLO). This may not seem like an enormous effect compared to typical experimental systematic uncertainties, however one should remember that the size of the difference depends also on the cuts and the choice of  $R$ . For example, with a larger  $R$  value (e.g.  $R = 0.7$ ) or a smaller rapidity range, one could easily envisage that these figures would double.

In the long-run, an alternative approach might be to use tools like MC@NLO [33] and POWHEG [34], which may eventually include a range of jet processes and thus provide both the NLO terms and an acceptable estimate of the large higher-order logarithms and

---

<sup>6</sup>Strictly speaking, many algorithms incorporate a seed threshold, e.g.  $p_t > 1$  GeV. This means that they are not truly infrared unsafe, in that they don't lead to infrared infinities in perturbative calculations (though they are then collinear unsafe if applied to particles rather than to calorimeter towers). However a 1 GeV seed threshold fails to remove the large logarithms in eq. (2) or to eliminate the non-perturbative uncertainties associated with IR unsafety. So the seed threshold does not make these algorithms any better than a formally IR unsafe one.

the non-perturbative effects.

### 2.1.5 Exact seedless cones

One full solution to the IRC safety issue avoids the use of seeds and iterations, and instead finds *all* stable cones through some exact procedure. This type of algorithm is often called a seedless cone (SC, thus SC-SM with a split–merge procedure).

In a seedless cone algorithm, the addition of a soft particle may lead to the presence of new stable cones, however none of those new cones will involve hard particles (a soft particle doesn’t affect the stability of a cone involving much larger momenta), and therefore the set of hard stable cones is infrared safe. As long as the presence of new soft stable cones (or of new soft particles inside hard stable cones) doesn’t change the outcome of the split–merge procedure (a non-trivial requirement), then a seedless cone will lead to an infrared safe collection of hard jets.

A computational strategy for identifying all cones was outlined in ref. [5]: one takes all subsets of particles and establishes for each one whether it corresponds to a stable cone — i.e. one calculates its total momentum, draws a circle around the resulting axis, and if the points contained in the circle are exactly as those in the initial subset, then one has found a stable cone. This is guaranteed to find all stable cones.

The above seedless procedure was intended for fixed-order calculations, with a very limited number of particles. It becomes impractical for larger numbers of particles because there are  $\mathcal{O}(2^N)$  possible subsets (think of an  $N$ -bit binary number where each bit corresponds to a particle, and the subset consists of all particles whose bit is turned on). Testing the stable-cone property takes  $\mathcal{O}(N)$  time for each subset and so the total time is  $\mathcal{O}(N2^N)$ . This exponential-time behaviour made seedless cones impractical for use on events with realistic numbers of particles (the  $N2^N$  approach would take about  $10^{17}$  years to cluster 100 particles). However in 2007 a polynomial-time geometrically-based solution was found to the problem of identifying all stable cones [24]. The corresponding algorithm is known as SIScone and it is described in section 3.2. An explicit test of the IR safety of SIScone is shown in fig. 4.

Seedless cone algorithms are also programmed into NLO codes like NLOJET++ [29] and MCFM [28]. Users should however be aware that there is some degree of confusion in nomenclature — for example the cone algorithm in MCFM v. 5.2 is referred to as the midpoint algorithm, but is actually a seedless implementation; in NLOJET++ v. 3 the algorithm is referred to as seedless, but has a midpoint option. Users of NLO codes are therefore advised to make sure they know *exactly* what is implemented in the NLO code’s native jet finder (i.e. they should carefully inspect the portion of code devoted to the jet finder). Alternatively they may use appropriately documented 3rd party libraries for their jet-finding.

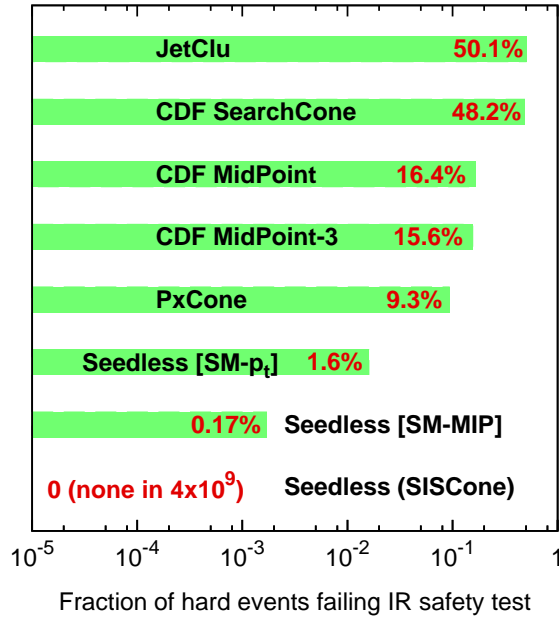


**Figure 4:** Failure rates for IR safety tests [24] with various algorithms, including a midpoint variant with 3-way midpoints and some seedless algorithms with commonly used, but improper, split-merge procedures. See table 2, p. 27, for the classification of the main different algorithms and [24] for a description of the different seedless variants. CDF MidPoint-3 is like the standard MidPoint algorithm except that it also uses midpoints between triplets of stable cones.

### 2.1.6 Dark towers

The xC-SM class of algorithms collectively suffers from a problem known as dark towers [35]: regions of hard energy flow that are not clustered into any jet. Dark towers arise because there exist configurations in which some particles will never end up in a stable cone. The stages of an iteration in which this is the case are shown in fig. 5, for which the rightmost particle cannot be in a stable cone: even when one uses it as a starting point for iteration, it is not contained in the final stable cone (nor is it contained in any stable cone in a seedless algorithm).

One solution to this problem in iterative algorithms is “ratcheting”: a particle that was included at any stage of the iteration is manually included in all subsequent stages

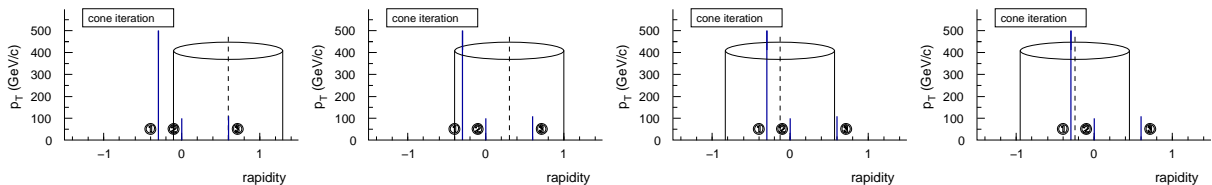


**Figure 5:** Some of the stages of a stable-cone iteration that starts on the rightmost particle and ends up in a position where that rightmost particle is not included in the stable cone.

of the iteration even if it is not within the cone boundary. This is used in CDF’s JetClu algorithm (though it is not actually described in the reference usually quoted by CDF for JetClu [20]).

Another fix to dark towers was proposed in [35], and referred to as the “searchcone”. It eliminates a large fraction of the dark towers by using a smaller radius to find stable cones and then expands the cones to their full radius, without further iteration, before passing them to the SM procedure. Unfortunately, when applied together with the midpoint procedure (IC<sub>se,mp</sub>-SM) it worsens its IR unsafety status from IR<sub>3+1</sub> back to IR<sub>2+1</sub> [36].

Perhaps the simplest solution [36] to dark towers is to identify any remainder energy flow that was not clustered by the xC-SM algorithm and run an extra pass of the algorithm on that remainder. This is the approach used in SIScone (which by default runs multiple passes until no energy is left).

## 2.2 Sequential recombination jet algorithms

Sequential recombination algorithms have their roots in  $e^+e^-$  experiments. A detailed overview of their history in  $e^+e^-$  studies is given in the introduction of [37]. The intention here is not to repeat that history, but rather to walk through the most widely used of the  $e^+e^-$  algorithms and then see how they lead to corresponding hadron-collider algorithms. It should be said that many of the ideas underlying today’s sequential recombination algorithms (including a momentum-related parameter to decide jet resolution and the use of relative transverse momenta) actually appeared first in the LUCLUS algorithm of Sjöstrand [38] (earlier work includes [39, 40, 41, 42]). However computational constraints at the time led to the algorithm including a preclustering phase, and it also involved a non-trivial procedure of reassignment of particles between clusters at each recombination. These two characteristics made it somewhat more complicated than its successors.

Today’s sequential recombination algorithms are all rather simple to state (far more so than the cone algorithms). Additionally they go beyond just finding jets and implicitly assign a “clustering sequence to an event”, which is often closely connected with approximate probabilistic pictures that one may have for parton branching.

### 2.2.1 Jade algorithm

The first simple sequential recombination algorithm was introduced by the JADE collaboration in the middle of the 1980’s [43, 44]. It is formulated as follows:

1. For each pair of particles  $i, j$  work out the distance

$$y_{ij} = \frac{2E_i E_j (1 - \cos \theta_{ij})}{Q^2} \quad (3)$$

where  $Q$  is the total energy in the event,  $E_i$  is the energy of particle  $i$  and  $\theta_{ij}$  the



angle between particles  $i$  and  $j$ . For massless particles,  $y_{ij}$  is just the (normalised) squared invariant mass of the pair.

2. Find the minimum  $y_{\min}$  of all the  $y_{ij}$ .
3. If  $y_{\min}$  is below some *jet resolution threshold*  $y_{\text{cut}}$ , then recombine  $i$  and  $j$  into a single new particle (or “pseudojet”) and repeat from step 1.
4. Otherwise, declare all remaining particles to be jets and terminate the iteration.

The number of jets that one obtains depends on the value of  $y_{\text{cut}}$ , and as one reduces  $y_{\text{cut}}$ , softer and/or more collinear emissions get resolved into jets in their own right. Thus here the number of jets is controlled by a single parameter rather than the two parameters (energy and angle) of cone algorithms.

Quite often in  $e^+e^-$  analyses one examines the value of  $y_{\text{cut}}$  that marks the transition between (say) an event being labelled as having  $n$  and  $n + 1$  jets,  $y_{n(n+1)}$ . Thus if  $y_{23}$  is small, the event is two-jet like, while if it is large then the event clearly has 3 (or more) jets.

The JADE algorithm is infrared and collinear safe, because any soft particle will get recombined right at the start of the clustering, as do collinear particles. It was widely used up to the beginning of the 1990s (and still somewhat beyond then), however the presence of  $E_i E_j$  in the distance measure means that two very soft particles moving in opposite directions often get recombined into a single particle in the early stages of the clustering, which runs counter to the intuitive idea that one has of a jet being restricted in its angular reach. As well as being physically disturbing, this leads to very non-trivial structure (non-exponentiated double logarithms) in higher-order calculations of the distribution of  $y_{23}$  [45, 46, 47] (later, this was also discussed in terms of a violation of something called recursive infrared and collinear safety [48]).

### 2.2.2 The $k_t$ algorithm in $e^+e^-$

The  $e^+e^-$   $k_t$  algorithm [11] is identical to the JADE algorithm except as concerns the distance measure, which is

$$y_{ij} = \frac{2 \min(E_i^2, E_j^2)(1 - \cos \theta_{ij})}{Q^2}. \quad (4)$$

In the collinear limit,  $\theta_{ij} \ll 1$ , the numerator just reduces to  $(\min(E_i, E_j)\theta_{ij})^2$  which is nothing but the squared transverse momentum of  $i$  relative to  $j$  (if  $i$  is the softer particle) — this is the origin of the name  $k_t$ -algorithm.<sup>7</sup> The use of the minimal energy ensures that the distance between two soft, back-to-back particles is larger than that between a soft particle and a hard one that’s nearby in angle.

---

<sup>7</sup>As mentioned above, the distance measured used in the earlier LUCUS algorithm [38],  $y_{ij} = 2 \frac{|\vec{p}_i|^2 |\vec{p}_j|^2}{(|\vec{p}_i| + |\vec{p}_j|)^2 Q^2} (1 - \cos \theta_{ij})$  (in the version given in [37]), was also a relative transverse-momentum type variable.

Another way of thinking about eq. (4) is that the distance measure is essentially proportional to the squared inverse of the splitting probability for one parton  $k$  to go into two,  $i$  and  $j$ , in the limit where either  $i$  or  $j$  is soft and they are collinear to each other,

$$\frac{dP_{k \rightarrow ij}}{dE_i d\theta_{ij}} \sim \frac{\alpha_s}{\min(E_i, E_j) \theta_{ij}} \quad (5)$$

There is a certain arbitrariness in this statement, because of the freedom to change variables in the measure on the left-hand side of eq. (5). However the presence of a power of just the minimum of the energy in the denominator (rather than some function of both energies as in the JADE distance measure) is robust.

The  $k_t$  algorithm's closer relation to the structure of QCD divergences made it possible to carry out all-order resummed calculations of the distribution of  $y_{n(n+1)}$  [11, 49, 50] and of the mean number of jets as a function of  $y_{\text{cut}}$  [51]. This helped encourage its widespread use at LEP. The relation to QCD divergences also means that the clustering sequence retains useful approximate information about the sequence of QCD splittings that occurred during the showering that led to the jet. This is of interest both in certain theoretical studies (for example CKKW matching of parton-showers and matrix elements [52]) and also for identifying the origin of a given jet (for example quark versus gluon discrimination [53]).

### 2.2.3 The $k_t$ algorithm with incoming hadrons

In experiments with incoming hadrons two issues arise. Firstly (as mentioned already for cone algorithms) the total energy is no longer well defined. So instead of the dimensionless distance  $y_{ij}$ , one might choose to use a dimensionful distance

$$d_{ij} = 2 \min(E_i^2, E_j^2) (1 - \cos \theta_{ij}) , \quad (6)$$

together with a dimensionful jet-resolution parameter  $d_{\text{cut}}$  (alternatively, one might maintain a dimensionless measure by choosing some convention for the normalisation scale). Secondly, the divergences in the QCD branching probability are not just between pairs of outgoing particles, but also between an outgoing particle and the incoming beam direction.

The first attempt at formulating a  $k_t$  algorithm in such cases was [54]. It introduced the idea of an additional *particle-beam* distance.

$$d_{iB} = 2E_i^2 (1 - \cos \theta_{iB}) , \quad (7)$$

which, for small  $\theta_{iB}$ , is just the squared transverse momentum of particle  $i$  with respect to the beam. The algorithm then remains the same as in  $e^+e^-$ , except that if a  $d_{iB}$  is the smallest, then the particle is recombined with the beam, to form part of the “beam-jet”. If there are two beams, then one just introduces a measure for each beam.

In  $pp$  collisions it is standard to use variables that are invariant under longitudinal boosts, however the  $d_{ij}$  and  $d_{iB}$  given above only satisfy this property approximately.

Thus ref. [12] introduced versions of the distance measures that were exactly longitudinally invariant

$$d_{ij} = \min(p_{ti}^2, p_{tj}^2) \Delta R_{ij}^2, \quad \Delta R_{ij} = (y_i - y_j)^2 + (\phi_i - \phi_j)^2, \quad (8a)$$

$$d_{iB} = p_{ti}^2, \quad (8b)$$

(this variant does not distinguish between the two beam jets).<sup>8</sup> It is straightforward to verify that in the relevant collinear limits, these measures just reduce to relative transverse momenta, like those in eqs. (6,7). Furthermore, since  $(y_i - y_j)$ , the  $\phi_i$  and  $p_{ti}$  are all invariant under longitudinal boosts, the  $d_{ij}$  and  $d_{iB}$  are too. Nowadays the procedure of section 2.2.1, with the distance measures of eqs. (8), is referred to as the *exclusive  $k_t$*  algorithm, in that every particle is assigned either to a beam-jet or to a final-state jet.

**Inclusive  $k_t$  algorithm.** At about the same time that ref. [12] appeared, a separate formulation was proposed in [13], which has almost the same distance measures as eq. (8),

$$d_{ij} = \min(p_{ti}^2, p_{tj}^2) \frac{\Delta R_{ij}^2}{R^2}, \quad \Delta R_{ij}^2 = (y_i - y_j)^2 + (\phi_i - \phi_j)^2, \quad (9a)$$

$$d_{iB} = p_{ti}^2, \quad (9b)$$

where the difference lies in the presence of a new parameter  $R$  (also called  $D$ ) in the  $d_{ij}$ , whose role is similar to  $R$  in a cone algorithm (see below). The other difference in this version of the algorithm is in how the  $d_{ij}$  get used:

1. Work out all the  $d_{ij}$  and  $d_{iB}$  according to eq. (8).
2. Find the minimum of the  $d_{ij}$  and  $d_{iB}$ .
3. If it is a  $d_{ij}$ , recombine  $i$  and  $j$  into a single new particle and return to step 1.
4. Otherwise, if it is a  $d_{iB}$ , declare  $i$  to be a [final-state] jet, and remove it from the list of particles. Return to step 1.
5. Stop when no particles remain.

Here, all particles are included in final-state jets, there is no concept of a beam jet, and there is no  $d_{\text{cut}}$  parameter — the question of what gets called a jet is determined by  $R$ : if a particle  $i$  has no other particles within a distance  $R$  then the  $d_{iB}$  will be smaller than the  $d_{ij}$  for any  $j$  and the particle will then become a jet. One consequence of this is that arbitrarily soft particles can become jets in their own right and therefore (just as for cone

---

<sup>8</sup>Ref. [12] also proposes a variant where  $\Delta R_{ij}^2 \equiv 2(\cosh(y_i - y_j) - \cos(\phi_i - \phi_j))$ , more closely related to the precise structure of the QCD matrix elements; however, to the author's knowledge, it has not seen extensive use.

algorithms), one should additionally specify a minimum transverse momentum that a jet should have for it to be of interest.

The above algorithm is most unambiguously referred to as the *inclusive*  $k_t$  algorithm, though when people mention the “ $k_t$  algorithm” in a collider context, it is nearly always the inclusive variant that they have in mind. It so happens that the exclusive and inclusive variants have identical clustering sequences — it is only the interpretation of those clustering sequences that differs.

The  $k_t$  algorithm has long been advocated by theorists because it is free of any infrared and collinear safety issues. On the other hand it had been criticised by experimenters on the grounds (a) that it was computationally slow, insofar as the two public implementations that were available in 2005, **KtClus** (Fortran) [55] and **KtJet** (C++) [56], both took times  $\sim N^3$  to cluster  $N$  particles; and (b) that it produces irregular jets, which complicates certain detector and non-perturbative corrections. We will return to the speed issue in section 3.1, while the irregularity is visible in fig. 6, p. 26 (related issues will be discussed in section 4.4).

Given the number of experimental objections that have been raised in the past regarding the  $k_t$  algorithm in a  $pp$  environment, it is worth commenting briefly on the two sets of hadron-collider measurements that have been carried out with the  $k_t$  algorithm. One, from DØ [57, 58], had to go to considerable lengths (introducing preclustering) to get around the speed issue (DØ’s fine calorimeter meant that it had many input towers) and found rather large non-perturbative corrections from the underlying event (UE); the latter issue perhaps discouraged further use of the  $k_t$  algorithm until CDF performed a similar measurement in 2005 [59, 60]. CDF did not suffer particularly from the speed issue, largely because their coarser calorimeter segmentation ensured modest input multiplicities. Also, crucially, they showed that DØ’s large UE corrections were probably a consequence of taking the jet radius parameter  $R = 1$ . When CDF instead took  $R = 0.7$  (as is common for cone algorithms), they found UE corrections that were commensurate with those for cone algorithms.

#### 2.2.4 The Cambridge and Aachen algorithms

The Cambridge algorithm [14] is a sequential recombination algorithm for  $e^+e^-$  collisions that introduces *two* distance measures between pairs of particles. It has  $v_{ij} = 2(1 - \cos \theta_{ij})$  (i.e. the squared angle) as well as the  $y_{ij}$  of eq. (3). It reads as follows

1. If only one particle is left, call it a jet and stop.
2. Otherwise find the pair of particles with smallest  $v_{ij}$ .
3. If the corresponding  $y_{ij} < y_{cut}$ , replace  $i$  and  $j$  with the recombined one and go to step 1.
4. Otherwise: take the less energetic of  $i$  and  $j$ , remove it from the list of particles, call it a jet, and go to step 1.

The idea here was to combine the  $y_{cut}$  jet resolution of the  $k_t$  algorithm with a clustering sequence dictated by angular ordering, i.e. one that relates closely to the powerful concept of angular ordering that arises when considering multiple gluon emission [61].

**Cambridge/Aachen.** The most widely discussed extension (and simplification) of the Cambridge algorithm to hadron colliders was given in [15] (another one [62] has seen less study). It is like the inclusive  $k_t$  algorithm in that it uses longitudinally invariant variables, introduces an  $R$  parameter, and does away with the  $y_{ij}$  cut on jets. It proceeds by recombining the pair of particles with the smallest  $\Delta R_{ij}$ , and repeating the procedure until all objects are separated by a  $\Delta R_{ij} > R$ . The final objects are then the jets.<sup>9</sup>

This algorithm was originally named the Aachen algorithm, though it is often now called the Cambridge/Aachen (C/A) algorithm, reflecting its angular-ordered Cambridge roots.

Like the  $k_t$  algorithm, the C/A algorithm gives somewhat irregular jets, and its original implementations took a time that scales as  $N^3$ . The latter problem is now solved (as for the  $k_t$  algorithm) and the fact that the C/A has a clustering hierarchy in angle makes it possible to consistently view a specific jet on many different angular scales, a feature whose usefulness will become apparent in section 5.3 and is also relevant for a “filtering” method discussed below.

### 2.2.5 The anti- $k_t$ algorithm

One can generalise the  $k_t$  and Cambridge/Aachen distance measures as [17]:

$$d_{ij} = \min(p_{ti}^{2p}, p_{tj}^{2p}) \frac{\Delta R_{ij}^2}{R^2}, \quad \Delta R_{ij}^2 = (y_i - y_j)^2 + (\phi_i - \phi_j)^2, \quad (10a)$$

$$d_{iB} = p_{ti}^{2p}, \quad (10b)$$

where  $p$  is a parameter that is 1 for the  $k_t$  algorithm, and 0 for C/A. It was observed in [17] that if one takes  $p = -1$ , dubbed the “anti- $k_t$ ” algorithm, then this favours clusterings that involve hard particles rather than clusterings that involve soft particles ( $k_t$  algorithm) or energy-independent clusterings (C/A). This ultimately means that the jets grow outwards around around hard “seeds”. However since the algorithm still involves a combination of energy and angle in its distance measure, this is a collinear-safe growth (a collinear branching automatically gets clustered right at the beginning of the sequence).<sup>10</sup> The result is an IRC safe algorithm that gives circular hard jets, making it an attractive replacement for certain cone-type algorithms (notably IC-PR algorithms).

One should be aware that, unlike for the  $k_t$  and C/A algorithms, the substructure classification that derives from the clustering-sequence inside an anti- $k_t$  jet cannot be usefully

<sup>9</sup>Alternatively, one can formulate it like the inclusive  $k_t$  algorithm, but with  $d_{ij} = \Delta R_{ij}^2/R^2$  and  $d_{iB} = 1$ .

<sup>10</sup>If one takes  $p \rightarrow -\infty$  then energy is privileged at the expense of angle and the algorithm then becomes collinear unsafe, and somewhat like an IC-PR algorithm.

related to QCD branching (essentially the anti- $k_t$  recombination sequence will gradually expand through a soft subjet, rather than first constructing the soft subjet and then recombining it with the hard subjet).

### 2.2.6 Other sequential recombination ideas

The flexibility inherent in the sequential recombination procedure means that a number of variants have been considered in both past and recent work. Some of the main ones are listed below.

**Flavour- $k_t$  algorithms.** If one is interested in maintaining a meaningful flavour for jets (for example in purely partonic studies, or when discussing heavy-flavour jets), then one may use a distance measure that takes into account the different divergences for quark and gluon branching, as in [63, 64]. The essential idea is to replace eq. (4) with

$$y_{ij}^{(F)} = \frac{2(1 - \cos \theta_{ij})}{Q^2} \times \begin{cases} \max(E_i^2, E_j^2), & \text{softer of } i, j \text{ is flavoured,} \\ \min(E_i^2, E_j^2), & \text{softer of } i, j \text{ is flavourless,} \end{cases} \quad (11)$$

where gluonic (or non-heavy-quark) objects are considered flavourless. This reflects the fact that there is no divergence for producing a lone soft quark, and correctly ensures that soft quarks are recombined with soft antiquarks. In normal algorithms, in contrast, a soft quark and anti-quark may end up in different jets, polluting the flavour of each one. Full details, and the hadron collider variants, are given in [63], while an application to  $b$ -jets was given [64], where it led to a much more accurate NLO prediction for the inclusive  $b$ -jet spectrum. Related ideas have also been used in a sequential-recombination jet-algorithm designed for combining QCD matrix elements and parton showers [65].

**Variable- $R$  algorithms.** A recent proposal in [66] suggests a class of hadron-collider distance measures of the following form

$$d_{ij} = \min(p_{ti}^{2p}, p_{tj}^{2p}) \Delta R_{ij}^2, \quad d_{iB} = p_{ti}^{2p} R_{\text{eff}}^2(p_{ti}^2), \quad (12)$$

where the radius of the jet (now placed in the  $d_{iB}$  term rather than  $d_{ij}$ ) becomes a function of the jet's transverse momentum  $R_{\text{eff}}(p_{ti}^2)$ . This provides an original way of having a jet radius that depends on the event structure, a feature which in general can be useful (cf. section 5.1). In [66] it was applied specifically to the question of dijet resonance reconstruction, with the aim of producing larger jets,  $R_{\text{eff}} \sim 1/p_t$ , (appropriate with  $p \leq 0$ ) for resonances that decay along the beam direction, and it led to improved resolution on the reconstructed mass peak.

**Filtering and pruning.** As we shall see in section 5, contamination from non-perturbative effects associated with beam-remnants (underlying event) in hadron colliders is a major

cause of degradation of resolution on jets' energies. One way of reducing this [67] is to first find the jets (with some given  $R$ ) and then reconsider each jet on a smaller angular scale,  $R_{\text{filt}} < R$  (either by reclustering, or by making use of the hierarchical angular information in the C/A algorithm). On that smaller angular scale one then takes (say) the two hardest subjets, corresponding physically to a hard parton and its hardest gluon emission, while rejecting the junk that comes from the underlying event. Initial studies [67, 68] indicate that this can provide non-negligible advantages in kinematic reconstructions.

A related idea, “pruning,” was suggested in ref. [69]. During the (re)clustering of the jet, if two objects  $i, j$  are separated by  $\Delta R_{ij} > R_{\text{filt}}$  and the softer one has  $z = \min(p_{ti}, p_{tj}) < p_{t,i+j} < z_{\text{cut}}$  (with  $z_{\text{cut}} = 0.1$  say), then that softer one is simply discarded.

One issue with filtering, pruning and the variable- $R$  approach discussed above, is that they all introduce extra degrees of freedom in the jet finding. Thus the gains that they may provide come at the expense of having to tune those choices to the specific physics analysis that is being carried out.

**3  $\rightarrow$  2 recombination.** Most sequential recombination algorithms are related to the idea of inverting successive  $1 \rightarrow 2$  perturbative branchings (as used in many parton-shower Monte Carlo programs). When simulating QCD branching it can also be useful to consider “dipole” branchings, i.e.  $2 \rightarrow 3$  splittings, as in Ariadne [70]. Correspondingly one can imagine a sequential-recombination jet algorithm that inverts these branchings by carrying out  $3 \rightarrow 2$  clusterings. This is the principle of the ARCLUS algorithm [71] for  $e^+e^-$  collisions. In practice its performance is similar to that of other  $e^+e^-$  algorithms (as discussed in [37]).

## 2.3 Jet finding as a minimisation problem

Several groups have considered jet finding as a minimisation problem. Though not the main subject of this review, for completeness it is worth devoting a few lines to describe these ideas, which fit into the top-down approach to jet-finding, and have been explored by several groups over the past decade.

One approach [72] relates to a method known as  $k$ -means in the more general computer science field of clustering [73]. It introduces a partition of particles  $i$  into  $n$  clusters  $L_k$  ( $k = 1 \dots n$ , with  $n$  chosen a priori). For a given partition, each cluster has a centroid  $C_k$  and one can evaluate a measure

$$S = \sum_k \sum_{i \in L_k} d(p_i, C_k) \quad (13)$$

where  $d(p_i, C_k)$  is some measure of the distance between particle  $i$  and the centroid  $k$ . One then chooses the assignment of particles into clusters that minimises  $S$ . Part of the motivation given for the approach of [72] is that it allows one to also include a range of physical constraints (such as the  $W$ -mass in top reconstruction) when carrying out the

minimisation. However there are open questions as to how it may fare in analyses where one doesn't actually know what the number of jets should be (for example because of background contamination).

Two other approaches, “deterministic annealing” (DA) [74] and the “optimal jet finder” (OJF) [75] do away with the idea that a particle belongs to any single jet. Essentially (and in a language closer to [75]), they argue that each particle  $i$  is associated with jet  $k$  with a weight  $w_{ik}$  such that  $\sum_k w_{ik} = 1$  (or alternatively also allowing for particles to be associated with no jet [75]). The momentum  $P_k$  of jet  $k$  is then given by  $P_k = \sum_i w_{ik} p_i$ . In the OJF approach, one makes an a-priori choice for the number of jets, and then a minimisation is carried out over all the entries of the  $w_{ik}$  matrix, so as to find the lowest value of some cost function, corresponding for example to some combination of the jet masses; one can then repeat the minimisation for a different number of jets and introduce some criterion for one's choice of the number  $n$  of jets, based on the value of the cost function for each  $n$ .

In the DA approach, roughly speaking, given some initial weights, one calculates the jet momenta  $P_k$ , and then one recalculates the weights according to

$$w_{ik} = \frac{P_{t,k} e^{-\beta d(p_i, P_k)}}{\sum_m P_{t,m} e^{-\beta d(p_i, P_m)}}, \quad (14)$$

where  $\beta$  is an inverse temperature and  $d(p_i, P_k)$  is some distance measure (for example  $\Delta R_{ik}^2$ ). One iterates until the weights converge. This is accompanied by the observation that for  $\beta = 0$ , whatever the starting conditions, the  $w_{ik}$  will be independent of  $i$ , which implies that whatever the initial conditions and value of  $n$ , all jets will have identical directions (i.e. there is only one jet); as one increases  $\beta$ , the system will then tend to develop a larger number of distinct jets. Thus  $\beta$  plays the role of  $1/d_{\text{cut}}$  in sequential recombination algorithms.

The ideas behind the OJF and DA algorithms are certainly interesting, especially the concept that a particle may be associated with more than one jet, though it is perhaps not obvious that the extra conceptual complexity that stems from this is offset by any particular benefits. In the corresponding initial studies [75, 74] physics performances were found to be comparable to that of the  $k_t$  algorithm, though a practical advantage at the time (no longer relevant nowadays) was a better scaling of the computational speed with particle multiplicity,  $\sim N$  for OJF,  $\sim N^2$  for DA.

The relation between minimisation and jet-finding has also been investigated in [35], where stable-cone finding (and cone iteration) has been interpreted in terms of the search for the local minima of the potential

$$F(\hat{n}) = \frac{1}{2} \sum_i E_{ti} \Delta R_{i\hat{n}}^2 \Theta(R^2 - \Delta R_{i\hat{n}}^2), \quad (15)$$

which is a function of the particle momenta and of a cone direction  $\hat{n}$  (a coordinate in  $\eta, \phi$ ). Each stable cone corresponds to a local minimum of the potential as a function of  $n$ . Investigations have also been carried out [76, 77] into whether one can directly use “potential” approaches as a replacement for jet finding altogether.



For completeness, it should be stated that the above approaches are infrared and collinear safe, as an almost direct consequence of the way in which they are constructed.

Finally, just as this review was about to be made public, it was brought to the author’s attention that code had just been released [78] for a further approach involving minimisation as well as weighted assignment of individual particles to multiple jets

## 2.4 Recombination schemes

The most widespread recombination scheme nowadays is the  $E$ -scheme, or 4-vector recombination scheme. To merge two particles, it just adds their 4-vectors (and it produces massive jets). This is the current recommendation according to [5].

A scheme that was widely used in the past at hadron-colliders was the  $E_t$  weighted recombination scheme, which had been put forward also in the Snowmass accord. To recombine a set of particles into a jet, it uses the following procedure:

$$E_{t,\text{jet}} = \sum_i E_{ti}, \quad (16a)$$

$$\eta_{\text{jet}} = \frac{1}{E_{t,\text{jet}}} \sum_i E_{ti} \eta_i, \quad (16b)$$

$$\phi_{\text{jet}} = \frac{1}{E_{t,\text{jet}}} \sum_i E_{ti} \phi_i, \quad (16c)$$

where the sum runs over the particles contained in the jet, and the jet is taken to be massless. This procedure has the drawback that it is not invariant under longitudinal boosts if the component particles are massive (though one can formulate boost-invariant alternatives in terms of rapidity  $y_i$  and transverse momentum  $p_{ti}$ ).

When other recombination schemes are used, this is usually stated explicitly in the corresponding publication. One should be aware that in some cases the recombination scheme used during the clustering (e.g. in the iteration of stable cones) differs from the recombination scheme that is used to obtain the final jet momenta once the particle assignments to the jets are known.

## 2.5 Summary

We have seen many different jet algorithms in this section. A summary of the main ones in common use in hadron-collider studies is given in table 2. Many of the algorithms (and all the IRC safe ones) are available from the FastJet [25] or SpartyJet [26] packages (the latter provides access to the IRC safe algorithms via FastJet).

A general recommendation is that hadron-collider algorithms that are IR or collinear unsafe should in future work be replaced by IRC safe ones, of which the inclusive  $k_t$ , C/A (possibly with “filtering”), anti- $k_t$  and SISCone are good choices. Specifically the xC-PR

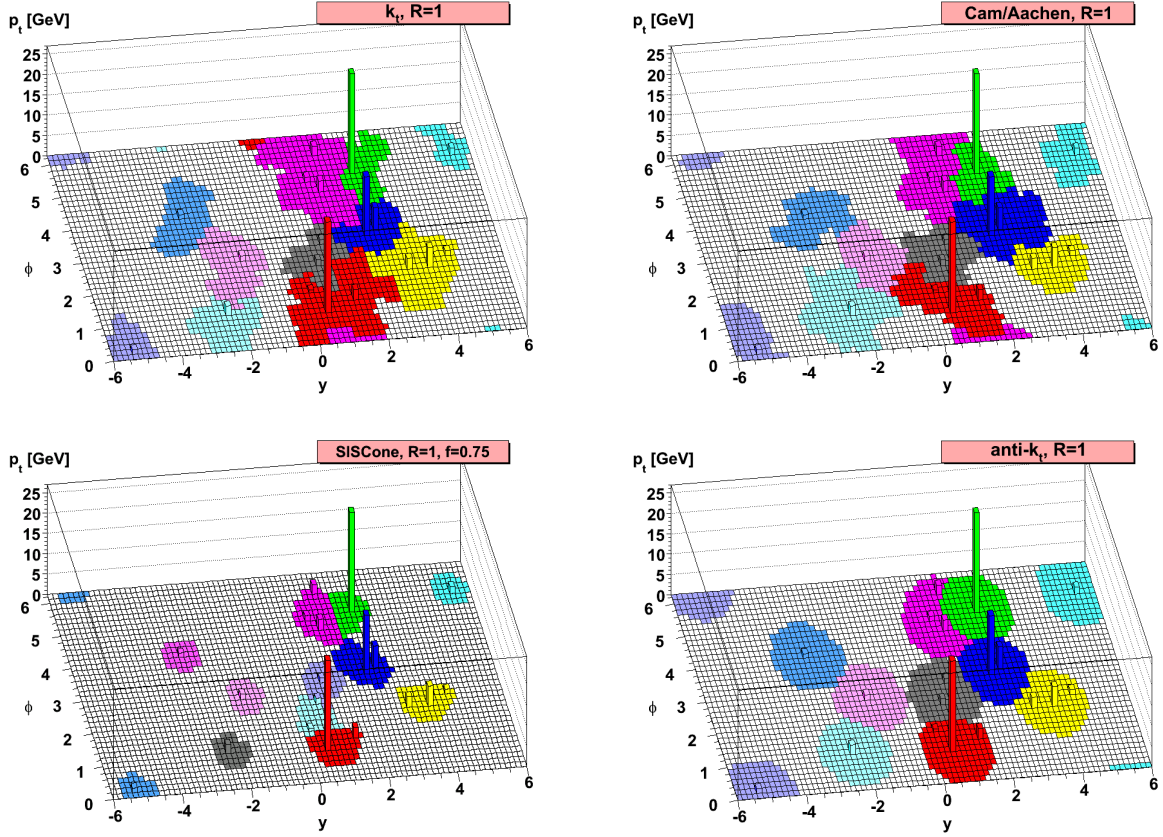


**Figure 6:** A sample parton-level event (generated with Herwig [80]), together with many random soft “ghosts”, clustered with four different jet algorithms, illustrating the “active” catchment areas of the resulting hard jets (cf. section 4.4). For  $k_t$  and Cam/Aachen the detailed shapes are in part determined by the specific set of ghosts used, and change when the ghosts are modified.

class of algorithms is naturally replaced by the anti- $k_t$  algorithm (which produces circular jets, as illustrated in figure 6, and has similar low-order perturbative properties), while SISCone is very much like the IC-SM algorithms, but ensures that the stable-cone finding is IRC safe.

Figure 6 illustrates the jets that are produced with the 4 “choice” IRC-safe algorithms in a simple, parton-level event (generated with Herwig), showing among other things, the degree of regularity (or not) of the boundaries of the resulting jets.

### 3 Computational geometry and jet-finding

It takes the human eye and brain a fraction of a second to identify the main regions of energy flow in a calorimetric event such as fig. 6. A good few seconds might be needed to quantify that energy flow, and to come to a conclusion as to how many jets it contains.

Algorithm	Type	IRC safe?	Ref.	Notes
inclusive $k_t$	$\text{SR}_{p=1}$	OK	[11, 12, 13]	also has exclusive variant
Cambridge/Aachen	$\text{SR}_{p=0}$	OK	[14, 15]	
anti- $k_t$	$\text{SR}_{p=-1}$	OK	[17]	
SISCone	SC-SM	OK	[24]	multipass, with optional cut on stable cone $p_t$
CDF JetClu	$\text{IC}_r\text{-SM}$	$\text{IR}_{2+1}$	[20]	
CDF MidPoint cone	$\text{IC}_{mp}\text{-SM}$	$\text{IR}_{3+1}$	[5]	
CDF MidPoint searchcone	$\text{IC}_{se,mp}\text{-SM}$	$\text{IR}_{2+1}$	[35]	
DØ Run II cone	$\text{IC}_{mp}\text{-SM}$	$\text{IR}_{3+1}$	[5]	no seed threshold, but cut on cone $p_t$
ATLAS Cone	IC-SM	$\text{IR}_{2+1}$	[2]	
PxCone	$\text{IC}_{mp}\text{-SD}$	$\text{IR}_{3+1}$	[22]	no seed threshold, but cut on cone $p_t$ ,
CMS Iterative Cone	IC-PR	$\text{Coll}_{3+1}$	[3]	
PyCell/CellJet (from Pythia)	FC-PR	$\text{Coll}_{3+1}$	[79]	
GetJet (from ISAJET)	FC-PR	$\text{Coll}_{3+1}$		

**Table 2:** Overview of some jet algorithms used in experimental or theoretical work in hadronic collisions in the past few years.  $\text{SR}_{p=x}$  = sequential recombination, with  $p = -1, 0, 1$  characterising the exponent of the transverse momentum scale, eq. (10); SC = seedless cone (finds all cones); IC = iterative cone (with midpoints  $mp$ , ratcheting  $r$ , searchcone  $se$ ), using either split–merge (SM), split–drop (SD) or progressive removal (PR) in order to address issues with overlapping stable cones; FC = fixed-cone. In the characterisation of infrared and collinear (IRC) safety properties (for the algorithm as applied to particles),  $\text{IR}_{n+1}$  indicates that given  $n$  hard particles in a common neighbourhood, the addition of 1 extra soft particle can modify the number of final hard jets;  $\text{Coll}_{n+1}$  indicates that given  $n$  hard particles in a common neighbourhood, the collinear splitting of one of the particles can modify the number of final hard jets. Where an algorithm is labelled with the name of an experiment, this does not imply that it is the only or favoured one of the above algorithms used within that experiment. Note that some of the corresponding computer codes for jet-finding first project particles onto modelled calorimeters.

Type of event	$N$
$e^+e^-$ event on the $Z$ peak	50
Tevatron ( $\sqrt{s} = 1.96$ TeV) dijet event	200
LHC ( $\sqrt{s} = 14$ TeV) dijet event	500
LHC low-luminosity event (5 pileup collisions)	1000
LHC high-luminosity event (20 pileup collisions)	4000
RHIC Au Au event ( $\sqrt{s} = 200$ GeV/nucleon)	3000
LHC Pb Pb event ( $\sqrt{s} = 5.5$ TeV/nucleon)	30000

**Table 3:** Orders of magnitude of the event multiplicities  $N$  (charged + neutral) for various kinds of event. The  $e^+e^-$  and  $pp$  events have been estimated with Pythia 6.4[81, 79], LHC PbPb with Pythia + Hydjet [82] and RHIC has been deduced from [83]. Note that in some cases algorithms may run on calorimeter towers or cells, which may be more or less numerous than the particle multiplicity.

Those are timescales that usefully serve as a reference when considering the speed of jet finders — if a jet finder takes a few seconds to classify an event it will seem somewhat tedious, whereas a few milliseconds will seem fast. One can reach similar conclusions by comparing to the time for a Monte Carlo event generator to produce an event (from tens of milliseconds to a fraction of a second), or for a fast detector simulation to process it. Or by considering the number of CPU hours needed to process a typical event sample, which might consist of  $\mathcal{O}(10^7)$  events.

The time taken for jet-finding by computer codes depends strongly on the number of input particles (or towers, etc.),  $N$ . We don’t yet know the exact average multiplicities of LHC events, but rough estimates are given in table 3. With the  $k_t$  algorithm’s “standard”  $N^3$  timing, assuming about  $10^9$  computer operations per second, one expects a time for clustering a low-luminosity LHC event of 1 s (this is also what one finds in practice). So this is close to being “tedious,” and becomes dissuasive for high-luminosity LHC and heavy-ion collisions, or if one wishes to try out many distinct jet definitions (e.g. several different  $R$  values to see which is best). A more extreme example is the exact seedless cone algorithm following the method in [5], which has a timing of  $N2^N$ . In practice (NLOJET++ implementation [29]), an event with  $\sim 20$  particles takes about a second, so one can extrapolate that even just 100 particles will take  $10^{17}$  years. This is beyond prohibitive.

To speed up jet finders one may consider the general class of computational algorithm that the jet-finder belongs to. For instance, all the SR jet finders are examples of “hierarchical clustering”, with a range of different distance measures. General solutions to the problem were discussed long ago in the computer science literature by Anderberg [84], with a set of rather good solutions proposed by Cardinal and Eppstein more recently in [85, 86], which scale roughly as  $N^2$ .

Generic hierarchical clustering is, however, a broad problem. For example, given three “points”,  $A$ ,  $B$  &  $C$ , generic distances are not ‘transitive’: if  $A$  is close to  $B$  and  $B$  is close

to  $C$ , this does *not* imply that  $A$  is close to  $C$  (the reader is encouraged to think up a concrete example for the  $k_t$  distance measure). On the other hand, jet-finding often has a geometrical component (since, at hadron colliders, the rapidity and azimuth coordinates represent the surface of a cylinder). In geometry, if  $A$  is close to  $B$  and  $B$  to  $C$ , then  $A$  and  $C$  are necessarily also close. This is of significant help, and a whole research field exists for such geometric proximity problems, computational geometry. Section 3.1 will show how we can make use of this to obtain  $N \ln N$  scalings for the  $k_t$  algorithm rather than the  $N^2$  of generic hierarchical clustering, or  $N^3$  of the older  $k_t$ -clustering codes. Then in section 3.2 we will examine how to apply computational geometry to cone algorithms.

### 3.1 Sequential recombination algorithms

The original implementations of the  $k_t$  algorithm [55, 56] set up a two-dimensional array of the  $d_{ij}$ , and at each stage of the clustering run through all entries of it in order to find the minimum, and then update the array with the entries for the newly created particle. Since the  $d_{ij}$  array is of size  $\mathcal{O}(N^2)$  and the minimum is searched for  $\mathcal{O}(N)$  times in total (i.e.  $\mathcal{O}(N)$  clusterings), these implementations take a time  $\sim N^3$ .

We have seen briefly above that there exist generic methods for hierarchical clustering, i.e. repeated recombination of the closest pair of objects, that take  $N^2$  time. In general  $N^2$  time is a lower bound because, at the very least, one has to consider all entries of the  $d_{ij}$  distance matrix in order to find the smallest. One may then be clever in keeping track of distance information as points are recombined, so as to side-step the  $N^3$  growth of some  $k_t$  algorithm implementations,<sup>11</sup> but the initial search for the minimum among all pairs of points seems unavoidable.

#### 3.1.1 $k_t$ algorithm

To see whether we can evade the  $N^2$  bound, let us examine the  $k_t$  algorithm's distance measure in more detail

$$d_{ij} = \min(p_{ti}^2, p_{tj}^2) \Delta R_{ij}^2, \quad \Delta R_{ij}^2 = (y_i - y_j)^2 + (\phi_i - \phi_j)^2. \quad (17)$$

We could equally well have considered a distance measure

$$D_{ij} = p_{ti}^2 \Delta R_{ij}^2, \quad (18)$$

The smallest of the  $D_{ij}$  across all  $i, j$  coincides with the smallest of all the  $d_{ij}$ , since  $\min(D_{ij}, D_{ji}) = d_{ij}$ . So it is irrelevant whether we use eq. (17) or (18) in the  $k_t$  algorithm.

Eq. (18) has the important property that the transverse-momentum part depends on just one of the two particles, so we can write

$$\min_j \{D_{ij}\} = p_{ti}^2 \min_j \{\Delta R_{ij}^2\}, \quad (19)$$

---

<sup>11</sup>Essentially, observing that at most  $\mathcal{O}(N)$  distances change at every pair recombination.

i.e. fixing  $i$ , the smallest of the  $D_{ij}$  involves  $i$ 's geometrical nearest neighbour (let's refer to it as  $\mathcal{G}_i$ ). So if we can find some efficient way of establishing and tracking that geometrical information, then rather than finding the minimum of  $N^2$   $D_{ij}$  values, the sequential recombination problem involves only finding the minimum of  $N$   $D_{i\mathcal{G}_i}$  values. This was the key observation of [87].

One is then left with the question of how to find the minimum of the  $\Delta R_{ij}^2$  for each  $i$ , since this still seems to involve a total of  $N^2$  points. Technically, the problem is that of establishing and maintaining a nearest-neighbour graph on the 2-dimensional surface of a cylinder. A rule of thumb when faced with such problems is to first ask how one might deal with them in 1 dimension, say rapidity  $y$ . That is easy: one sorts the points according to their  $y$  coordinate, and the nearest neighbour of a point is the one that immediately precedes or follows it.

Let us do the bookkeeping for this case with just a rapidity coordinate:

Initialisation:

- Sort points according to  $y$  coordinate (with a balanced binary tree), find nearest neighbours, and find all  $d_{i\mathcal{G}_i}$ . [ $N \ln N$ ]
- Place the  $d_{i\mathcal{G}_i}$  in a “priority queue” (a structure for efficient minimum-finding and updates; often simply a balanced binary tree) [ $N \ln N$ ]

Iteration:

- Recombine the pair with smallest  $d_{i\mathcal{G}_i}$ , remove the corresponding two points from the rapidity-sorted tree, add the new one, establish the new point's nearest neighbours and establish if it has become the nearest neighbour of any of the existing points. [ $\ln N$  per recomb.]
- Update the priority queue of  $d_{i\mathcal{G}_i}$  values and find the new minimum (only a finite number of  $d_{i\mathcal{G}_i}$  will change per round). [ $\ln N$  per recomb.]

This gives a total time of  $\mathcal{O}(N \ln N)$ .

With two geometrical dimensions, nearest-neighbour finding is more complex, however it has been the subject of research by the computational geometry community. One structure that can help is the Voronoi diagram [88], or its dual, the Delaunay triangulation. A Voronoi diagram divides the plane into cells (one per vertex), such that every point in the cell surrounding a vertex  $i$  has  $i$  as its nearest vertex. The structure is useful for nearest-neighbour location because the vertex  $\mathcal{G}_i$  nearest to vertex  $i$  is always in one of the (few, *expected*<sup>12</sup>  $\mathcal{O}(1)$ ) cells that share an edge with the cell of vertex  $i$ . An example is shown in figure 7.

Voronoi diagrams for  $N$  points can be constructed with  $\mathcal{O}(N \ln N)$  operations [89]. Maintaining dynamic point sets is more complicated, however there exists an approach [90]

---

<sup>12</sup>“Expected” means that there can be special cases where the number is parametrically larger.

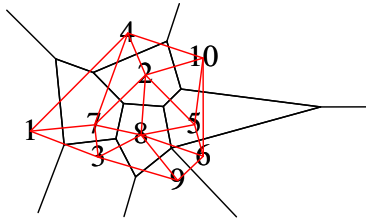


**Figure 7:** The Voronoi diagram for ten random points. The Delaunay triangulation (red) connecting the ten points is also shown. In this example the points 1, 4, 2, 8 and 3 are the ‘Voronoi’ neighbours of 7, and 3 is its nearest neighbour. Taken from [87].

that takes  $\mathcal{O}(N \ln N)$  for the initial construction and expected  $\ln N$  per insertion/deletion and it is available as a public code, CGAL [91, 92].

A complete expected  $N \ln N$  implementation that makes use of CGAL is available in the FastJet program [25]. In practice,  $\ln N$  terms in computational geometry come with a large coefficient — typically  $\ln N$  might be smaller than  $N$  only for  $N \gtrsim 10^3$ . Therefore for moderate  $N$  it is useful to include alternative computational strategies. One particularly successful one (optimal in the range  $50 \lesssim N \lesssim 10^4$ ) makes use of the fact that only for  $\Delta R_{ij} < R$  will a  $d_{ij}$  distance be smaller than  $d_{iB}, d_{jB}$  in eq. (6)— therefore one can restrict one’s search for  $i$ ’s geometric nearest neighbours to the region within  $R$  of  $i$ . Denoting by  $n$  the typical number of points in such a region, one then has a  $\mathcal{O}(Nn)$  algorithm.

Further details are available in the FastJet documentation (from the web site [25]) and from an unpublished preprint [93].

### 3.1.2 Special cases

The above approaches can be used for the whole class of generalised (longitudinally invariant)  $k_t$  algorithms, however some special cases deserve comment.

**Cambridge/Aachen.** For the C/A jet-finder, there is no momentum scale, so rather than having a dynamic planar nearest-neighbour problem, one has a dynamic planar closest pair problem,  $d_{ij} \equiv \Delta R_{ij}$ . This is simpler — essentially one can maintain a nearest neighbour candidate for each point, but it only need be correct for the closest pair. One remarkable solution to this problem<sup>13</sup> was given by Chan in [94]. It is included natively in FastJet, and is slightly faster than the CGAL based solution (as well as avoiding the need for a separate package).

Note: Chan’s solution relies on the use of integer arithmetic (part of its cleverness lies in its implicit use of the binary representation of integers). However since rapidities and azimuths do not extend to large values, one can safely rescale them by some large constant

<sup>13</sup>Which can be stated in a paragraph, though this does not mean that it is simple to understand!

and represent them as integers.

**Anti- $k_t$ .** The generalised  $k_t$  algorithm with  $p < 0$  (and specifically anti- $k_t$ , with  $p = -1$ ) has the property that it effectively produces jets that grow outwards in a circular pattern around a high- $p_t$  seed. This leads to configurations with one particle at the centre of a circle and many on the edge (the first layer of points on the edge contains  $\mathcal{O}(\sqrt{n})$  particles).

This is precisely the configuration in which the ‘expected’  $N \ln N$  behaviour of the clustering breaks down: the central point has many Voronoi neighbours, and, furthermore, is involved in each clustering (so it is removed, reinserted, and then one must go around all the points on the edge to see which now is its nearest neighbour). This means that for very large  $N, n$ , the timing for anti- $k_t$  type algorithms is closer to  $N\sqrt{n}$  than to  $N \ln N$ .

According to [95] there exist approaches to the planar nearest-neighbour problem that have worst-case behaviour  $N^\epsilon$  with arbitrarily small  $\epsilon$ , however these have not been investigated in the context of jet-finding.

### 3.2 A polynomial-time seedless cone

We saw in section 2.1.4 that the use of particles as seeds, i.e. starting points for cone iterations, gets us into trouble with IRC safety: if one finds jets based on the ordering of the seeds in  $p_t$ , then one is sensitive to collinear splittings; if one uses the stable cones obtained from iterating all seeds, then one becomes sensitive to the addition of new soft seeds.

We also saw an exact seedless approach that takes all subsets of particles and establishes for each one whether it corresponds to a stable cone — i.e. for each subset one calculates its total momentum, draws a circle around the resulting axis, and if the points contained in the circle are exactly those in the initial subset, then one has found a stable cone. This is guaranteed to find all stable cones.

For large multiplicities, this is inherently wasteful insofar as most of the  $2^N$  subsets of particles don’t fit into a circle of radius  $R$  on the rapidity-azimuth plane, so there is no way for them to form a stable cone.

The obvious corollary of that observation is that one should only consider subsets of points in which the members of the subset are contained within a circle of radius  $R$ , and any point not in the subset is outside the circle. It is only these subsets that can ever form a stable cone. Therefore rather than considering all subsets of points, one can restrict one’s attention to all distinct ways of separating points on the surface of a cylinder (or plane) into two subsets, those points inside a circle of radius  $R$ , all others outside — a “planar all distinct circular enclosures” problem.

This problem is a clear example of a computational geometry problem. Let’s first see how we would deal with it in one dimension, for which a “circular enclosure” just reduces to a line segment enclosure. Given points on a line and a segment of length  $2R$ , we can



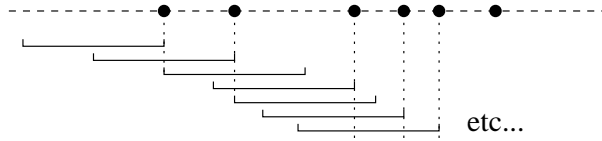


**Figure 8:** Representation of points on a line and the places where a sliding segment has a change in its set of enclosed points.

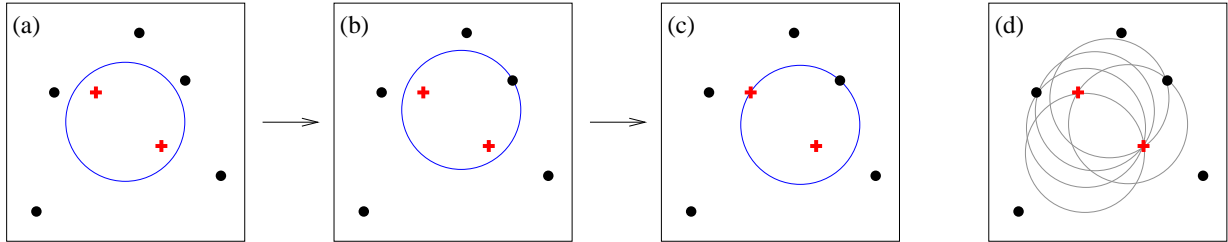


**Figure 9:** (a) Some initial circular enclosure; (b) moving the circle in a random direction until some enclosed or external point touches the edge of the circle; (c) pivoting the circle around the edge point until a second point touches the edge; (d) all circles defined by pairs of edge points leading to the same circular enclosure.

order the points, place the segment to the left of the leftmost point, and then slide it sideways. Each time the left or right edge of the segment touches a point, the contents of the enclosure change. The cost of finding all enclosures is just that of ordering the points ( $N \ln N$ ).

How do we extend this to two dimensions? The central idea is that the enclosed point set changes when a point touches the enclosure. In 1d we can always shift the enclosure, without changing its contents, until its edge touches a point (either in or out of the enclosure). In 2d we can first shift the circular enclosure until one point touches the edge, then pivot the circle around that point until its circumference touches a second point (fig. 9). Conversely if we consider all pairs of points (within  $2R$  of each other) and draw all possible circles that go through those pairs, then we will have found all possible enclosures (one should remember that edge points can be either in or out of the enclosure; special treatment is also needed for points that are alone, i.e. further than  $2R$  from the nearest other point).

There are  $\mathcal{O}(Nn)$  relevant pairs of points.<sup>14</sup> One could directly check the stability of each one (at a cost of at least  $\mathcal{O}(n)$ ), giving an  $\mathcal{O}(Nn^2)$  algorithm. Alternatively one can establish a traversal order in which the circle contents change by one point at a time, avoiding (with the help of a few other tricks) the need to pay a price of  $\mathcal{O}(n)$  for the stable-cone check for each distinct enclosure. This is the basis of the (expected)  $Nn \ln n$

<sup>14</sup>There is a correspondingly large number of distinct cones, and this has implications for proposal [96] to use a Fast Fourier Transform for the stable-cone search (cf. also the FFTJet package [78], which was released just as this review was being finalised), essentially because it implies the need for a Fast Fourier Transform grid of size  $\mathcal{O}(Nn)$ .

algorithm that is known as SISConc (Seedless Infrared Safe Cone) [24].<sup>15</sup>

Some comments are due concerning SISConc’s timing. There are usually only  $\mathcal{O}(N)$  stable cones, parametrically fewer than the number of distinct enclosures. Might there be a way of somehow skipping all the unstable enclosures? It is not clear, because the upper bound on the number of stable cones is actually  $\mathcal{O}(Nn)$  (the much lower expected value holds for random point sets [24]). This worst case can actually occur (for example with regular sets of “ghosts,” cf. section 4.4), with implications then for the split–merge procedure. Normally the split–merge procedure is significantly faster than the stable-cone search, in that it takes time  $\mathcal{O}(N^2)$  ( $\ll Nn \ln n$  in practice<sup>16</sup>) in SISConc’s fairly straightforward implementation. However if the number of stable cones is  $\mathcal{O}(Nn)$ , then the split–merge step becomes  $\mathcal{O}(N^2n)$  unless one applies additional dedicated techniques (such as quad-trees or  $k$ -d trees, as discussed in [24] and also suggested in [96]).

A further comment is due on memory usage: SISConc maintains a hash of circular enclosures that it has already seen (and whether they are candidates for stable cones or not). That hash has as many entries as distinct enclosures,  $\mathcal{O}(Nn)$ , and this can become problematic for very large multiplicities.<sup>17</sup> In such cases one could in principle reduce the memory use to  $\mathcal{O}(N)$ , at the expense of a slower run-time  $\mathcal{O}(Nn^{3/2})$ , but this has not been implemented.

### 3.3 Speed summaries

Statements of timings in terms of their scaling with  $N$  can hide large coefficients and significant preasymptotic corrections. Another issue is that as  $N$  increases so does memory usage, requiring (slower) access to the main memory rather than the CPU cache, and this too can affect practical timing results.

Timings for a subset of commonly used algorithms are shown in fig. 10. One conclusion from that figure is that SISConc, the slowest of the IRC safe algorithms, is still competitive in speed with the main public Midpoint-cone code and is acceptably fast unless one goes to  $N$  larger than several thousand. FastJet’s implementation of the  $k_t$  algorithm (and C/A and anti- $k_t$ ) is much faster, with clearly healthier scaling at large  $N$ , and it beats even the fast IRC unsafe cone codes, like CDF’s JetClu.

---

<sup>15</sup>It has been pointed out by Sjöstrand [97] that SISConc’s use of all pairs of points to provide the full list of distinct circular enclosures bears a close relation to a technique used in the  $N^3$  computation of the Thrust [98]. There, all pairs of particles are used to generate all relevant separations of the surface of a sphere into two hemispheres. A corollary of this observation is that SISConc’s idea of a traversal order could also be used in the context of the thrust, to reduce its computation time to  $N^2 \ln N$ .

<sup>16</sup>In QCD events and with typical values of the jet-finding radius  $R = 0.4 - 1.0$ ,  $N/n$  is usually between 10 and 100; in 2-dimensional problems, for the multiplicities that are of relevance here, a rule of thumb seems to be that  $\ln n$  is very roughly equivalent to a factor of order  $10^3$ .

<sup>17</sup>If we suppose  $n \sim 0.1N$ , and that each entry needs 12 bytes for the hash, two double-precision numbers (8 bytes each) to describe the center of the cone, and a pointer to the next hash element, plus various overheads, then we get a memory usage of about  $4N^2$  bytes, i.e. nearly 4 GB for  $N \sim 30\,000$ , which is a typical expected LHC heavy-ion multiplicity.

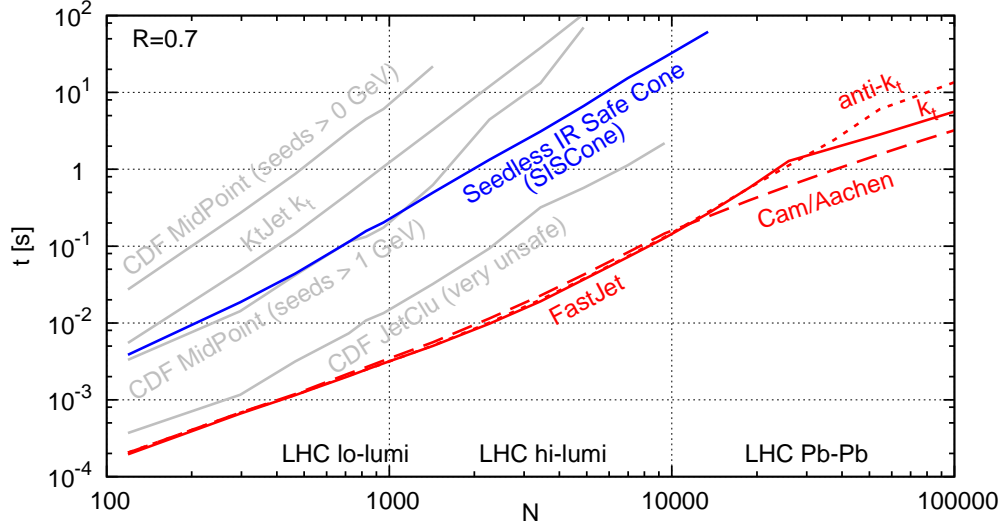


**Figure 10:** Timings for the clustering of a simulated  $\sim 50$  GeV dijet event, to which increasing numbers of simulated minimum-bias events have been added (both simulated with Pythia). In dark colours one sees SISCone and the FastJet  $k_t$  implementation (with automatic optimal choice been  $Nn$  and  $N \ln N$  strategies), while in grey one sees results for the KtJet implementation [56] of the the  $k_t$  algorithm, the Midpoint cone ( $IC_{mp}$ -SM) in CDF’s implementation (with and without a 1 GeV cutoff on seeds) and the JetClu iterative cone ( $IC_r$ -SM, with a 1 GeV seed threshold). All non-FastJet algorithms (except KtJet) have been accessed through FastJet plugins.

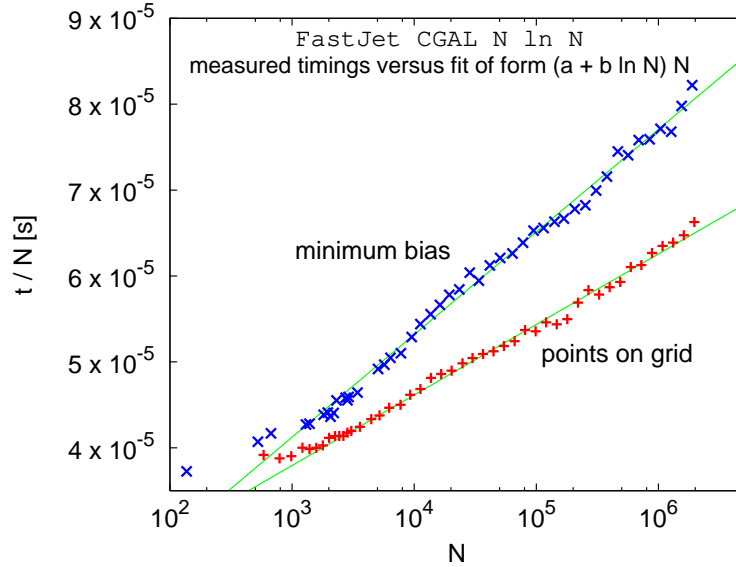


**Figure 11:** Verification of the  $N \ln N$  timing behaviour of the CGAL-based implementation of the  $k_t$  algorithm in FastJet. The timings are divided by  $N$  so as to highlight the remaining  $\ln N$  dependence. Taken from [93].

The FastJet curve has a clear kink at  $N \sim 15000$ . This is the point where FastJet switches from an  $Nn$  (tiled) algorithm to the  $N \ln N$  CGAL-based one. One can explicitly verify that the CGAL-based algorithm does have an  $N \ln N$  behaviour, by dividing the run times by  $N$  and plotting the result. This is shown in fig. 11.

To conclude this part, we have seen how the computational geometry aspect of jet-related problems can be exploited to help resolve many of the practical computational issues that arise if one is to carry out infrared-safe hadron-collider jet-finding. It is probably fair to say that this is playing a crucial role in encouraging the LHC experiments to switch to QCD-compatible jet-finders. In particular, all the LHC experiments now incorporate FastJet and its SIScone plugin in their software frameworks (and ATLAS also has its own  $\sim N^2$  implementation of the sequential recombination algorithms) [2, 99].

## 4 Understanding jets

Ideally, one would really like to be able to measure partons in experiments. Jets are the closest, physically, that we get to partons. How close are they exactly? And what about the fact that a “parton” isn’t actually a well-defined concept in the first place. An understanding of these questions is part of the key to knowing how best to use jet algorithms at colliders, both in terms of choosing which algorithm to use and setting its parameters.

The precise issues that one might investigate fall into various categories. For example, how broadly will a jet reach for its constituents (section 4.1)? This information is important in terms of one’s ability to disentangle different partons in heavy-particle decays (for example hadronic  $t\bar{t}$  events, which decay to 6 hard partons). Often, one will use jets to reconstruct the kinematics of some ‘parent object’ (again, a heavy particle that decayed; or, in inclusive-jet measurements, a scattered parton from the incoming proton). How does the jet’s energy relate to that of the ‘parent object’? This is affected both by perturbative (section 4.2) and non-perturbative (section 4.3) radiation. Finally LHC is special in that it will have significant underlying-event activity (maybe 15 GeV per unit rapidity) and even larger pileup (easily 100 GeV per unit rapidity). How do jets react to this (section 4.4)?

It is probably fair to say that our understanding of all these questions is still incomplete. But the material below outlines some of what we do know.

### 4.1 Reach

#### 4.1.1 Two-particle case

Given just two massless particles, separated by a distance  $\Delta R$  on the  $y - \phi$  cylinder, will they be recombined into a single jet? This is the simplest of the questions one might ask about a jet definition’s reach. It was discussed in [13] for the inclusive  $k_t$  algorithm and for a partially specified cone, which behaves somewhat like SIScone.

It is convenient to take the transverse momenta of the two particles,  $p_{t1}$ ,  $p_{t2}$  (defined as the softer one) to be related by

$$p_{t2} = xp_{t1}, \quad x < 1. \quad (20)$$

Writing the sum of the two particles' momentum as  $p_J$ , with  $p_{tJ} = p_{t1} + p_{t2}$ ,<sup>18</sup> and imagining the two partons as coming from a common ancestor, we can also write

$$p_{t1} = (1 - z)p_{tJ}, \quad p_{t2} = zp_{tJ}, \quad \left( z = \frac{x}{1 + x} < \frac{1}{2} \right). \quad (21)$$

According to the context, results are more simply expressed either in terms of  $x$  or  $z$ , which is why it is useful to introduce both.

In the  $k_t$  algorithm, the two particles will form a single jet if  $d_{12} < d_{1B}, d_{2B}$  (as defined in eqs. (9)), or equivalently if

$$\Delta R_{12} < R. \quad (22)$$

In the case of an algorithm like SIScone, based on stable cones, the question is whether particles 1 and 2 can both belong to a single cone. This happens if both are within  $R$  of  $p_J$ ,

$$\left. \begin{aligned} \Delta R_{1J} &= z\Delta R_{12} \\ \Delta R_{2J} &= (1 - z)\Delta R_{12} \end{aligned} \right\} < R \quad (23)$$

Since we have defined  $z < 1/2$ , it is the lower condition that is more constraining and it leads to

$$\Delta R_{12} < (1 + x)R, \quad (24)$$

i.e. the same as the  $k_t$  algorithm condition, eq. (22), when  $p_2$  is soft,  $x \ll 1$ , but reaching twice as far when  $p_{t2} \simeq p_{t1}$ .

The conditions eq. (22,24) basically account for the behaviours of nearly all jet algorithms:

- eq. (22) holds for the  $k_t$  algorithm, as well as Cambridge/Aachen, anti- $k_t$ , and the xC-PR cone algorithms;
- eq. (24) holds for IC<sub>mp</sub>-SM (“midpoint”), IC<sub>mp</sub>-SD (Pxcone) and SC-SM (SIScone) algorithms;
- IC-SM algorithms without midpoint seeds (JetClu, Atlas Cones) have ill-defined behaviour. For just two particles, they lead to a single jet based on eq. (22), but if additional soft seeds are present then this transforms into eq. (24). This is a manifestation of their infrared unsafety.

---

<sup>18</sup>In the widespread 4-vector ( $E$ -scheme) recombination scheme, this is exact only if the particles are very close in angle. However it remains a good approximation even for  $\Delta R_{12} \sim 1$  and so it is an approximation that will recur in this section.

### 4.1.2 General case

The complexity of tracing the behaviour of a jet algorithm precludes general results about the reach of different jet algorithms for multi-particle configurations. One question that has however seen some attention is that of how the results of section 4.1.1 get modified in the presence of parton showering and hadronisation.

This is a delicate question because to answer it one has to know something about the *environment* that created the two partons: did they come from the branching of a single parent quark, or a parent gluon, or even the decay of a colour-singlet particle? And what was the parent parton colour-connected to? All of these issues relate to the fact that there is no rigorous way of defining partons in the first place. Furthermore, even in a probabilistic Monte-Carlo type approximation, the way partons shower and hadronise depends on the environment.

One approach [20, 100] to the question involved superposing pairs of events and establishing under what conditions jets that had been identified in the individual events became a single jet if one applied the jet finder to the two events combined together. This study was performed for IC-SM type algorithms and came to the conclusion that the individual jets were merged if there were within  $1.3R$  of each other.<sup>19</sup> This corresponds roughly to expectations based on eq. (24), if one performs some reasonable averaging over the jet momenta, i.e.  $x$  (indeed we will see the value 1.3 appear again below in section 4.2.1). However it fails to provide a direct link with the  $x$ -dependence of eq. (24).

Another approach to testing eqs. (22,24) was taken in [24]. There, jets were initially found with a “reference,”  $R = 1$  hierarchical-clustering algorithm. The hierarchy was used to identify the two main subjets,  $S_1$  and  $S_2$ , within the jet. Each event was also clustered with a test algorithm  $T$ , with  $R_T = 0.4$ . One then looked to see if there was a jet with algorithm  $T$  that contained at least half of the  $p_t$  of each of  $S_1$  and  $S_2$ . If there was, the conclusion was that the two subjets had ended up (dominantly) in a single jet from the test algorithm. The procedure was repeated for many events and one could then plot the fraction of  $k_t$ -algorithm jets for which this occurs,  $P_{2 \rightarrow 1}(\Delta R, x)$ , as a function of the distance  $\Delta R \equiv \Delta R_{S_1 S_2}$  and the momentum ratio  $x \equiv p_{t, S_2}/p_{t, S_1}$ .

In ref. [24] it was the  $k_t$  algorithm that was used as a reference. Here we shall instead use the C/A algorithm as a reference and the subjets are the two objects whose merging in the reference jet’s clustering sequence involves the largest  $k_t$  distance (i.e. the hardest merging).<sup>20</sup> The results will be based on dijet events simulated with Herwig 6.5 [80], both at parton and hadron levels (the latter including Herwig’s default soft UE). Reference jets

---

<sup>19</sup>The value 1.3 has also inspired a practice in NLO calculations, still current within the CDF collaboration (e.g. [101]), that involves placing an artificial cut on the separation between partons within a jet at  $\Delta R = R_{sep} \times R$ , with  $R_{sep} = 1.3$ . Such ad-hoc modifications of the jet algorithm used in a theory prediction defeat the purpose of a NLO calculation. It is probably fair to say, however, that in most contexts where  $R_{sep}$  has been used, its impact is smaller than the dominant theory and experimental uncertainties.

<sup>20</sup>This is inspired by the use of a  $k_t$  and an angular distance measure in the original Cambridge algorithm, and gives clearer results than the  $k_t$  algorithm’s subjets.

were required to have  $p_t > 50$  GeV.

Results are shown in fig. 12, for various jet-algorithms  $T$ , with parton-level results on the left and hadron level on the right. In the regions in black, the two C/A subjects always end up in a common  $T$ -jet, while in the region in white this does not occur. For the IR-safe algorithms one sees rough agreement with the expectations from eqs. (22,24), though for SISCone the boundary is quite broad and shifted to the left of  $\Delta R/R_T = 2$  at  $x = 1$ . This is probably partly a consequence of the showering and hadronisation, which limit the stability of configurations in which the two subjects are near opposing edges of a cone, as has been extensively discussed in [35]. The dependence of the effect also on the split–merge overlap threshold  $f$  suggests that the split–merge dynamics have a non-trivial impact as well. Fig. 12 also shows results two very IR unsafe algorithms, a plain IC-SM variant (CDF’s Midpoint algorithm with the midpoint option turned off) and JetClu. Among the relevant features, one notes the somewhat different shape for the IC-SM algorithm at parton and hadron level, a consequence of the IR unsafety. JetClu bears little resemblance to the plain IC-SM algorithm, even though it is IC-SM based. More detailed study reveals that this is only partially due to its use of ratcheting.

## 4.2 Perturbative properties, $p_t$ and mass

Gluon radiation is inevitable from fast-moving partons. How does it affect the properties of a jet? Basically the gluon may be radiated beyond the reach of the jet definition (“splash-out”) and thus reduce the jet’s energy compared to that of the parton. Alternatively it may be radiated within the reach of the jet-definition and then generate a mass for the jet (assuming a 4-vector-addition recombination scheme). The aim of this section is to give some simple analytical understanding of the effect of perturbative radiation on a jet’s transverse momentum and mass — rules of thumb — as well as references to the literature for more detailed analyses.

### 4.2.1 Jet $p_t$

In many uses of jets, one needs to know how a jet’s energy (or  $p_t$ ) relates to the underlying hard scale of the process — for example to the mass of a decaying heavy particle (top quark, Higgs boson, new particle), or to the momentum fraction carried by a scattered parton in an inclusive jet cross section.

One approach to this is to take a Monte Carlo event generator, let it shower a parton from some source and then compare the jet’s  $p_t$  to that of the parton. This often gives a reasonable estimate of what’s happened, even if the Monte Carlo basically acts as a black box, and brings a somewhat arbitrary definition of what is meant by the initial “parton” (or of the mass of the top quark).

Another approach is to take a program for carrying out NLO predictions, like MCFM [28] or NLOJET++ [29], and for example determine the relation between the jet  $p_t$ -spectrum

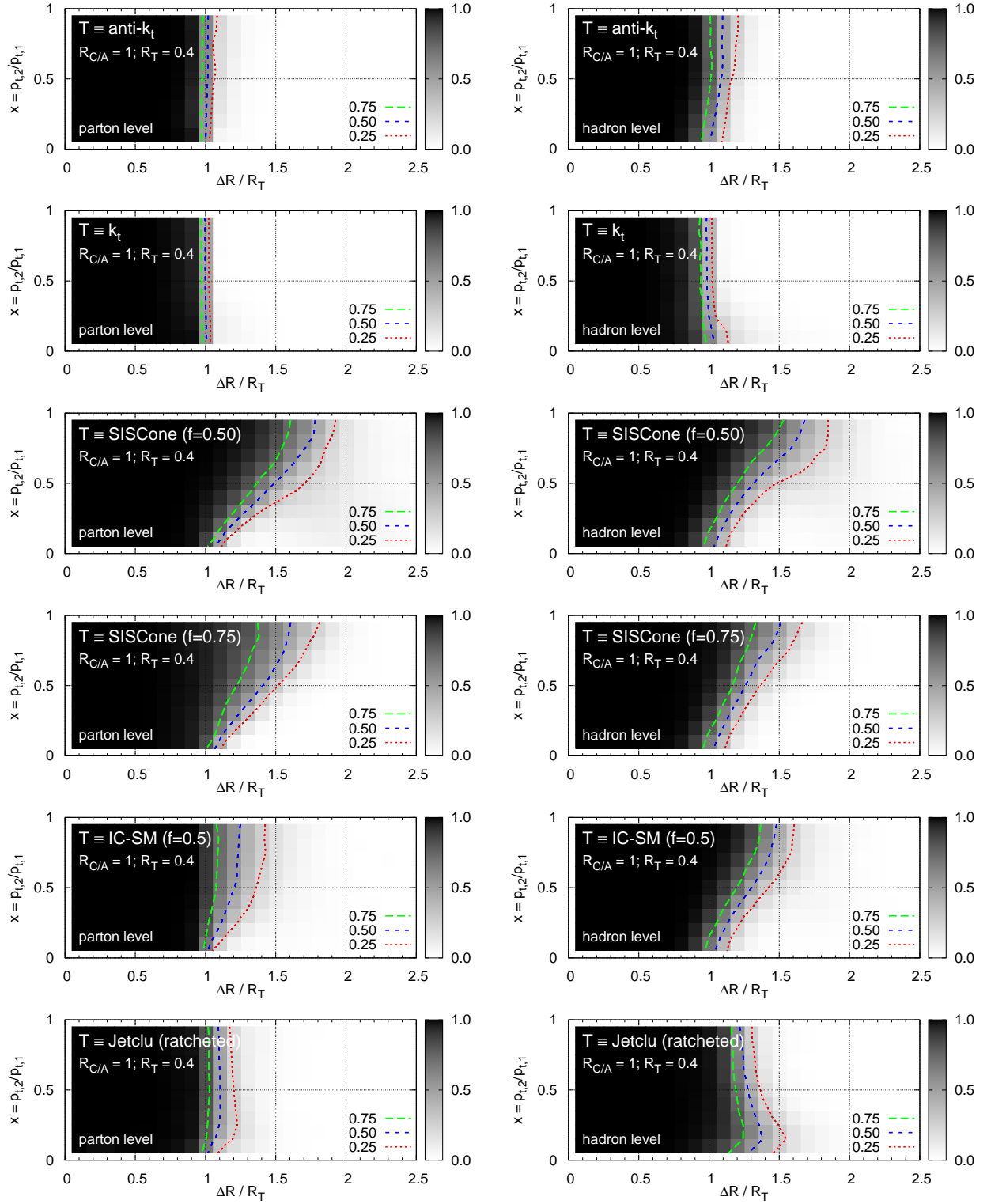


**Figure 12:** Shade/contour plot of the probability for two C/A subjects to each have at least 50% (blue contour; 25% and 75%: red, green contours) of their transverse momentum within a single test-algorithm (T) jet. Shown based on a sample of dijet events simulated with Herwig 6.5 at parton-level and at hadron-level (with Herwig’s default soft UE), using all C/A jets with  $p_t > 50$  GeV. Carried out for Tevatron Run II conditions,  $p\bar{p}$  at  $\sqrt{s} = 1.96$  TeV.



and the parton distribution functions. NLO calculations are perhaps even blacker boxes than Monte Carlo generators, on the other hand they do have the advantage of giving predictions of well-defined precision; however, one loses all relation to the intermediate (ill-defined) “parton” (this holds also for tools like MC@NLO [33] and POWHEG [34]).

Some insight can be obtained from analytical NLO calculations of jet cross sections, such as [102, 103, 104, 105, 106]. A feature that is common to them is that at the first non-trivial order, cross sections acquire a  $\ln R$  dependence in the small- $R$  limit. The small- $R$  limit is one case where one *can* say something meaningful the relation between a jet’s  $p_t$  and that of the original parton (another is the threshold limit, for example [107, 108, 109, 110, 106]), because the emitting parton decouples from its environment, a consequence of angular ordering. Working in a collinear approximation and considering an initial quark, with a gluon emission matrix element proportional to the real  $P_{qq}(z)$  splitting function ( $P_{qq}(z) = C_F(1+z^2)/(1-z)$ ), one can simply write the average difference  $\delta p_t = p_{t,\text{jet}} - p_{t,\text{quark}}$  as

$$\langle \delta p_t \rangle_{\text{pert}} = \int \frac{d\theta^2}{\theta^2} \int dz \underbrace{p_t(\max[z, 1-z] - 1)}_{\delta p_t} \frac{\alpha_s(\theta(1-z)p_t)}{2\pi} P_{qq}(z) \Theta(\theta - f_{\text{alg}}(z)R), \quad (25)$$

where one integrates over the angle  $\theta$  between the quark and an emitted gluon and over the momentum fraction  $z$  that is kept by the quark, weighting the matrix element with the loss of momentum from the leading jet,  $p_t(\max[z, 1-z] - 1)$ , when the gluon and quark form two separate jets,  $\theta > f_{\text{alg}}(z)R$  (throughout this section,  $\theta$  is to be understood as a boost-invariant angle,  $\theta \equiv \Delta R_{qg}$ ). The quantity  $f_{\text{alg}}(z)$  reflect the algorithm’s reach, cf. eqs. (22,24) and is given by

$$f(z) = \begin{cases} 1 & k_t, \text{ C/A, anti-}k_t \\ 1 + \min(\frac{z}{1-z}, \frac{1-z}{z}) & \text{SISCone} \end{cases} \quad (26)$$

Carrying out the integration in a fixed-coupling approximation gives

$$\frac{\langle \delta p_t \rangle_{\text{pert}}}{p_t} = \frac{\alpha_s}{\pi} L_i \ln R + \mathcal{O}(\alpha_s), \quad R \ll 1, \quad (27)$$

with  $L_i$  a coefficient that depends on whether it is a quark or a gluon that is the initiating parton (cf. [111]):

$$L_q = C_F \left( 2 \ln 2 - \frac{3}{8} \right) \simeq 1.01 C_F, \quad (28a)$$

$$L_g = C_A \left( 2 \ln 2 - \frac{43}{96} \right) + n_f T_R \frac{7}{48} \simeq 0.94 C_A + 0.15 T_R n_f, \quad (28b)$$

One notes that for small  $R$  the result of eq. (27) is negative. The unspecified pure  $\mathcal{O}(\alpha_s)$  term reflects the result’s dependence on the large-angle environment. It can be defined

unambiguously only in the threshold limit. Neglecting it, one comes to the conclusion that with  $R = 0.4$ , a quark-induced jet has, on average, a  $p_t$  that is about 4 – 5% smaller than the initiating parton, while a gluon jet's  $p_t$  is 8 – 10% smaller.

One can also evaluate the small- $R$  limit of the average difference between the  $p_t$  of a SISCone jet and (say) a  $k_t$  jet (again following [111])

$$\frac{\langle \delta p_t^{\text{SISCone}} \rangle_{\text{pert}} - \langle \delta p_t^{k_t} \rangle_{\text{pert}}}{p_t} = \frac{\alpha_s}{\pi} K_i \quad (29)$$

with

$$K_q = \left( -\frac{15}{16} + \frac{9}{8} \ln 2 + \ln^2 2 \right) C_F \simeq 0.323 C_F, \quad (30a)$$

$$K_g = \left( -\frac{1321}{1152} + \frac{133}{96} \ln 2 + \ln^2 2 \right) C_A + \left( \frac{241}{576} - \frac{25}{48} \ln 2 \right) n_f T_R \simeq 0.294 C_A + 0.057 n_f T_R. \quad (30b)$$

Numerically,  $K_i \sim 0.3 L_i$ , or equivalently the average behaviour of SISCone and the  $k_t$  (and related) algorithms are similar perturbatively when  $\ln R_{k_t} \simeq 0.3 + \ln R_{\text{SISCone}}$ , that is  $R_{k_t} \simeq 1.35 R_{\text{SISCone}}$ . This feature was originally observed for a generic cone algorithm in [13].

#### 4.2.2 Jet mass

Partons (except for heavy quarks) are essentially massless. Jets, in particular those with significant substructure, are not. Jet masses are interesting in part because hadronic decays of very high- $p_t$  top quarks and electroweak bosons will be collimated by the Lorentz boost factor and so form a single jet, whose invariant mass might provide a means to identify the origin of the jet (cf. section 5.3).

The simplest quantity to examine is the mean squared invariant mass of a jet. This was studied in a hadron-collider context in [6] and it was pointed out that to first non-trivial order,

$$\langle M^2 \rangle \simeq C \cdot \frac{\alpha_s}{\pi} p_t^2 R^2, \quad (31)$$

where  $C$  is a coefficient that depends on the relative fraction of quarks and gluons and on the type of jet algorithm.<sup>21</sup> This is easily derived in the small- $R$  limit, e.g. for a quark-induced jet:

$$\langle M^2 \rangle_{\text{pert}} \simeq \int \frac{d\theta^2}{\theta^2} \int dz \cdot \underbrace{p_t^2 z(1-z)\theta^2}_{M^2} \cdot \frac{\alpha_s(\theta(1-z)p_t)}{2\pi} P_{qq}(z) \Theta(f_{\text{alg}}(z)R - \theta), \quad (32)$$

---

<sup>21</sup>Results for jet masses at  $\mathcal{O}(\alpha_s)$  are sometimes quoted as being NLO. It would be more accurate to state that they are LO results, since  $\mathcal{O}(\alpha_s)$  is the first order at which the mass is non-zero. True NLO results would go up to  $\mathcal{O}(\alpha_s^2)$ . Jet masses can be calculated to NLO in dijet events using the 3-jet NLO component of a program like NLOJET++ [29].

In a fixed-coupling approximation, the results can be summarised as

$$C_q^{k_t} = \frac{3}{8}C_F \quad C_g^{k_t} = \frac{7}{20}C_A + \frac{1}{20}n_f T_R, \quad (33)$$

for  $k_t$ -like algorithms and

$$C_q^{\text{SIS}} = C_F \left( \frac{7}{4} - \frac{3}{2} \ln 2 \right) \simeq 0.71 C_F, \quad (34a)$$

$$C_g^{\text{SIS}} = C_A \left( \frac{49}{24} - 2 \ln 2 \right) + n_f T_R \left( \ln 2 - \frac{7}{12} \right) \simeq 0.66 C_A + 0.11 n_f T_R, \quad (34b)$$

for SIScone type algorithms (consistent with the observation that  $k_t$  and SIScone type algorithms behave similarly for  $R_{k_t} \simeq 1.35 R_{\text{SIScone}}$ ). These results coincide roughly with the rule of thumb given in [6] that to within 25%,  $\sqrt{\langle M^2 \rangle} \simeq 0.2 R p_t$ , with the exact value depending on the mix of quarks and gluons, and subject also to finite- $R$  effects as well as threshold modifications for high jet transverse momenta. Ref. [6] also emphasises that eqs. (34) will be subject to significant higher-order corrections, associated with the fact that SIScone's effective clustering reach is somewhat smaller for  $z \simeq 1/2$  than the two-parton reach  $f(z = 1/2) \simeq 2$ , cf. fig. 12.

When using jet masses for tagging hadronically-decaying boosted heavy objects, it is also of interest to know the distribution of the jet mass. At leading order,  $d\sigma/dM^2$  diverges with a logarithmic enhancement  $\sim \frac{\alpha_s}{M^2} \ln \frac{R^2 p_t^2}{M^2}$  for small masses (cf. the analytical result in [112]). Higher order terms are enhanced by further powers of  $\ln R p_t/M$  and can in principle be resummed. Analytical results exist however only for certain specific cases in  $e^+e^-$  [113, 114, 115] and DIS [116] and have not been extended to hadron-collider jets, in part because of issues such as the non-trivial process dependence [117, 118] and jet-algorithm dependence [119, 120] of soft logarithms associated with delimited (“non-global” [115, 121, 122]) regions of phase-space.

### 4.2.3 Other properties

Many other properties of jets can be predicted perturbatively. Among them one may mention the scale associated with subjets within a jet [11, 49, 123], multiplicities of subjets [124, 125] and of particles (see e.g. [126] and references therein) and jet shapes [23] (radial moments and the fraction of energy that is within a certain central core of the jet). As well as providing important handles on our understanding of the QCD dynamics within jets, these observables can also be useful for example in discriminating quark and gluon jets. One such application is given in [53].

## 4.3 Hadronisation

The properties of jets are affected not just by perturbative radiation, but also by low- $p_t$ , non-perturbative effects. It is useful to divide such effects into two classes: hadronisation

and the underlying event. Hadronisation corresponds to the transition between partons and hadrons, and occurs in all high-energy QCD processes ( $e^+e^-$ , DIS and  $pp$ ). The underlying event (UE) consists of the multiple low- $p_t$  interactions that occur between the two hadron remnants in a  $pp$  or a resolved  $\gamma p$  collision. Physically, in a  $pp$  collision, hadronisation and the UE cannot be unambiguously separated (the question of what hadronises depends on what has interacted). Nevertheless it is useful to consider them separately, because they affect jets in rather different ways. Hadronisation is discussed here, and the UE in section 4.4.

With current techniques, the impact of hadronisation cannot be calculated (or even easily defined) from first principles. However, in the mid 1990's, methods were developed [127, 128, 129, 130, 131, 132] (reviewed in [133]) that allowed one to predict the main features of hadronisation, based on ambiguities that arise in perturbative calculations related to the Landau pole.

A somewhat oversimplified statement of the idea is that if a perturbative calculation involves an integral over  $\alpha_s(\mu)$ , then one can estimate the size of the non-perturbative contribution by replacing  $\alpha_s(\mu)$  with a purely non-perturbative piece  $\alpha_s^{\text{NP}}(\mu) = \Lambda\delta(\mu - \Lambda)$  where  $\Lambda$  is commensurate with the Landau scale. So, for example, to estimate the non-perturbative correction to a quark jet's transverse momentum in the small- $R$  limit one takes eq. (25) and writes

$$\langle \delta p_t \rangle_{\text{NP}} \sim p_t \int \frac{d\theta^2}{\theta^2} \int dz (\max[z, 1-z] - 1) \frac{\alpha_s^{\text{NP}}(\theta(1-z)p_t)}{2\pi} P_{qq}(z) \Theta(\theta - f_{\text{alg}}(z)R), \quad (35a)$$

$$\sim p_t \int_{R^2} \frac{d\theta^2}{\theta^2} \int dz (z-1) \frac{\alpha_s^{\text{NP}}(\theta(1-z)p_t)}{2\pi} \frac{2C_F}{1-z}, \quad (35b)$$

$$\sim -\frac{2C_F\Lambda}{\pi R}, \quad (35c)$$

where in the second line one makes use of the knowledge that the  $\delta$ -function will select  $1-z = \Lambda/(\theta p_t) \ll R$ . For gluon jets the result is the same except for the replacement  $C_F \rightarrow C_A$ . A crucial idea in calculations such as eqs. (35) is that one can apply the same procedure to a wide range of observables and the same value of  $\Lambda$  should hold for each.<sup>22</sup> This is known as “universality”. Universality has been investigated in some detail for event shapes in  $e^+e^-$  and DIS collisions and there is some debate as to just how well it works (e.g. [134] as compared to [135]). However for the purpose of understanding the essentials of the hadronisation of jets it is probably an adequate assumption, and one can take  $\Lambda \simeq 0.6$  GeV.

The basic result that hadronisation removes transverse-momentum  $\mathcal{O}(\Lambda/R)$  from a jet was presented in [127] (and could be deduced from the results of [23]; hadronisation as

---

<sup>22</sup>As long as they all share the same  $p_t$ -dependence in the infrared — a less oversimplified formulation of the idea in eq. (35) is that observables with the same IR  $p_t$ -dependence are all sensitive to a common moment of the coupling in the infrared.

a shift in  $p_t$  was also discussed in [136]). Aside from the quark/gluon jet difference it is a process-independent result, as long as  $R$  is much smaller than the angle between jets. It seems, however, that this result had largely been forgotten until the advent of a more recent calculation [111], which goes beyond the small  $R$  limit (in a threshold approximation for dijet production). As an example, the result for the case of the  $qq' \rightarrow qq'$  subprocess of dijet production is

$$\langle \delta p_t \rangle_{\text{NP}}^{qq' \rightarrow qq'} = \frac{\Lambda}{\pi} \left[ -\frac{2}{R} C_F + \frac{1}{8} R \left( 5C_F - \frac{9}{N_c} \right) + \mathcal{O}(R^2) \right]. \quad (36)$$

A feature of eq. (36) is that the first correction to the  $1/R$  term is fairly small even for  $R = 1$  (less than 20%). Consequently for most purposes it is adequate to take just the  $1/R$  piece. This is what is done in fig. 13, whose lower set of curves in each quadrant compares the hadronisation correction as deduced from Herwig (solid lines) and from Pythia (dashed lines) with the  $1/R$  part of the analytical expectation given above (dot-dashed lines). Generally speaking the agreement is good, even in the large- $R$  region where the  $1/R$  approximation might be expected to break down.

To obtain a closer relation to studies of hadronisation for  $e^+e^-$  and DIS event shapes (for a review see e.g. [138]), one may replace

$$\frac{\Lambda}{\pi} \rightarrow \frac{2}{\pi} \mathcal{M} \mathcal{A}(\mu_I). \quad (37)$$

Here  $\mathcal{A}(\mu_I)$  is defined as the integral over a non-perturbative contribution to  $\alpha_s$ ,  $\delta\alpha_s$ , up to some infrared matching scale  $\mu_I$  (usually 2 GeV),  $\mathcal{A}(\mu_I) = \frac{1}{\pi} \int_0^{\mu_I} d\kappa_t \delta\alpha_s(\kappa_t)$ . Following [128], it is often written in terms of yet another parameter  $\alpha_0(\mu_I)$ , the integral of the full coupling in the infrared  $\alpha_0(\mu_I) = \int_0^{\mu_I} d\kappa \alpha_s(\kappa)$ , via

$$\mathcal{A}(\mu_I) = \frac{1}{\pi} \mu_I \left[ \alpha_0(\mu_I) - \alpha_s(p_t) - \frac{\beta_0}{2\pi} \left( \ln \frac{p_t}{\mu_I} + \frac{K}{\beta_0} + 1 \right) \alpha_s^2(p_t) \right], \quad (38)$$

where  $K = C_A \left( \frac{67}{18} - \frac{\pi^2}{6} \right) - \frac{5}{9} n_f$ , and the subtracted terms in eq. (38) remove double counting with contributions already included in NLO calculations. Fits to data in DIS and  $e^+e^-$  usually give  $\alpha_0(2 \text{ GeV}) \simeq 0.5$ .

The factor  $\mathcal{M}$  in eq. (37) is known as the Milan factor [139, 140, 141, 142, 143]. It accounts for the corrections that arise when one considers two non-perturbative “gluons” rather than a single one. For all known event shapes,  $\mathcal{M}$  has been calculated to be  $\mathcal{M} = 1.49$  — this “universality” of the Milan factor is due to the fact that event-shape observables are effectively linear in the momenta of soft gluons [140]. For jets it had been argued that only the anti- $k_t$  algorithm satisfied this linearity property [17]. This was recently confirmed in an explicit calculation by Dasgupta and Delenda [144], who showed that the  $k_t$  algorithm instead has  $\mathcal{M}_{k_t} = 1.01$ . This smaller value is consistent with the somewhat reduced hadronisation corrections observed for the  $k_t$  algorithm compared to anti- $k_t$  in fig. 13, though a detailed quantitative comparison has not yet been performed. Future

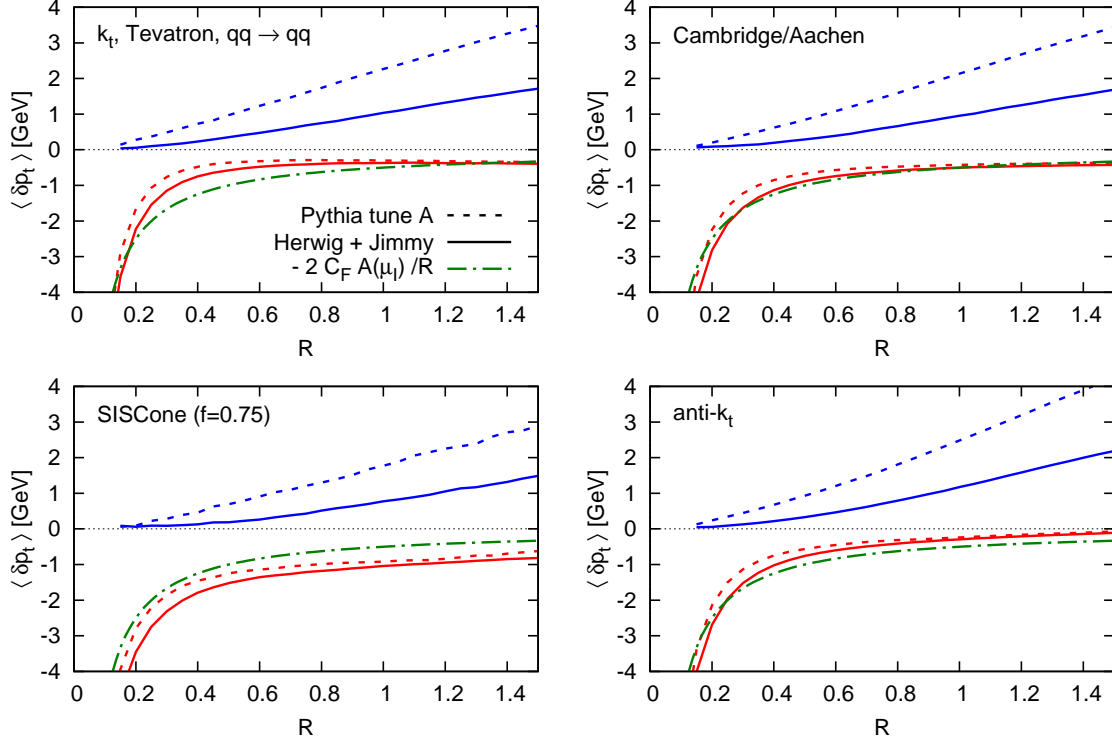


**Figure 13:** Modification of the  $p_t$  of jets due to the underlying event (upper curves in each plot) and hadronisation (lower curves), for  $qq \rightarrow qq$  scattering at the Tevatron Run II ( $p\bar{p}$ ,  $\sqrt{s} = 1.96$  TeV), comparing Pythia 6.412 [79] (tune A, dashed lines) and Herwig 6.510 [80] with Jimmy 4.3 [137] (solid lines). In the case of hadronisation, the Monte Carlo outputs are compared to the  $1/R$  part of the analytical result, eq. (36) (dot-dashed lines). Dijet events are selected containing an underlying  $qq \rightarrow qq$  scattering, and with the requirement that at parton-shower level the hardest jet has  $55 \text{ GeV} < p_t < 70 \text{ GeV}$ . The non-perturbative corrections shown correspond to the average for the two hardest jets. Taken from [111].

calculations of the Milan factor for C/A and SISCone will hopefully also fit in with the pattern of slight differences that are observed in fig. 13 with respect to the algorithm-independent behaviour that is given by eqs. (35c,36).

A point emphasised in [136] is that even if the non-perturbative modification of a jet's  $p_t$  is rather modest,  $\mathcal{O}(1 \text{ GeV})$ , it can nevertheless have a significant impact on steeply falling cross sections. Given a jet  $p_t$  spectrum that falls as  $p_t^{-n}$ , the full result for the jet spectrum can be expressed in terms of the perturbative spectrum and the non-perturbative shift as

$$\frac{d\sigma_{\text{full}}}{dp_t}(p_t) \rightarrow \frac{d\sigma_{\text{PT}}}{dp_t}(p_t - \langle \delta p_t \rangle_{\text{NP}}) \simeq \frac{d\sigma}{dp_t}(p_t) \cdot \left( 1 - n \frac{\langle \delta p_t \rangle_{\text{NP}}}{p_t} \right). \quad (39)$$

Thus for typical values of  $n$  in an inclusive-jet spectrum, a 2% change in  $p_t$  can lead to a 10 – 15% change in the cross section (this observation holds also for  $p_t$  shifts due to the underlying event, which are discussed below).

A final point is that the above methods can also be used to calculate the non-perturbative corrections to the squared jet mass,

$$\langle \delta M^2 \rangle_{\text{NP}} \simeq \frac{2C_F}{\pi} \Lambda p_t (R + \mathcal{O}(R^3)) \equiv \frac{4C_F}{\pi} \mathcal{MA}(\mu_I) p_t (R + \mathcal{O}(R^3)), \quad (40)$$

where the  $R^3$  terms have small coefficients [111]. Note that for jet algorithms other than anti- $k_t$ , the Milan factors for  $\langle \delta p_t \rangle_{\text{NP}}$  and  $\langle \delta M^2 \rangle_{\text{NP}}$  will not be the same.

#### 4.4 UE, pileup, jet areas

While the process of hadronisation may well be reasonably universal between  $e^+e^-$ , DIS and  $pp$  collisions, the latter have the additional feature of the “underlying event” (UE), which can be thought of as the semi- or non-perturbative interactions that occur between hadron remnants in a  $pp$  collision. Our understanding of the UE is somewhat less developed than that of hadronisation. One way that one can model it is by saying that it induces an extra amount of transverse momentum per unit rapidity,  $\Lambda_{\text{UE}}$ .<sup>23</sup> In this case a jet should receive a position contribution to its  $p_t$  from the UE that is proportional to the region of the rapidity-azimuth region that it covers, i.e.  $\sim R^2$ :

$$\langle \delta p_t \rangle_{\text{UE}} \simeq \Lambda_{\text{UE}} R J_1(R) = \Lambda_{\text{UE}} \left( \frac{R^2}{2} - \frac{R^4}{8} + \dots \right). \quad (41)$$

where terms at  $R^4$  and beyond [111] hold for the a 4-vector ( $E$ ) recombination scheme. The corresponding formula for the change to the squared jet-mass is

$$\langle \delta M^2 \rangle_{\text{UE}} \simeq \Lambda_{\text{UE}} p_t \left( \frac{R^4}{4} + \frac{R^8}{4608} + \dots \right). \quad (42)$$

---

<sup>23</sup>Later we will talk of transverse momentum  $\rho$  per unit area on the rapidity-azimuth plane;  $\Lambda_{\text{UE}} = 2\pi\rho_{\text{UE}}$ .

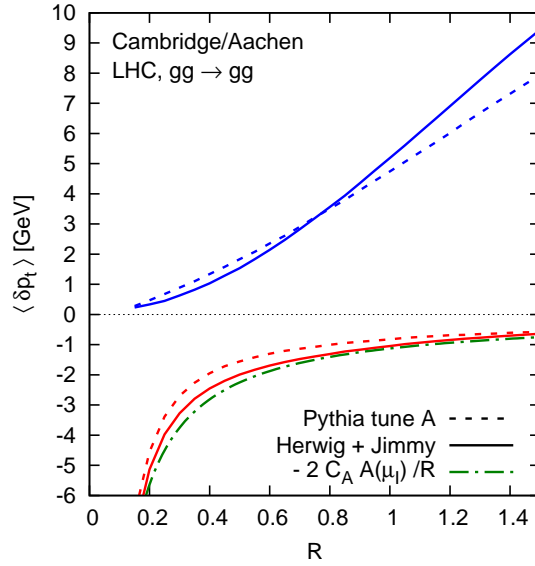


**Figure 14:** Similar to Fig. 13, but for just one algorithm, at the LHC ( $pp$ ,  $\sqrt{s} = 14$  TeV) rather than the Tevatron, and for  $gg \rightarrow gg$  collisions (rather than  $qq \rightarrow qq$ ). Taken from [111].

In fig. 13, the upper curves represent the UE contributions to the  $p_t$  of Tevatron jets, as determined from the UE models in Pythia [79] (tune A [36]) and Jimmy [137] (with the ATLAS tune [36]). Three features are worth commenting on: (a) the curves agree with a rough  $R^2$  dependence, (b) the two models disagree by a factor of two even though they have both been tuned to Tevatron data and (c) the value that one extracts for  $\Lambda_{\text{UE}}$ , in the range 2 – 4 GeV, is quite a bit larger than the  $p_t$  per unit rapidity that would be generated by normal hadronisation for a quark or gluon dipole stretched between the two beams (respectively 0.5 GeV and 1 GeV).

For the LHC, the models predict an even larger contribution from the UE, cf. fig. 14 from which one deduces  $\Lambda_{\text{UE}} \sim 10$  GeV, and for a large range of  $R$  it dominates over hadronisation. Furthermore pileup (multiple  $pp$  collisions in a given beam crossing) is expected to add up to an extra 100 GeV of soft “junk” per unit rapidity.

All of this implies that it is important to understand in more detail how jets are affected by “low- $p_t$ ” noise that is roughly uniformly distributed in rapidity. Two things can happen: firstly, the soft junk can end up in the jet — to study this it is useful to refer to the “jet area” [21], a measure of the extent of the region in rapidity and azimuth over which a jet captures UE or pileup; secondly, the presence of the UE (and pileup) can modify the way non-UE particles get clustered into jets, a process named back-reaction in [21].

#### 4.4.1 Jet areas

A jet’s “area” is a way of measuring its susceptibility to contamination from soft radiation. Two definitions were proposed for it in [21] and the results quoted here are all taken from



there. The *passive* area is a measure of the jet’s susceptibility to pointlike radiation. One introduces a “ghost” particle,  $g(y, \phi)$  with infinitely low transverse momentum and situated at some rapidity and azimuth  $y, \phi$ , and then defines the area for jet  $J$  in terms of the region in  $y, \phi$  over which the ghost is clustered with the jet:

$$a(J) \equiv \int dy d\phi f(g(y, \phi), J) \quad f(g, J) = \begin{cases} 1 & g \in J \\ 0 & g \notin J \end{cases} . \quad (43)$$

For an infrared safe algorithm  $J$  itself is of course unaffected by the addition of the infinitely soft particle  $g$ . If  $J$  consists of a single (hard) particle then its passive area is  $\pi R^2$  for all algorithms.

An alternative definition of area is the *active* area, which measures a jet’s susceptibility to diffuse radiation. Here one imagines a large number of very soft ghost particles, uniformly distributed in rapidity and azimuth (with some optional randomness). One can define a jet’s active area for a given ensemble  $\{g_i\}$  of ghost particles,

$$A(J | \{g_i\}) = \frac{\mathcal{N}_g(J)}{\nu_g} . \quad (44)$$

where  $\mathcal{N}_g(J)$  is the number that end up in the jet and  $\nu_g$  their number density in  $y, \phi$ . One then often considers the average active area, an average over many ghost ensembles

$$A(J) = \lim_{\nu_g \rightarrow \infty} \langle A(J | \{g_i\}) \rangle_g , \quad (45)$$

taken in the limit of many ghost particles (with fixed infinitesimal total  $p_t$  per unit area).<sup>24</sup>

Given that one usually imagines the UE as being fairly diffuse, it is the active area that is probably the most natural measure of sensitivity to the UE. However, there are two reasons why it is useful to consider both passive and active areas. Firstly, the UE is actually somewhere in between diffuse and pointlike and a full understanding of UE contamination benefits from considering both limits. Secondly, of the two, the passive area is often simpler to treat analytically.

Let’s illustrate these points for the case of a jet that has just one, hard particle (1PJ). As mentioned above, the passive area is  $\pi R^2$ . This statement holds for all jet algorithms. The average active area and its standard deviation over ghost ensembles are given in table 4. For one algorithm, anti- $k_t$ , the active area is identical to the passive area and  $A(J | \{g_i\})$  is independent of the particular ghost ensemble. This can be seen as advantageous, insofar as it implies that the contamination of an anti- $k_t$  jet will be independent of the detailed structure of the UE.

---

<sup>24</sup> These two areas are strictly speaking both “scalar” areas. Passive and active areas also come in “4-vector” variants, which take into account the ghosts’ full impact on a jet’s 4-vector. Though useful for subtracting pileup and other noise, most of their features are quite similar to those of scalar areas, so we shall not discuss them separately in this section.

Algorithm	$k_t$	C/A	SISCone	anti- $k_t$
$\frac{A(1PJ) \pm \Sigma(1PJ)}{\pi R^2}$	$0.812 \pm 0.277$	$0.814 \pm 0.261$	$\frac{1}{4} \pm 0$	$1 \pm 0$
$\frac{A(GJ) \pm \Sigma(GJ)}{\pi R^2}$	$0.554 \pm 0.174$	$0.551 \pm 0.176$	—	—

**Table 4:** the average active area  $A(1PJ)$ , eq. (45), for an isolated one-particle jet in various jet algorithms and its standard deviation  $\Sigma(1PJ)$  over ghost ensembles. Results are also given for the area of jets that are purely composed of ghosts (GJ), in the cases where this makes sense (in SISCone the result depends critically on the distribution of ghosts, while for anti- $k_t$  the distribution of ghost-jet areas has two peaks, one at 0, the other at  $\pi R^2$ ).

SISCone also has the property that its active area is independent of the ghost ensemble, but the actual value is much smaller than for the passive area (a consequence of the split-merge step which eats away from the main jet). This is good insofar as it means less overall sensitivity to noise, but bad because the exact amount of contamination will depend on the details of just how pointlike the UE is (a feature that therefore needs to be well tuned in Monte Carlo programs).

The  $k_t$  and C/A algorithms are unlike the other two in that  $A(J | \{g_i\})$  depends significantly on the exact set of ghosts, as indicated by the standard deviations in table 4, which are about one third of the average area. The non-zero standard deviation arises because ghosts tend to cluster between themselves before clustering with the hard particle, and slight shifts in the layout of the ghosts lead to significant differences in the final clustering. This implies an extra source of fluctuations from UE contamination: one has not only the intrinsic fluctuations in the amount of  $p_t$  in a given event's UE, but also a fluctuation in how much of the UE the jet actually captures. The consequent (moderate) worsening of the kinematic resolution of the jets seems to be an inevitable feature of jet algorithms with a QCD-motivated hierarchical clustering sequence: the algorithm is trying to assign meaningful QCD substructure to the jet, and the absence of such substructure in the UE induces a degree of randomness in the outcome of the clustering (this is related also to the irregularity of the jet boundaries in fig. 6).

The above results hold for 1-particle jets (1PJ). Real jets are more complex because QCD branching gives them substructure. To a first approximation, one can examine what happens if one adds a single soft gluon at an angle  $\theta$  with respect to the jet axis. This gives a modified jet area, e.g.  $a_{JA,R}(\theta)$  in the passive case, illustrated in fig. 15. After integration over the (soft, collinear) QCD branching matrix element one obtains

$$\langle a_{JA,R} \rangle = \pi R^2 + d_{JA,R} \frac{C_1}{\pi b_0} \ln \frac{\alpha_s(Q_0)}{\alpha_s(Rp_{tJ})}, \quad (46)$$

where the anomalous dimension (i.e. the  $p_t$ -dependent rightmost term) stems from the

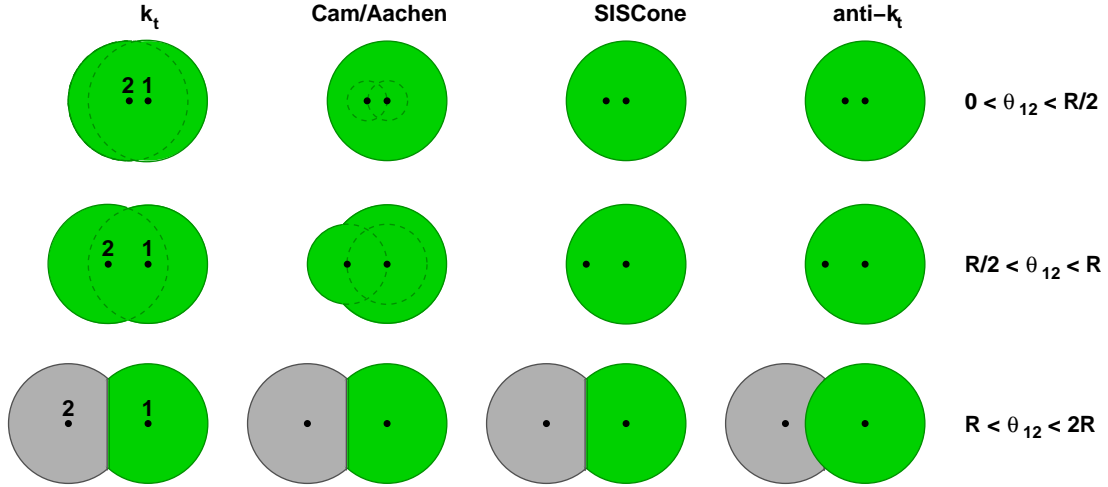


**Figure 15:** Schematic representation of the passive area of a jet containing one hard particle “1” and a softer one “2”,  $a_{JA,R}(\theta_{12})$ , for various separations between them and for the usual 4 jet algorithms. Different shadings represent distinct jets. Figure adapted from [21].

	$a(1PJ)$	$A(1PJ)$	$\sigma(1PJ)$	$\Sigma(1PJ)$	$d$	$D$	$s$	$S$
$k_t$	1	0.81	0	0.28	0.56	0.52	0.45	0.41
Cam/Aachen	1	0.81	0	0.26	0.08	0.08	0.24	0.19
SIScone	1	1/4	0	0	-0.06	0.12	0.09	0.07
anti- $k_t$	1	1	0	0	0	0	0	0

**Table 5:** A summary of main area results for our four jet algorithms: the passive ( $a$ ) and active ( $A$ ) areas for 1-particle jets (1PJ), the magnitude of the passive/active area fluctuations ( $\sigma$ ,  $\Sigma$ ), followed by the coefficients of the respective anomalous dimensions ( $d$ ,  $D$ ;  $s$ ,  $S$ ), in the presence of perturbative QCD radiation. All results are normalised to  $\pi R^2$ , and rounded to two decimal figures. For algorithms other than anti- $k_t$ , active-area results hold only in the small- $R$  limit, though finite- $R$  corrections are small.

integration over the energy of the soft gluon, and its coefficient is given by

$$d_{JA,R} = \int_0^{2R} \frac{d\theta}{\theta} (a_{JA,R}(\theta) - \pi R^2). \quad (47)$$

In eq. (46)  $b_0 = \frac{11C_A - 2n_f}{12\pi}$  and  $C_1$  is the colour factor of the hard particle in the jet ( $C_F$  or  $C_A$ ). The scale  $Q_0$  is a non-perturbative cutoff scale, introduced by hand, and which is necessary because jet areas are not IR safe (except in the case of anti- $k_t$ ). The physically natural value for  $Q_0$  will depend on the characteristics of the UE/pileup: given an amount of transverse momentum  $\rho$  per unit area, one expects  $Q_0$  to be  $\mathcal{O}(\rho R^3)$ .<sup>25</sup>

Formulae analogous to eqs. (46,47) hold for the active area ( $\pi R^2 \rightarrow A(1PJ)$ ,  $d \rightarrow D$ ),

<sup>25</sup>That is: a transverse momentum with respect to the beam  $\mathcal{O}(\rho R^2)$ , which translates to a transverse momentum with respect to the jet  $\mathcal{O}(\rho R^3)$ , it being the latter that corresponds to  $Q_0$  in eqs. (46) etc.

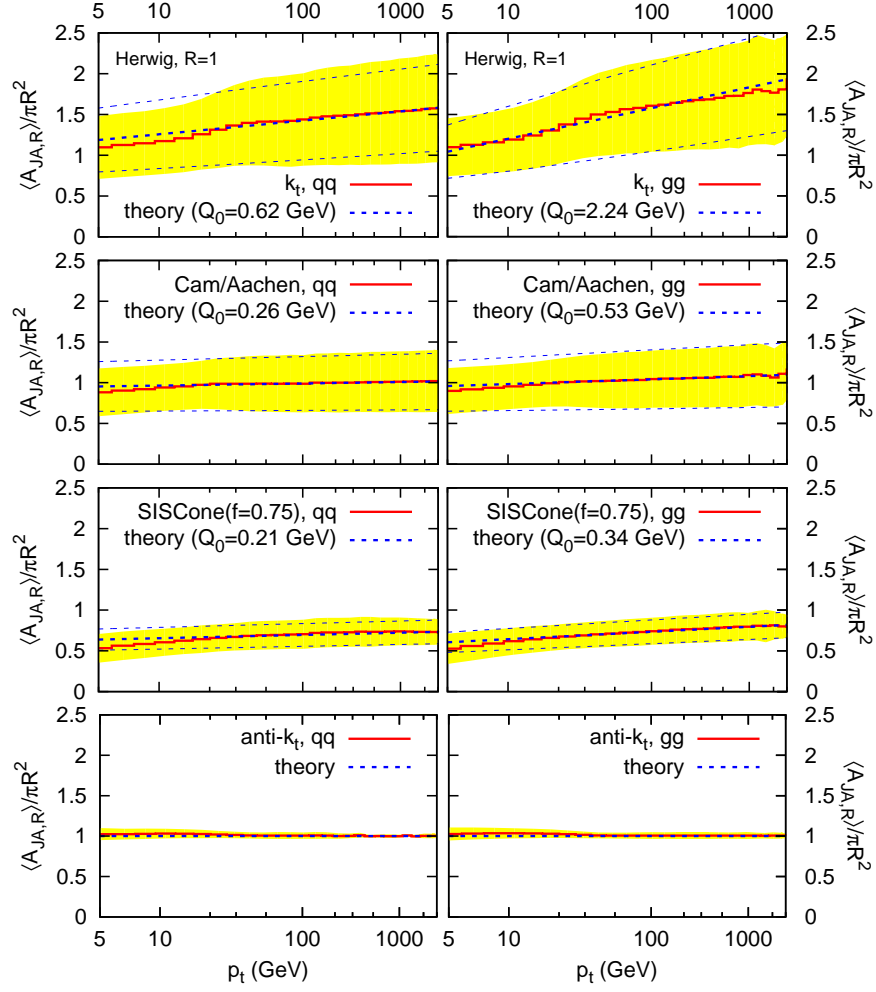


**Figure 16:** Average active area and standard deviation (solid lines and band) in simulated Herwig 6.5 events (default UE) compared to analytical expectations (dashed lines) with a fitted  $Q_0$  value; shown separately for 4 algorithms and for  $qq \rightarrow qq$  and  $gg \rightarrow gg$  events. Adapted from [21, 17].

and also for the standard deviations  $\sigma_{\text{JA},R}$  of the passive area,

$$\langle \sigma_{\text{JA},R}^2 \rangle = s_{\text{JA},R}^2 \frac{C_1}{\pi b_0} \ln \frac{\alpha_s(Q_0)}{\alpha_s(Rp_{t1})}, \quad s_{\text{JA},R}^2 = \int_0^{2R} \frac{d\theta}{\theta} (a_{\text{JA},R}(\theta) - \pi R^2)^2 \quad (48)$$

and the active area

$$\langle \Sigma_{\text{JA},R}^2 \rangle = \Sigma_{\text{JA},R}^2(1\text{PJ}) + S_{\text{JA},R}^2 \frac{C_1}{\pi b_0} \ln \frac{\alpha_s(Q_0)}{\alpha_s(Rp_{t1})}. \quad (49)$$

The various coefficients are all summarised in table 5, while in fig. 16 the resulting predictions are compared to jet areas measured in Herwig Monte Carlo simulations (with  $Q_0$  fitted on a case-by-case basis). One sees how  $k_t$  has a fairly large area, large fluctuations and strong  $p_t$  dependence, C/A an area  $\sim \pi R^2$  with moderate fluctuations and little  $p_t$  dependence, SISCone an area smaller than  $\pi R^2$  (but still larger than  $\pi R^2/4$ ), small fluctuations and moderate  $p_t$  dependence and, finally, anti- $k_t$  an area very close to  $\pi R^2$ , with almost no fluctuations or  $p_t$  dependence. A corollary of the  $k_t$  algorithm's strong  $p_t$  dependence is that if one increases the UE density  $\rho$ , the jet area will *shrink*, a consequence of the presence of  $\alpha_s(Q_0)$  in eq. (46), with  $Q_0 \sim \rho R^3$ .

A final comment concerns the relation between passive and active areas. They differ in sparse events because there is an ambiguity in how one assigns “empty” parts of the event to the jets — the two kinds of area simply consist of different prescriptions for doing this. In very dense events, where the jet boundaries are well delimited by the event's particles, the passive and active areas become identical (as should any other sensible definition of area).

#### 4.4.2 Back reaction

Suppose you have an event with particles numbered 1–100, and in which numbers 1–10 end up in jet  $a$ . Now immerse that event in a soft background with *finite*  $p_t$ . The background will add its own particles to the jet, but it can alter the behaviour of the clustering with respect to the original particles. So maybe only particles 1–9 would end up in jet  $a$ , or maybe jet  $a$  would additionally contain particle 11. This is back reaction.

The study of back-reaction bears similarities to that of jet areas: in particular one can study it with pointlike noise, or with diffuse noise. The former can be dealt with analytically, whereas the latter is tractable only numerically.

Full details are given in [21], but the basic analytical result is that the average net change in a jet's  $p_t$  due to back-reaction in the presence of diffuse noise has an asymptotic behaviour of the form

$$\langle \Delta p_{t,\text{JA},R}^{BR} \rangle \simeq \mathcal{B}_{\text{JA},R} \rho \cdot \frac{C_1}{\pi b_0} \ln \frac{\alpha_s(\rho R^3)}{\alpha_s(p_{t1} R)} + \mathcal{O}(\alpha_s \rho), \quad (50)$$

where the coefficients are  $\mathcal{B}_{k_t,R} \simeq \mathcal{B}_{\text{C/A},R} \simeq -0.10\pi R^2$  and  $\mathcal{B}_{\text{SISCone},R} = \mathcal{B}_{\text{anti-}k_t,R} = 0$ . In practice, given the small size of the  $\mathcal{B}$  coefficients (and the fact that the  $\frac{C_1}{\pi b_0} \ln \frac{\alpha_s(\rho R^3)}{\alpha_s(p_{t1} R)}$

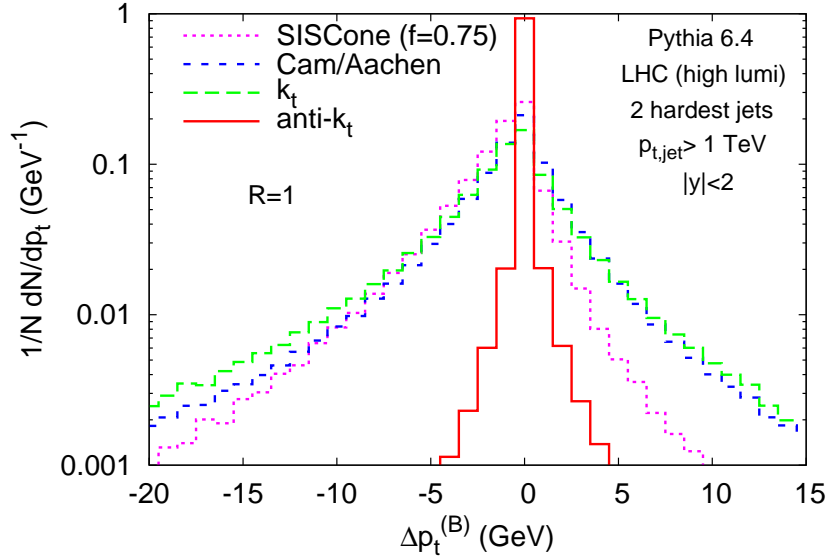


**Figure 17:** The distribution of back-reaction for high- $p_t$  jets ( $p_t > 1$  TeV) immersed in pileup corresponding to high-luminosity LHC running ( $\rho \sim 15$  GeV per unit area). Simulated with Pythia 6.4 and shown for 4 algorithms.

factor is often  $\mathcal{O}(1)$ ), the term of order  $\alpha_s \rho$  is usually as important as the formally leading term. Both terms are generally small compared to the direct contamination of the jet from UE/pileup noise,  $\mathcal{O}(\rho \cdot \pi R^2)$ .

The concrete situation for the various algorithms is illustrated in fig. 17, which shows the distribution of back reaction for a high- $p_t$  jet immersed in pileup ( $\rho \sim 15$  GeV). In about 1% of events one has a back-reaction of order of  $\rho$ , except for anti- $k_t$ , whose back-reaction is far more suppressed. Fig. 17 confirms that back-reaction is a modest effect compared to the direction contamination of a jet from background noise. Essentially it is relevant only when trying to determine a jet's energy to very high precision, or in the presence of extreme noise (as in heavy-ion collisions).

## 4.5 Summary

We have seen a number of results here. Let us summarise them:

- Most jet algorithms will cluster a pair of particles if they are within  $R$  of each other; SISCone reaches out to  $2R$  (somewhat less in real events) if the two particles are of similar hardness.
- At small  $R$ , a jet's  $p_t$  is reduced relative to a parton's by an amount  $\sim \alpha_s p_t \ln 1/R$ . With  $R = 0.4$ , that's of order 5% for a quark, 10% for a gluon. The mean squared jet mass goes as  $\alpha_s R^2 p_t^2$ .

- Hadronisation reduces a quark jet’s  $p_t$  by an amount  $\sim 0.5 \text{ GeV}/R$  at small  $R$  (roughly double this for a gluon jet), with modest differences between algorithms.
- The underlying event and pileup induce contaminations proportional to  $\sim R^2$ . Because the intrinsic energy scale associated with the underlying event ( $p_t$  per unit rapidity of  $10 - 15 \text{ GeV}$  at the LHC) is an order of magnitude larger than that from hadronisation (and pileup is yet another order of magnitude larger), one should devote special effort to understanding different jet algorithms’ susceptibility to them. This can be done via the concept of jet areas. The  $k_t$  algorithm has the largest jet area (with noticeable  $p_t$  dependence and fluctuations), SISCone the smallest, and anti- $k_t$  has the most stable jet area, nearly always  $\pi R^2$ .
- The UE (and pileup) modifies how an event’s original particles get clustered into jets — this is back-reaction. Its impact is an order of magnitude smaller than the direct contamination, but can be relevant for precision studies. It is essentially zero for the anti- $k_t$  algorithm.

The differing impact of various physical effects across algorithms and as a function of  $R$  might seem like a source of considerable complication in jet finding, and in some ways it is. However, it can also be used to our advantage. One example is in studies like top-mass measurements that are in part limited by physics-modelling systematics. If one uses multiple jet definitions with different sensitivities to UE, gluon radiation and hadronisation, and then finds that the final Monte Carlo-corrected top mass is independent of the choice of jet definition, then this provides a powerful cross check of the physics modelling within the Monte Carlo generator. And, in the next section, we shall see how our understanding of jets can help guide the choice of “optimal” jet definitions for various reconstruction tasks.

## 5 Using jets

So far at hadron colliders, jets have mostly been used as fixed objects — universal, if imperfect proxies for partons. Generally, experiments have settled on one or two main jet definitions for nearly all their analyses: for example at CDF the Midpoint algorithms with  $R = 0.7$  for most inclusive-jet studies,<sup>26</sup> and JetClu with  $R = 0.4$  for top-quark physics and for searches.

Such a strategy was probably not too far from optimal at the Tevatron, where most of the physics being looked at is in a modest range of scales, from a few tens of GeV to a few hundred, and pileup is present, but not overwhelming.

The LHC, in contrast, will cover a broader range of scales from a few tens of GeV to a few TeV, events with multiple simultaneous scales will be common (e.g. EW bosons and top quarks with  $p_t \gg m$ ) and pileup will range from almost none to 20 – 30 simultaneous

---

<sup>26</sup>Though in recent years they also studied the  $k_t$  algorithm with three  $R$  values [59, 60], and this probably played a key role in convincing the LHC experiments that the  $k_t$  algorithm is viable.

$pp$  interactions in each bunch crossing. This begs the question: could analyses benefit from more flexible jet-finding?

The work examined below tries to examine this question by concentrating on two characteristic types of analysis — standard mass reconstructions, with attention also to the issue of pileup; and the task of identifying highly boosted massive particles. Our discussion will be restricted to studies at “particle level” (also referred to as hadron level) and won’t go into detector-specific effects. For a discussion of the latter, see for example [145, 99, 2].

## 5.1 Choosing an algorithm and a radius

Which jet algorithm is “best”? This is a widespread question, and a natural follow-on question is “which  $R$  should one use”? This question cannot be answered in isolation. It inevitably goes with the issue of what one wants to use the jet algorithm for.

The most reliable way of answering the question is to carry out a detailed study of the process one is interested in, with many jet algorithms, and many  $R$  values for each. Then one may devise some “quality measure” and establish which algorithm optimises it. This can be a big job (4 algorithms, maybe 10  $R$  values) and is seldom done in a systematic way. In what follows we’ll see how even crude analytical estimates can give guidance on the question, and then examine some Monte Carlo studies.

### 5.1.1 Analytical study

In a QCD measurement like that of the inclusive jet spectrum, one will compare data to a perturbative QCD prediction. At moderate  $p_t$ , the largest ambiguity in the comparison comes from non-perturbative effects (since perturbative effects are calculable to some accuracy), so one might want to choose an algorithm and  $R$  value that minimises hadronisation and UE contributions. One can choose to ignore the relatively modest differences between algorithms, and just take the analytic formulae of sections 4.3, 4.4. From these, one deduces a value of  $R$  that minimises the squared sum of hadronisation and UE pieces [111],

$$R = \sqrt{2} \left( \frac{2C_i \mathcal{MA}(\mu_I)}{\pi \Lambda_{\text{UE}}} \right)^{1/3}, \quad (51)$$

where only the leading  $R$  terms have been used,  $C_i$  is the appropriate colour factor ( $C_F, C_A$ ) for quark/gluon jets, and we have assumed a jet area of  $\pi R^2$  for simplicity. The resulting numerical  $R$  values are given in table 6.<sup>27</sup>

If one uses jets for kinematic reconstruction, the considerations are different: when trying to identify a mass peak, for example, it is of little consolation that one can calculate the perturbative degradation of the peak if that degradation in any case causes the

---

<sup>27</sup>In practice, an additional issue is that perturbative uncertainties from missing higher-order contribution may also depend on  $R$ . The interplay between this and non-perturbative uncertainties has not been studied.



	quark jets	gluon jets
Tevatron	0.56	0.73
LHC (14 TeV)	0.41	0.54

**Table 6:**  $R$  values that minimise the two non-perturbative contributions in various circumstances for Tevatron and LHC running, based on eq. (51), with  $2\mathcal{MA}(\mu_I)/\pi = 0.19$  GeV and  $\Lambda_{UE} = 4$  GeV (10 GeV) at the Tevatron (LHC).

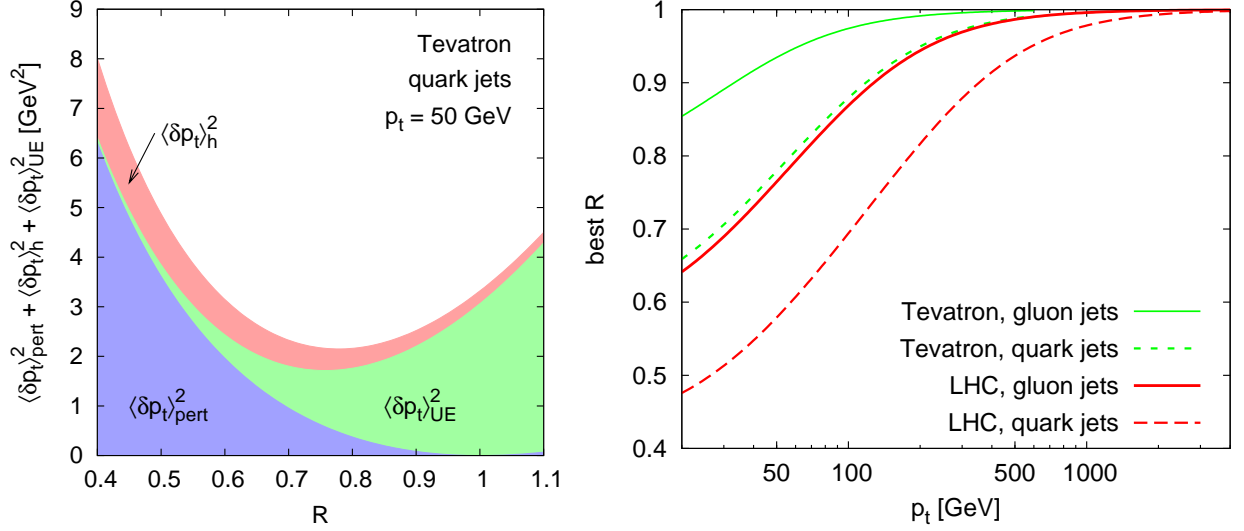


**Figure 18:** Left: sum of the squares of the mean shifts of a jet's momentum due to perturbative gluon radiation, hadronisation and the UE, as a function of  $R$  for  $p_t \sim 50$  GeV quark jets at the Tevatron; right: the resulting crude estimate for the “best”  $R$  as a function of jet  $p_t$ , for quark and gluon jets at the Tevatron and LHC (14 TeV). These values are to be taken as indicative of general trends rather than reliable estimates of the best  $R$ . The plots use the same parameters as table 6 and the perturbative contribution is taken in the small- $R$  limit. Taken from [111].

peak to disappear under the background. A *very* crude estimate of what goes on can be had by assuming that fluctuations in a jet's momentum due to perturbative radiation, hadronisation and UE are each proportional to their average effect. Adding the squared averages in quadrature gives fig. 18 (left) and the minimum provides an idea of the optimal  $R$  (as before, ignore differences between algorithms), and illustrates how the main relevant interplay is between perturbative radiation and the UE. The right-hand plot shows how the resulting optimal  $R$  varies with  $p_t$ : gluon jets and high  $p_t$  jets prefer larger  $R$  values (because of the greater relative importance of perturbative radiation), while one needs smaller  $R$  values at the LHC than at the Tevatron (the former has more UE).

While fig. 18 is useful for understanding general trends (notably the need for large  $R$  at high  $p_t$ ), it is not quantitatively reliable: the fluctuations in a jet's kinematics and the mean energy-loss due to gluon radiation are for example *not* proportional to each other; also, for  $R \sim 1$ , the  $\alpha_s p_t \ln R$  approximation for perturbative energy loss is in itself poor

since it neglects terms of  $\mathcal{O}(\alpha_s p_t)$ ; finally, for simplicity, it has been obtained neglecting differences between algorithms and this is not entirely legitimate.

### 5.1.2 Numerical studies

Given that a complete analytic treatment is not yet available, one usefully can use Monte Carlo event simulation to examine the optimisation of the choice of jet definition.

Historically the approach taken to studying the quality of jet-definitions has been to take hard partons in a Monte Carlo, let them shower and hadronise, and then see how closely the reconstructed hadron-level jets match the original partons (see for example [146]). This procedure has the drawback that it is conceptually impossible to extend it to advanced Monte Carlo tools like MC@NLO [33], because the “original parton” is no longer identifiable. Furthermore it leads to several distinct quality measures: whether the number of jets is equal to the number of “partons”, the angular distance between the jets and the partons, and the  $p_t$  difference between the jets and the partons. It is then often not clear which of these measures is most representative of the algorithm’s usefulness in a real physics analysis.

The most robust way of proceeding would be, for each possible experimental study, to carry out a full signal and background analysis with a wide variety of jet definitions and then see which provides the best signal to background (or root-background) ratio. As well as being a major undertaking, this can have subtleties: for example, optimal cuts in an analysis may depend on the jet definition and so may need to be reoptimised for each new jet definition.

An approach taken in [147, 148, 68, 66] attempts to carry out a simplified version of this procedure. It takes a physical process, for example the production of a narrow  $Z'$  that decays to  $q\bar{q}$ , or a  $t\bar{t}$  event ( $t \rightarrow \text{hadrons}$ ) and attempts to reconstruct the massive object. The “better” the reconstructed mass peak, the better the jet algorithm. This ignores issues like how the jet algorithm performs with respect to background events (which was however additionally studied in [66]), but is well-defined (no reference to partons) and avoids the appearance of multiple quality measures (angular dispersion, energy dispersion, etc.). Note: the physical process itself need not necessarily be realistic — e.g. it is highly unlikely that there exists an as-yet undiscovered, hadronically decaying  $Z'$  with mass 100 GeV. But it still serves as a useful stand-in for a generic  $q\bar{q}$  resonance, whose mass scale can easily be varied.

Quantifying the quality of the mass peak is, as it turns out, is a non-trivial issue. This is evident from fig. 5.1.2. It is tempting to measure the peak quality by fitting a Gaussian. However, the fit is poor; the results of the fit depend on the choice of fit-window; and then it’s not clear which parameters of the Gaussian would serve as the quality measure: the normalisation? The width? Some combination of the two? The approach of [147, 148, 68] is to avoid the fit-function and instead to find the width of the smallest window that contains a specified fraction  $z$  of the events,  $Q_{f=z}^w$ . A sharper (i.e. better) peak corresponds to a

lower  $Q_{f=z}^w$  value. There is still some arbitrariness in this, for example the choice of the fraction of events  $z$  (defined with respect to all events before cuts). However  $z$  is easily varied to check the robustness of the procedure and one can also examine other quality measures.<sup>28</sup>

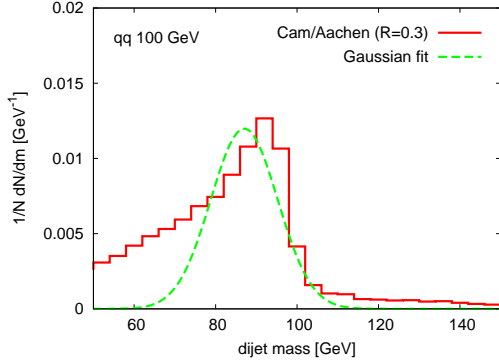


**Figure 19:** Distribution of the reconstructed invariant mass of a 100 GeV  $q\bar{q}$  system for the C/A algorithm with  $R = 0.3$ , simulated with Pythia 6.4, together with a Gaussian fit.

discussed in section 5.1.1: the larger the importance of perturbative gluon radiation, the larger the preferred  $R$  value. The optimal  $R$  as a function of mass scale, for the different algorithms and for the  $q\bar{q}$  and  $gg$  cases, is illustrated in fig. 22. The overall trend is not unlike the rough analytical estimate, fig. 18 (right), but the details differ: for example the full result doesn't show as rapid an  $R$  dependence, and it is not clear to which extent the optimal  $R$  saturates at the highest scales in fig. 22.

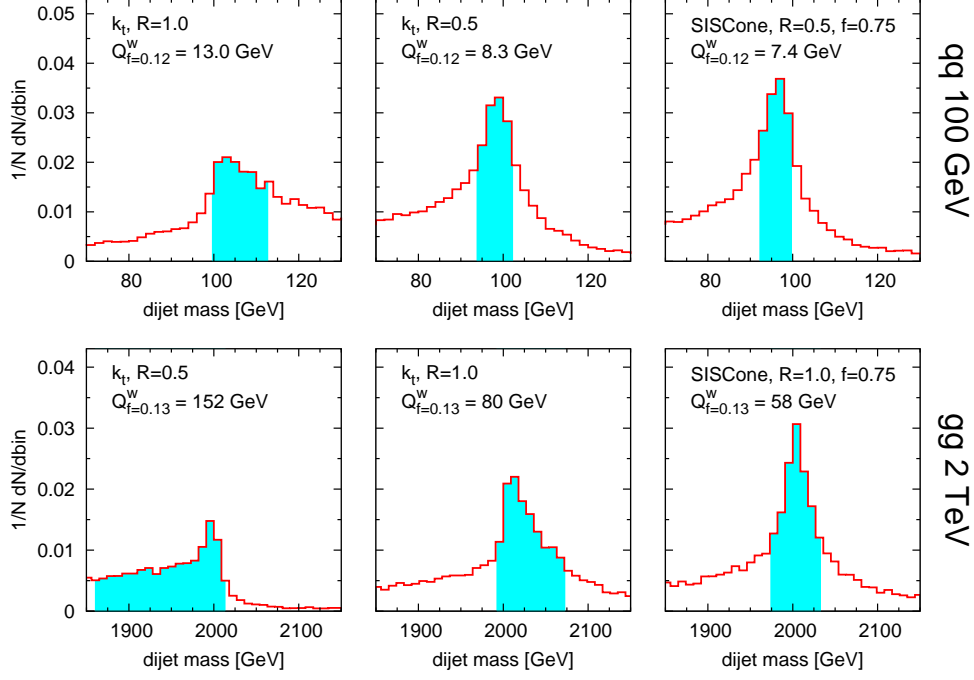
Figure 21 shows that even at the optimal  $R$  there are differences between algorithms. The origin of these differences has not been analysed in full detail, but can almost certainly be traced back to the very different area properties of the various algorithms:  $k_t$  fares worst because its larger area allows more UE into the jet, causing enhanced fluctuations of the kinematics from event to event; meanwhile SISCone, with its small area, fares well, as does the filtered version of the C/A algorithm, which resolves each jet on an angular scale  $R/2$  and takes just the two hardest subjets (cf. section 2.2.6).

<sup>28</sup>One alternative is to fix the window width to be  $x$  GeV, place the window so as to maximise the number of events that it contains, and then use the inverse fraction of contained events  $Q_{w=x}^{1/f}$  as the quality measure. A better peak concentrates more events in a given window, giving a lower result for  $Q_{w=x}^{1/f}$ .

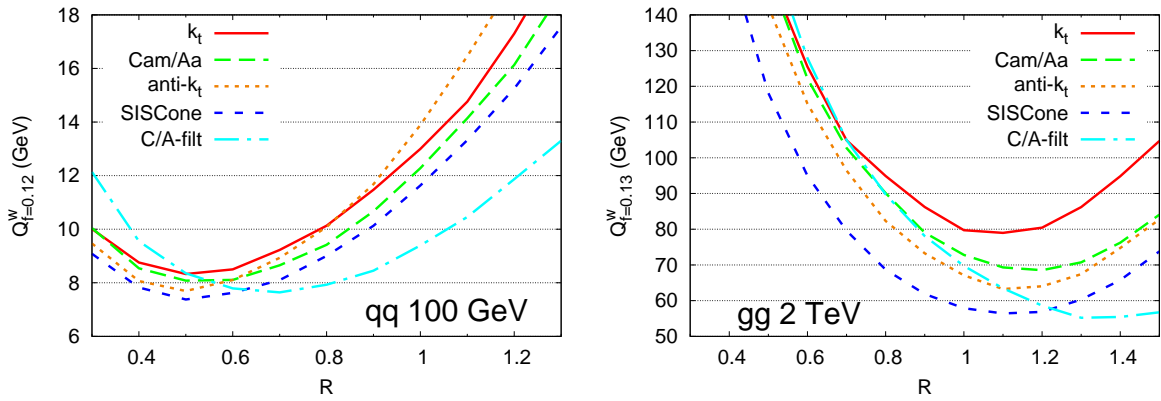
<sup>29</sup>This and other figures in this subsection are all taken from [68], to which the reader is referred for full details. In the dijet case, a mass is reconstructed from the two hardest jets, with a cut  $|\Delta y| < 1$  on the rapidity interval between the two jets (because in studies with background, such a cut greatly reduces the background).

Fig. 20 illustrates the procedure for a 100 GeV  $q\bar{q}$  resonance and a 2 TeV  $gg$  resonance, examining three jet definitions (the use of  $z = 0.12$  corresponds to taking about 25% of events after cuts).<sup>29</sup> One sees how better peaks have lower values for  $Q_{f=z}^w$ , together with the extent of the differences between algorithms, and the relevance of the choice of  $R$ .

The full  $R$ -dependence of the quality measure is shown for 5 algorithms in fig. 21, for the same two physics cases. The minimum of each curve indicates the best  $R$  for that particular algorithm, while the differences between the curves are illustrative of the different behaviour of the various algorithms. In particular, one sees the preference for larger  $R$  in the 2 TeV  $gg$  case. This is in accord with the expectations



**Figure 20:** Illustrative dijet invariant mass distributions for two processes (above:  $q\bar{q}$  case at  $M = 100$  GeV; below:  $gg$  case at  $M = 2$  TeV), comparing three jet definitions for each process. The shaded bands indicate the regions used when obtaining the  $Q_z^w$  quality measure. Note that different values of  $R$  have been used for the  $q\bar{q}$  and  $gg$  cases.



**Figure 21:** The quality measure  $Q_{f=z}^w$ , for different jet algorithms as a function of  $R$ , for the 100 GeV  $q\bar{q}$  case (left) and 2 TeV  $gg$  (right).

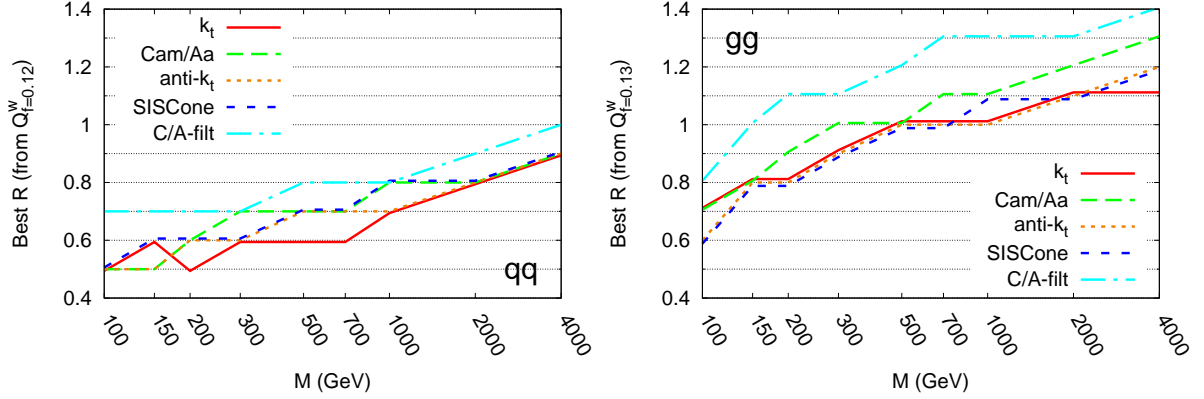


**Figure 22:** The optimal value for  $R$  as a function of the mass of the  $q\bar{q}/gg$  system (left/right), as determined from the  $Q_{f=z}^w$  quality measure for various jet algorithms. Note that the exact results for the optimal  $R$  depend a little on the choice of quality measure, however the observed trends do not.

A key question in examining results such as those in fig. 20 and 21 is how much the differences between algorithms (and  $R$ -values) matter: from this information an experiment can then decide whether it is worthwhile investing in the calibration of multiple jet definitions (or in the inherent flexibility that allows easy use of any jet definition). One way of making such an estimate is to assume that the peak is being reconstructed in the context of a search with significant background. If one can assume that the amount of background basically scales as the width of the window that comes out of the  $Q_{f=z}^w$  quality measure, then the significance  $S/\sqrt{B}$  of any signal will just be inversely proportional to  $\sqrt{Q_{f=z}^w}$ . One can then define a measure  $\rho_L$ , which is the extra factor in luminosity that is needed to see the signal with given significance when using one jet-definition (JD) relative to another.

Results for  $\rho_L$  are given in fig. 23. One sees that the impact of the jet algorithm choice is greatest at large mass scales (not surprising perhaps, given that large scales prefer large  $R$ , where the area-sensitivity matters particularly). That figure also illustrates how, at large mass scales, especially for gluon jets (as discussed first in [148]), standard choices of  $R \sim 0.5$  are extremely poor — requiring up to twice as much luminosity to see a mass peak above a background. This conclusion is relatively robust: fig. 23 actually has results for two different quality measures, which agree remarkably well (the solid line derives from  $Q_{f=z}^w$ , discussed above, while the dashed line stems from an alternative measure, cf. footnote 28, or [68] for full details).

A reader who wishes to examine these quality measures further is encouraged consult a web-tool [149], which provides access to over 100,000 plots, two different quality measures and  $z$  values, with histograms for a wide range of jet definitions and mass scales as well as summary plots of the quality measures and resulting  $\rho_L$  values.

Two important comments are due concerning the above discussion. Firstly, it applies

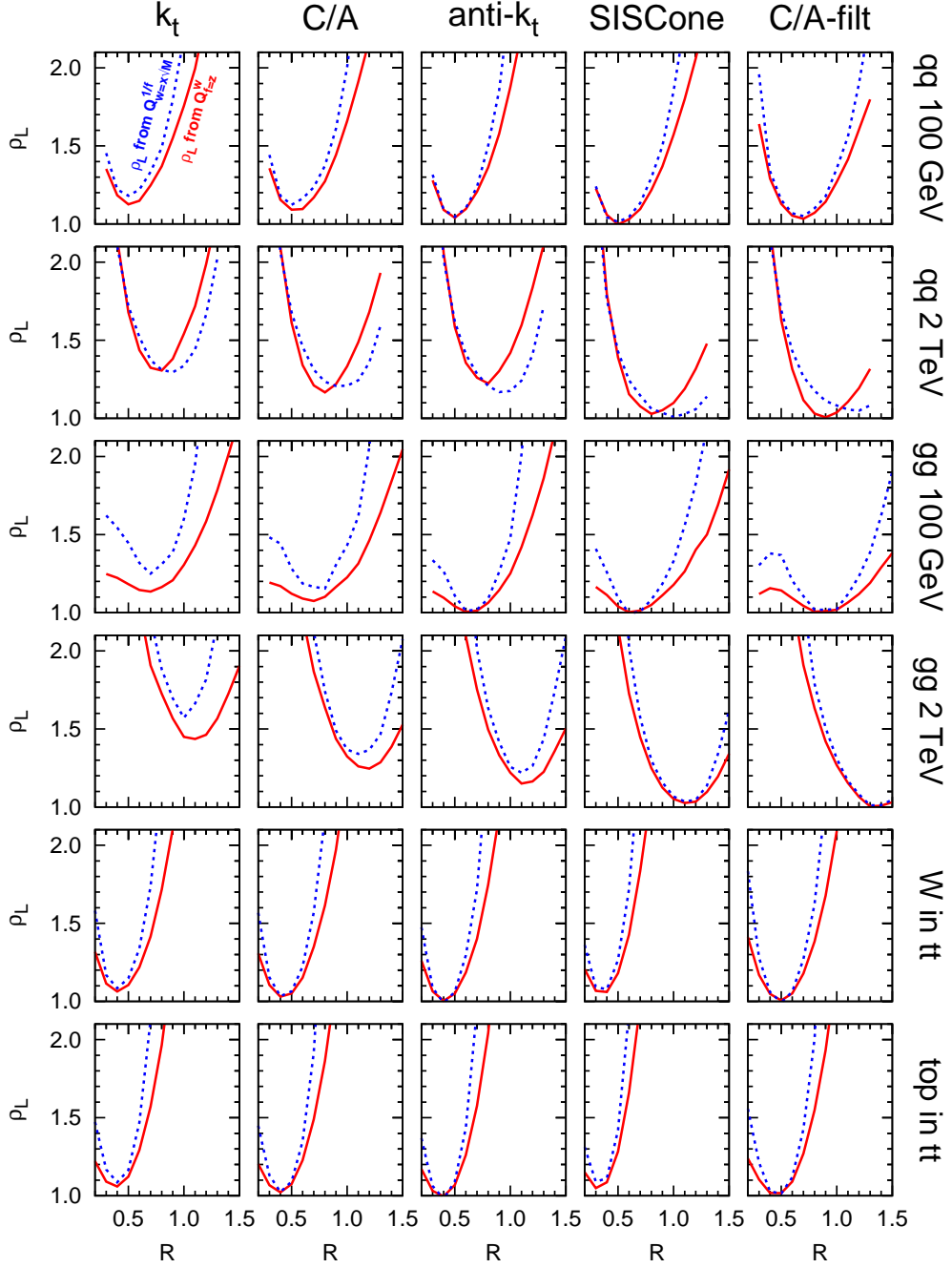


**Figure 23:** For each process (one per row) this plot shows the extra factor in luminosity,  $\rho_L$ , required in order to obtain the same significance as with the best jet definition, as a function of  $R$ . The (red) solid line corresponds to the estimate of  $\rho_L$  based on the minimal width  $Q_{f=z}^w$ , while the (blue) dotted line corresponds to that based on the maximal fraction  $Q_{w=1.25\sqrt{M}}^{1/f}$  (cf. footnote 28).

Algorithm	500 GeV	1 TeV	2 TeV	3 TeV
anti- $k_t \rightarrow$ anti- $k_t$ VR	18% (0.9, 200)	14% (1.0, 450)	10% (1.2, 1000)	8% (1.3, 1500)
C/A $\rightarrow$ C/A VR	17% (0.9, 175)	14% (1.0, 400)	7% (1.2, 1000)	9% (1.3, 1500)

**Table 7:** Percentage improvement in the number of events from a resonance  $X$  that have been reconstructed in the mass window  $m_X \pm 25$  GeV, comparing a fixed- $R$  algorithm at its best  $R$  (first number in brackets) with the variable- $R$  algorithm (the second number in brackets,  $\rho$ /GeV, sets the jet radius as  $R(p_t) = \rho/p_t$ ). Results taken from [66].

directly only to simple dijet events. There have also been studies with multijet events from top-quark decays, cf. the two bottom rows of fig. 23, as well as an extensive analysis in [150]. What emerges from these studies is that the best choices in dijet events (where SISCone works very well) may not be optimal in multijet cases. For example, in [150] SISCone had more difficulty resolving all relevant jets, while in fig. 23 the acceptable range of  $R$  is somewhat narrower for SISCone than for other algorithms. A related point is that in multijet events the conclusion about the need for larger  $R$  at high scales is likely to conflict with the need to resolve the multiple jets. These are important issues and call for further study.

A second comment is that refs. [147, 148, 68] did not carry out any detailed tests of how the presence of realistic background events affects the relation between mass scale and optimal  $R$ . However, the analysis to be described below, ref. [66], did include a study with background events, and confirms that at high masses large- $R$  values are preferred (though the cuts and other details differ somewhat from those in [68]).

**Variable  $R$ .** One should be aware that there may also be benefits to be had by moving away from the use of a single  $R$  value even when studying a single mass scale. For example, one might choose to adapt  $R$  according to the amount of noise (UE, pileup) in each given event. Alternatively, other kinematic variables, like the rapidity separation between the leading jets, can also affect the optimal  $R$  choice on an event-by-event basis.

This last point was studied recently by Krohn, Thaler and Wang (KRT) [66] with a variable- $R$  jet algorithm (cf. section 2.2.6). Their  $R$  value is actually not directly a function of the rapidity difference,  $\Delta y$ , between the two hardest jets, but rather scales as  $1/p_{t,jet}$ , which for two hard jets stemming from a resonance of given fixed mass translates to a rapidity dependence  $R \sim \cosh \frac{\Delta y}{2}$ . This was motivated on the grounds that jets from a resonance decay emit gluons on an angular scale that is independent of whether the jets are transverse or along the beam direction; in the centre-of-mass frame of the resonance, for two partons at rapidity  $y/2$ , separated by an angle  $\theta_{ij} \ll 1$ , the boost-invariant angular distance  $\Delta R_{ij}$  is given by  $\theta_{ij} \cosh \frac{y}{2}$ . Hence the scaling used for the jet radius.<sup>30</sup>

<sup>30</sup>The optimal  $R$  depends choice should of course depend also on initial state radiation and the underlying event, and further studies might benefit by taking into account this information too.

Table 7 illustrates the improvements in signal reconstruction that are obtained with this approach as compared to fixed- $R$  algorithms. The benefit is at the level of tens of percent. This is similar in magnitude to the improvement seen above by optimising the choice of algorithm, or optimising a fixed  $R$  as compared to a standard  $R = 0.5$  or  $R = 0.7$  choice.

The KRT analysis was performed using the two leading jets reconstructed from all particles with  $|\eta| < 3$ . This means that significant numbers of events involve two leading jets with large rapidity separations. In this respect, the KRT analysis differs from that discussed above [68], which only studied events in which the leading jet pair was separated by  $|\Delta y| < 1$ . With the latter requirement, since  $\cosh \frac{\Delta y}{2}$  would be close to 1, one might expect the  $p_t$ -dependent variable- $R$  choice to have a more modest impact.

KRT also studied jet performance for resonance reconstruction that includes a dijet background. Here too they found improvements with a variable  $R$  choice (and again at the level of about 10 – 15%), but only if they supplemented their analysis with a “jet quality” cut which requires that the energy be deposited centrally within the jet. The corresponding fixed- $R$  analysis confirmed the need for large  $R$  values at high mass scales.

## 5.2 Pileup subtraction

The LHC will collide protons with an unprecedented instantaneous luminosity of up to  $10^{34} \text{ cm}^{-2} \text{ s}^{-1}$  and a bunch spacing of 25 ns, corresponding to  $0.25 \text{ mb}^{-1}$  per bunch crossing. While this high luminosity is essential for many searches of rare new physics processes at high energy scales, it also complicates analyses, because at each bunch crossing there will be of the order of 20 minimum bias  $pp$  interactions, which pollute any interesting hard events with many soft particles. The beams at LHC will have a longitudinal spread, and it may be possible experimentally to associate each charged particle with a distinct primary vertex that corresponds to a single  $pp$  interaction and so eliminate some fraction of the soft contamination. However, for neutral particles this is not possible, and many jet measurements are in any case expected to be carried out with calorimeters, which do not have the angular resolution needed to reconstruct the original primary vertex. Therefore kinematic measurements for jets will be adversely affected by pileup (PU), with resolution and absolute energy measurements suffering significantly.

The impact of PU is illustrated in the upper row of fig. 24, which shows histograms for the same 2 TeV  $gg$  resonance used above, but now with varying degrees of pileup: none, low-luminosity LHC running ( $0.05 \text{ mb}^{-1}$  per bunch crossing) and high-luminosity running ( $0.05 \text{ mb}^{-1}$  per bunch crossing). The degradation of the peak and its shift to higher masses are clearly evident here. While the shift is perhaps not overly consequential (it could be corrected for by comparing to MC simulation of the pileup), the loss of resolution is a serious issue.

Both the Tevatron and LHC experiments have examined the question of pileup. Some approaches to limiting its impact are based on average correction procedures, for example



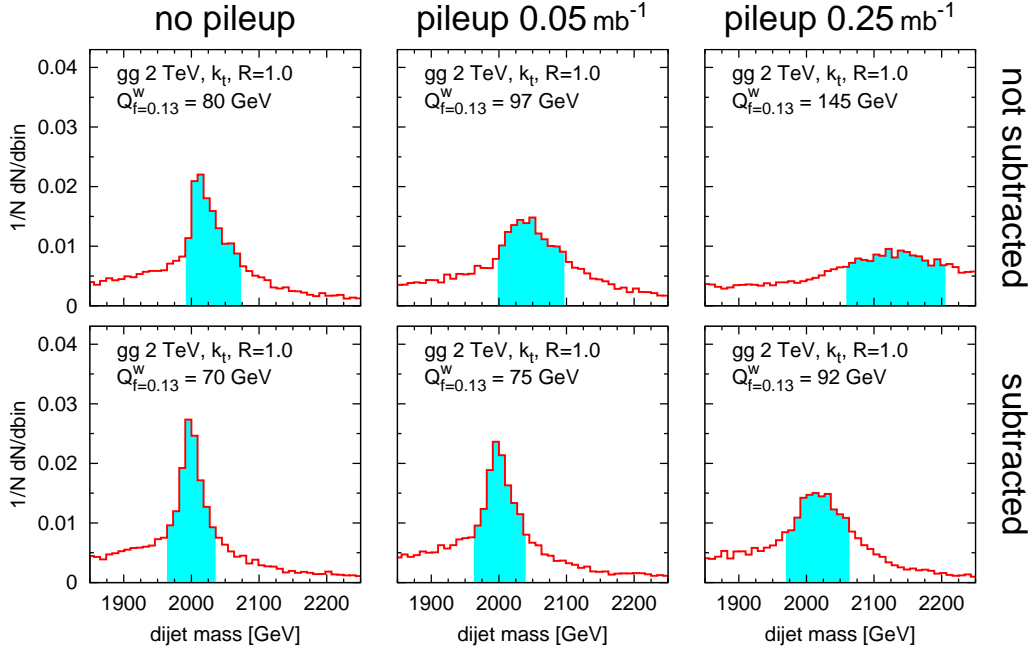


**Figure 24:** Invariant mass distributions for the 2 TeV  $gg$  process of section 5.1.2, for the  $k_t$  algorithm with  $R = 1$ , shown with no pileup (left), low pileup (middle) and high pileup (right), without subtraction (upper row) and with pileup subtraction as outlined in [151] (lower row). The shaded bands indicate the region used to calculate the  $Q_{f=z}^w$  quality measure in each case. Figure taken from [68].

the requirement that final measured distributions should be independent of luminosity [59], or a correction to each jet given by some constant times the number of primary interaction vertices (minus one) [152]. These approaches have the advantage of being simple, but their averaged nature limits the extent to which they can restore resolution lost through pileup. Other approaches involve event-dependent corrections that are applied to calorimeter towers either before or during the clustering [153, 154]. These can give better restoration of resolution than average-based methods. One drawback that they have is that they are tightly linked to the specific experimental setup (for example calorimeter cell-size), and require ad-hoc transverse-momentum thresholds to distinguish pileup from hard jets. Additionally they are sometimes tied to specific (legacy) jet algorithms, and so may not always be readily applied to more modern jet algorithms.

The above issues triggered the development of an experiment-independent pileup subtraction approach in [151]. The essential observation is that pileup roughly modifies a jet's  $p_t$  as follows:

$$\Delta p_t = A\rho \pm \sigma\sqrt{A} + \Delta p_t^B, \quad (52)$$

where  $A$  is the jet's area (after addition of the pileup),  $\rho$  is the mean amount of transverse momentum per unit area that has been added to the event by pileup;  $\sigma$  measures the fluctuations of the pileup from point-to-point within the event (defined as the standard

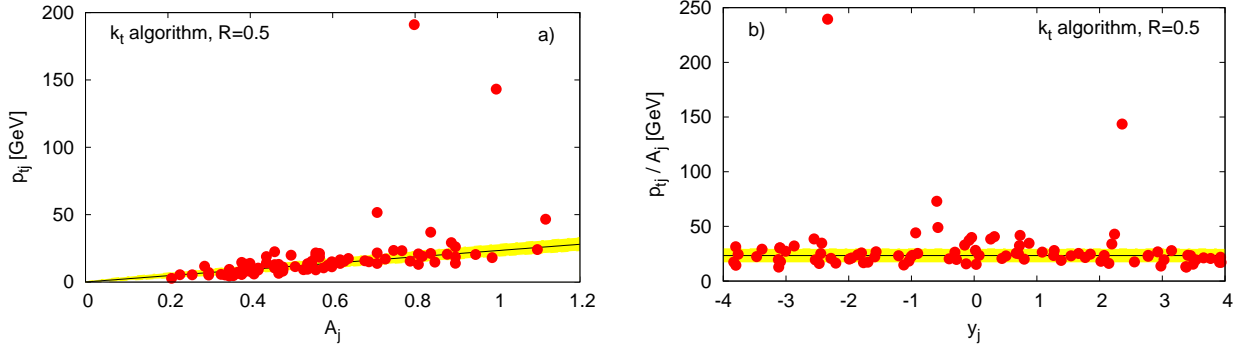


**Figure 25:** a) Scatter plot of the jet transverse momentum  $p_{tj}$  versus its area  $A_j$ , for an LHC dijet event with a pileup of 22 minimum bias interactions (simulated with the default tune of Pythia 6.325 [81]). The line and band are given by  $\rho A_j \pm \sigma \sqrt{A_j}$ . b) The ratio  $p_{tj}/A_j$  as a function of the rapidity,  $y_j$ , for the same event; the line and band are given by  $\rho \pm \sigma/\sqrt{\langle A \rangle}$ . Taken from [151].

deviation of the distribution of pileup across many squares of area 1); and  $\Delta p_t^B$  is the net change in transverse momentum due to back reaction. Fluctuations in the jet  $p_t$  arise because  $A$  varies from jet-to-jet,  $\rho$  from event-to-event, because the pileup density fluctuates from place to place within an event (the  $\sigma$  term) and because of back-reaction. The approach of [151] involves first running the jet algorithm, estimating  $\rho$  and then subtracting the  $A\rho$  term from each jet. This leaves just the  $\sigma\sqrt{A}$  piece and the back-reaction term and should significantly reduce both the fluctuations and the mean offset in jet energy.<sup>31</sup>

The estimation of  $\rho$  (without using detector-specific information, such as the origin of tracks) is non-trivial because one must decide what part of the event belongs to the hard event and which part comes from pileup. Ideally one wants to do this without introducing any explicit threshold to distinguish the two, given that the natural threshold would vary significantly from event to event. One observation of [151] is that this can be done using the jets themselves. Fig. 25a shows a scatter plot of jet  $p_t$  versus jet area for a single Monte Carlo event and one sees a clear correlation from nearly all the jets. Fig. 25b shows  $p_t/A$  for each jet as a function of rapidity for the same event and one sees that the  $p_t/A$  results cluster around a value that is fairly independent of rapidity (it is still unclear just how true this will actually be at the LHC). These two features led to the proposal to take the distribution of  $p_t/A$  for all jets in an event, up to some maximum rapidity, and to then use its median (robust with respect to outliers, i.e. hard jets) as an estimate of  $\rho$ .<sup>32</sup> That

<sup>31</sup>One might eliminate the back reaction too if one could subtract the PU before running the jet-finder — subtracting PU directly at particle level leads, however, to negative momenta, with consequent non-trivial issues within many jet-algorithms.

<sup>32</sup>One technical detail is that only certain jet algorithms, essentially  $k_t$  and C/A, are suitable for estimating  $\rho$ , while the subtraction itself can be performed for any algorithm. When trying to optimise the subtraction there are also issues with the choice of the correct  $R$  value in the JD used to estimate  $\rho$ , with  $R \sim 0.5 - 0.6$  being a generally reasonable choice.

estimate gives the black line in fig. 25, while the yellow band's width is controlled by the value of  $\sigma$  obtained from examining the width of the  $p_t/A$  distribution.

With  $\rho$  estimated in this fashion, one can correct each jet by an amount:

$$p_{tj}^\mu \rightarrow p_{tj}^\mu - \rho A_j^\mu, \quad (53)$$

where  $A_j^\mu$  is the jet's 4-vector area. This approach was used to obtain the lower row of fig. 24, illustrating the substantial gain in peak quality that is to be had with the method (as well as nearly correct reconstruction of peak position). In this specific case there is even an improvement in the peak quality in the case without pileup, a consequence of the fact that the above method also subtracts UE.

One comment is that pileup subtraction does not completely eliminate the effect of pileup. In the area-based approach just described, this is because of the last two terms on the RHS of eq. (52) are still present after subtraction. Nevertheless it reduces the impact of pileup sufficiently that conclusions about optimal jet definitions drawn from fig. 23 in the absence of pileup also hold with pileup. This is important, because it means that analyses that use data taken at different luminosities can successfully use a common jet algorithm, independently of the pileup.

**Subtraction in heavy-ion collisions.** The techniques described above have the potential to be useful also in heavy-ion (HI) jet finding, where the problem is to identify jets given the large soft background of particles that results from the hot dense matter that is formed in a heavy-ion collision. This is of interest in the heavy-ion community (see for example the review [7]) because the modification of jets as they traverse the hot dense medium may provide insight into the nature of the medium.

The proposal for area-based pileup subtraction [151] also included an application to the HI case and it has been investigated by the STAR collaboration at RHIC in a first preliminary measurement of jet-cross sections in Au Au gold collisions at  $\sqrt{s_{NN}} = 200$  GeV [8].

The value of  $\rho$  in the heavy-ion case is up to an order of magnitude larger than in high-luminosity  $pp$  running. This places particularly stringent constraints on the accuracy that is required in the subtraction and has spurred various ongoing investigations. Given the similarities between HI and high-pileup  $pp$  jet-finding, it is to be expected that these investigations will be beneficial in both environments.

Among the issues that are being considered is that of how to estimate  $\rho$  without recourse to the whole event, given that there is significant rapidity dependence (and even azimuth dependence in some cases) in the production of soft particles, both in HI and  $pp$  collisions (the event in fig. 25b is a little unusual in its degree of rapidity-independence). Other issues are those of minimising systematic residual shifts from back-reaction (for which the anti- $k_t$  algorithm is beneficial) and reducing the impact of point-to-point fluctuations in the noise (in this respect C/A filtering seems to offer a promising avenue).

## 5.3 Substructure

A key feature of the LHC is that it will be the first collider to probe scales that are significantly above the EW scale. This is what will allow the LHC to investigate the nature of electroweak symmetry breaking and explore new territory in the search for particles and phenomena beyond those of the standard model.

The importance of physics at transverse momenta  $p_t \gg m_Z$  has implications for the structure of the final state because at high transverse momenta, “signature” particles, W’s, Z’s, Higgs bosons and top-quarks, have very collimated decays (due to their relativistic boost). Standard approaches for identifying these particles (i.e. recombining different jets) fail because all the decay products end up in a single jet.

The work so far on identifying hadronic decays of boosted heavy particles has fallen into two broad classes: particles with two-pronged decays (the EW bosons), and those with three-pronged decays (top quarks). In each case, the mass of the jet is one indicator of its origin (as discussed recently for example in [155, 156, 157, 158, 159]). However, even for massless partons, QCD branching generates a significant fraction of jets with large masses (or equivalently with 2 or 3-pronged substructure): assuming a given jet  $p_t$ , the leading-order (fixed-coupling) differential QCD jet-mass distribution goes as

$$\frac{1}{n} \frac{dn}{dM^2} \sim \frac{1}{M^2} \frac{\alpha_s C_i}{\pi} \left( \ln \frac{R^2 p_t^2}{M^2} + \mathcal{O}(1) \right) \quad (54)$$

(see [112] for more detailed analytic expressions, or [113, 115] for corresponding resummed results in  $e^+e^-$  collisions) and the logarithm can in part compensate the smallness of  $\alpha_s$ , especially at larger  $p_t$ . Two main questions that need to be answered are then: how can one reduce the background of QCD jets of a given mass, and how can one get the best resolution on jet mass so as to be able to use a small jet-mass window in selecting candidate heavy particles?

### 5.3.1 Two-pronged decays

The first detailed discussion of advanced jet techniques for two-pronged decays, over 15 years ago, was given by Seymour in [160] in the context of a search for a heavy Higgs boson decaying to  $WW$  with one  $W$  decaying leptonically, the other hadronically. He mainly considered the issue of mass resolution and investigated two approaches. One method involved the (inclusive)  $k_t$  algorithm, with  $R = 1$ , in which the clustering sequence for the hardest jet was essentially undone by one step, so as to resolve the jet into the two subjets from the  $W$  decay. The resulting separation of the subjets could then be used to set a smaller  $R$  for a second run of the  $k_t$  algorithm, which helped improve the mass resolution. Another method involved the use of a cone algorithm with quite small  $R$ ,  $\sim 0.25$  in order to directly identify the two subjets. This small  $R$  was needed in order to robustly resolve the two subjets, but that then caused it to lose significant gluon radiation from the  $W \rightarrow q\bar{q}$  system, giving worse mass resolution than the  $k_t$  algorithm. The basic observation was

therefore that the  $k_t$  algorithm's intrinsic internal information on substructure allowed one to be more flexible in the compromise between identifying substructure and capturing the bulk of the relevant radiation.

The next development on the subject was made by Butterworth, Cox and Forshaw [161] who examined  $WW$  scattering, again with one leptonically and one hadronically decaying  $W$ . They observed that the distribution of  $k_t$  distance,  $d_{ij}$  (eq. (8)), between the two  $W$  subjects was close to the  $W$  mass in  $W$  decays, but tended to have lower values in generic massive jets. This allowed them to obtain a substantial reduction in the background. The same idea was used later for electroweak-boson reconstruction in the context of a SUSY search [162]. The tool associated with this technique is often referred to as “Y-splitter”.

It is worthwhile looking at some simple analytic results that relate to the techniques of [161] and [160]. For a quasi-collinear splitting into two objects  $i$  and  $j$ , the total mass is  $m^2 \simeq p_{ti}p_{tj}\Delta R_{ij}^2$ . Labelling  $i$  and  $j$  such that  $p_{tj} < p_{ti}$  and defining  $z = p_{tj}/p_t$  ( $p_t = p_{ti} + p_{tj}$ ), then

$$m^2 \simeq z(1-z)p_t^2\Delta R_{ij}^2, \quad (55)$$

$$d_{ij} = z^2p_t^2\Delta R_{ij}^2 \simeq \frac{z}{(1-z)}m^2. \quad (56)$$

It is the fact that electroweak bosons decay with a fairly uniform distribution in  $z$  (exactly uniform for a Higgs boson), whereas a QCD splitting has a soft divergence, e.g.

$$P_{gq} \propto \frac{1+(1-z)^2}{z}, \quad (57)$$

that means that for a fixed mass window, the background will have lower  $d_{ij}$  values than the signal. Indeed, the logarithm in eq. (54) comes from the integral over the  $1/z$  divergence in eq. (57), with lower limit  $z \gtrsim m^2/p_t^2R^2$ . If one places a cut on  $d_{ij}$ , or analogously on  $z$ , then one eliminates that logarithm, thus reducing the QCD background (one can even calculate, analytically, what the optimal cut is for given signals and backgrounds).

A second set of observations concerns mass resolution. Firstly, with a small cone of size  $R \ll \Delta R_{ij}$  used to reconstruct the two prongs of a colour-singlet  $q\bar{q}$  state, then there will be an average loss of mass, dominated by a contribution from perturbative gluon radiation,

$$\langle \delta m^2 \rangle \simeq 2m^2 \cdot \frac{\alpha_s L_q}{\pi} \left( \ln \frac{R}{\Delta R_{ij}} + \mathcal{O}(1) \right), \quad R \ll \Delta R_{ij}, \quad (58)$$

with  $L_q \simeq C_F$  as given in eq. (28). If instead a single jet is used to reconstruct the whole  $q\bar{q}$  system, then one can show that most of the perturbative radiation from the  $q\bar{q}$  system will be contained in the jet. However there may then be significant contamination from the UE and pileup,

$$\langle \delta m^2 \rangle \simeq \rho p_t \frac{\pi R^4}{2}, \quad (59)$$

for a circular jet (cf. eq. (42), with  $\rho \equiv \Lambda_{UE}/2\pi$ ), with an additional contribution coming also from perturbative radiation from the beam. Even though the above two equations

represent major oversimplifications of the full dynamics, one can understand the task of optimising mass resolution as one of minimising both types of contribution (in analogy with section 5.1.1).

This understanding provided the backdrop to a two-pronged subjet technique given in [67], used there for a high- $p_t$  Higgs boson search in association with a back-to-back high- $p_t$  vector boson. The approach involved the Cambridge/Aachen algorithm, because its sequential recombination in increasing angular distance is ideally suited to dealing with problems that involve multiple or unknown angular scales. The basic procedure that was used to identify a  $H \rightarrow b\bar{b}$  decay went as follows:

1. Break a C/A jet  $j$  into two subjets by undoing its last stage of clustering. Label the two subjets  $j_1, j_2$  such that  $m_{j_1} > m_{j_2}$ .
2. If there was a significant mass drop (MD),  $m_{j_1} < \mu m_j$ , and the splitting is not too asymmetric,  $y = \frac{\min(p_{tj_1}^2, p_{tj_2}^2)}{m_j^2} \Delta R_{j_1, j_2}^2 > y_{\text{cut}}$ , then deem  $j$  to be the heavy-particle neighbourhood and exit the loop ( $\mu$  was taken to be 0.67 and  $y_{\text{cut}} = 0.09$ ). Note that  $y \simeq \min(p_{tj_1}, p_{tj_2}) / \max(p_{tj_1}, p_{tj_2})$ .<sup>33</sup>
3. Otherwise redefine  $j$  to be equal to  $j_1$  and go back to step 1.

The search for a mass-drop, step 2, served to identify the point in the decomposition that involved significant hard substructure and, in the context of a Higgs-boson search, one can verify that the two subjets at that stage both have a  $b$ -tag. The cut on  $y \simeq z/(1-z)$  allows one to kill the logarithm for (fake  $b$ -tag) QCD backgrounds in eq. (54). By virtue of angular ordering [61], the two C/A subjets produced at that stage, each with opening angle equal to  $\Delta R_{j_1, j_2}$ , should contain nearly all the perturbative radiation from the  $b\bar{b}$  system (i.e. eq. (58) is close to zero). They still tend to include too much contamination from the UE however, so one can then apply a filtering technique in which the two subjets are reexamined on a smaller angular scale  $R_{\text{filt}}$  and only the three hardest components (i.e.  $b\bar{b}g$ ) were retained. This essentially reduces the coefficient of the UE contamination in eq. (59). The value used for  $R_{\text{filt}}$  was specific to the jet,  $R_{\text{filt}} = \min(0.3, R_{b\bar{b}}/2)$ , though this could perhaps be further optimised.

A comparison of different jet algorithms for the  $ZH$  search channel for  $m_H = 115$  GeV, with  $Z \rightarrow e^+e^-, \mu^+\mu^-$  for  $p_{tH}, p_{tZ} > 200$  GeV (and other cuts detailed in [67]) is shown in table 8. The C/A algorithm with the mass-drop and filtering (MD-F) is clearly the best both at extracting the signal and limiting the background. The  $k_t$  algorithm fares poorly mainly because of its poor mass resolution (its larger area and fluctuations, cf. section 4.4, make it intrinsically worse than the C/A algorithm, and it is shown without any filtering). SISCone does quite well on the reconstruction of the signal, mainly because of its particularly low sensitivity to UE contamination, but does poorly on the background rejection

---

<sup>33</sup>This  $y_{\text{cut}}$  is related to, but not the same as, that used to calculate the splitting scale in [161, 162], which use a dimensionful  $d_{\text{cut}}$ .

Jet definition	$\sigma_S/\text{fb}$	$\sigma_B/\text{fb}$	$\sigma_S/\sqrt{\sigma_B \cdot \text{fb}}$
C/A, $R = 1.2$ , MD-F	0.57	0.51	0.80
$k_t$ , $R = 1.0$ , $y_{cut}$	0.19	0.74	0.22
SISCone, $R = 0.8$	0.49	1.33	0.42
anti- $k_t$ , $R = 0.8$	0.22	1.06	0.21

**Table 8:** Cross section for signal ( $\sigma_S$ ) and the  $Z$ +jets background ( $\sigma_B$ ) in the leptonic  $Z$  channel of  $HZ$  production at a 14 TeV LHC, for  $200 < p_{TZ}/\text{GeV} < 600$  and  $110 < m_J/\text{GeV} < 125$ , with perfect  $b$ -tagging; the C/A algorithm uses the procedure outlined in the text; the  $k_t$  algorithm uses the first step of decomposition to identify two subjets with a cut on  $y_{ij}$  as for C/A; SISCone and anti- $k_t$  do not use any subjet analysis, but each require two  $b$ -tags within the jet. In each case  $R$  has been chosen to give near optimal significance with that algorithm.

because it fails to correlate the  $b$  tagging with the subjet momentum structure, as does anti- $k_t$ . It is probably fair to say that the defects of the algorithms could to some extent be resolved with refinements such as the use of jet-finding with multiple  $R$  values. However it is only in the C/A algorithm that the use of multiple  $R$  values fits in naturally within the context of a single run of the jet finder, and the C/A algorithm provides an internal representation of the jet structure that makes it particularly easy to establish the right  $R$  values.

For completeness, fig. 26 shows the results of the Monte Carlo simulation of the boosted  $pp \rightarrow HV$  Higgs-boson search, illustrating how this becomes a relevant search channel at the LHC (and one that provides clean access to the product of  $Hbb$  and  $ZZH$ ,  $WWH$  couplings).

### 5.3.2 Three-pronged decays

Three-pronged decays have been studied mainly in the context of top decays.<sup>34</sup> This is motivated in part because high-mass  $t\bar{t}$  resonances are a feature of many new physics scenarios (see for example [164, 155, 165, 166, 167] and references therein).

The use of subjet structure in identifying hadronically decaying tops is a much more recent topics than for EW bosons, having developed mainly in the last year. However many of the ideas are directly inspired from the two-pronged case. Aside from examining the jet-mass (whose distribution is calculated in detail at leading order in [112]), techniques that have been investigated include subjet-decomposition with the  $k_t$  algorithm [168, 169], C/A subjet techniques [170] and pruning [69]. Among the discriminating variables that are used, there are  $d_{ij}$  type variables [169],  $z$ -type variables [168, 170, 69] and event-shape variables [168, 112] (in both cases, a sphericity-like variable in the plane transverse to the jet), constraints on a  $W$ -subjet mass [168, 170] as well as other interjet correlation variables

<sup>34</sup>Though there has also recently been work on the three-pronged hadronic decay of a neutralino in an  $R$ -parity violating SUSY scenario [163].

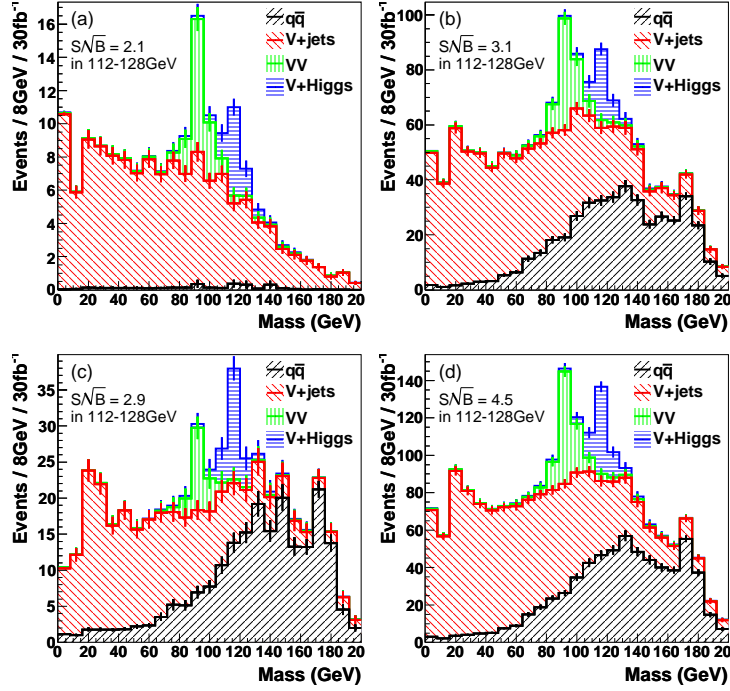


**Figure 26:** Signal and background for a 115 GeV SM Higgs in the  $pp \rightarrow VH$  channels, with  $H \rightarrow b\bar{b}$ , simulated using Herwig 6.5 and Jimmy 4.31 (an ATLAS tune), C/A MD-F with  $R = 1.2$  and  $p_t > 200$  GeV, for  $30 \text{ fb}^{-1}$ . The  $b$  tag efficiency is assumed to be 60% and a fake-tag probability of 2% is used. The  $q\bar{q}$  sample includes dijets and  $t\bar{t}$ . The vector boson selections are (a) two leptons, (b) missing energy and (c) lepton plus missing energy, while (d) shows the sum of all three channels (see [67] for details). The errors reflect the statistical uncertainty on the simulated samples, and correspond to integrated luminosities  $> 30 \text{ fb}^{-1}$ .

(a helicity angle  $\theta_h$  in [170]).

A summary of results for top-tagging efficiencies and fake rates in the various methods is given in table 9. What emerges from this is that the C/A-based method of [170] seems to offer good efficiencies and very good QCD-jet rejection, with the best signal significance and signal-to-background ratio (“better than  $b$ -tagging at high  $p_t$ ”). Compared to the C/A-based method of [67] for Higgs decays, particularly relevant differences are that it avoids any reference to mass-drops (thus simplifying the method), and introduces a minimal distance between subjects, which needs to be adjusted with the jet  $p_t$ . Its signal efficiency and fake-tag rates are shown as a function of transverse momentum in fig. 27 (left). The decrease in efficiencies at high transverse momenta is simply a consequence of the inclusion of finite calorimeter tower sizes ( $0.1 \times 0.1$ ), and could perhaps be alleviated experimentally with the use of tracking and electromagnetic calorimetry, both of which have finer angular resolution

One important point in top-tagging is that to obtain the best tagging at high transverse momenta, one should use an  $R$  value that scales as  $1/p_t$ , because the top-quark decay is



	Method	efficiency	fake fraction
(from [168])	just jet mass	50%	10%
Brooijmans [169]	3,4 $k_t$ subjets, $d_{cut}$	45%	5%
Thaler & Wang [168]	2,3 $k_t$ subjets, $z_{cut}$ + shape	40%	5%
Kaplan et al. [170]	3,4 C/A subjets, $z_{cut}$ + $\theta_h$	40%	1%

**Table 9:** Efficiencies for reconstructing top quarks with  $p_t \sim 1$  TeV and the fraction of normal QCD jets that get a fake “top-tag”. Shown for the various tagging methods that quoted numbers easily amenable to interpretation in this manner. Insofar as results involve different detector and resolution assumptions, Monte Carlo generator choices, as well as slightly different  $p_t$  cuts, the comparison should be considered indicative rather than precise. Furthermore the results of the various methods have different dependences on the transverse momenta being studied.

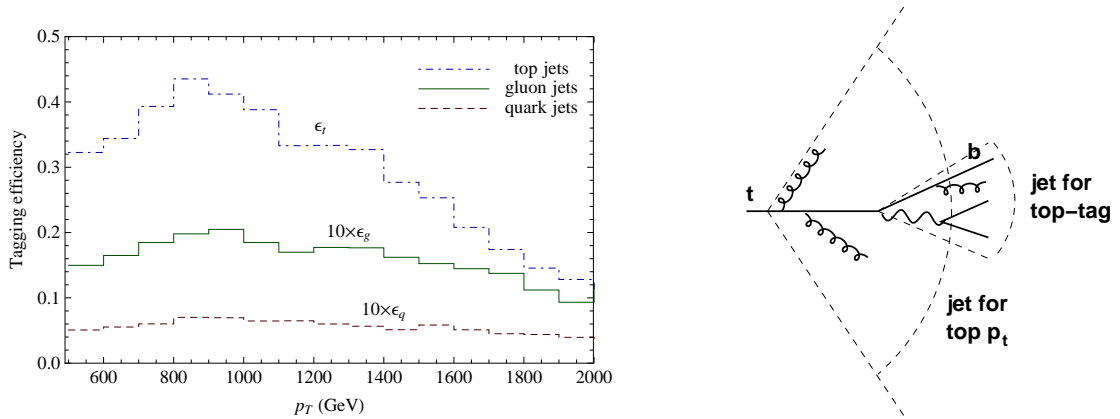


**Figure 27:** Left: signal efficiency for boosted top ID,  $\epsilon_t$ , and fake-tag rates for quark and gluon jets ( $\epsilon_q$ ,  $\epsilon_g$ , both multiplied by 10 for visibility) for the Kaplan et al. C/A-based top-tagger, as a function of jet  $p_t$  (reproduced from [170]). Right: the use of two jet sizes for top reconstruction: the inner cone, of order a few times  $m/p_t$ , includes the top decay products, but excludes radiation from the top quark itself (dead-cone). To capture that radiation and reconstruct the correct top  $p_t$ , one should use the outer cone.

mostly contained in a cone of width of order  $2 - 3$  times  $m/p_t$ . Using a jet-opening angle that is much larger than this will lead to considerable degradation in mass resolution, not only because of UE contamination (as in the colour-singlet two-body decay case), but also because the top quark, a coloured object, itself radiates gluons, which will tend to increase the jet mass. The C/A-based approach of [170] is to some extent able to find the right  $R$  automatically for a given top-decay, and this is part of its strength.

Finding the top-quark is only half the task however: one must also establish its momentum. Barely any of the gluons emitted from a fast-moving top-quark are contained in the small jet used to identify the top — this is the dead-cone phenomenon for radiation from a massive quark. To capture them one should instead use a jet with large opening angle, as one would for a high- $p_t$  light quark [68], cf. section 5.1. This is essential if one is to obtain good mass resolution on a  $t\bar{t}$  resonance and is summarised in fig. 27 (right).

Thus, when studying highly boosted tops, one needs to examine the event on two angular scales: quite small  $R \sim 3m_t/p_t$  to tag the top-decay structure, and large  $R \sim 1$  to reconstruct the top-quark momentum before the top started emitting gluons.

## 5.4 Summary

It is probably fair to say that the question of how best to use jets is still in its infancy. Nevertheless, some clear results have emerged from the above discussion.

- There will not be a single “best” jet-definition (i.e.  $R$  and jet-algorithm) at the LHC. What’s optimal will depend on what one wants to measure. The trade-off will be between resolving separate jets (not really discussed here), capturing their perturbative radiation and limiting UE contamination, and depends on the momentum scale of an event, the number of jets, and so forth. In particular, kinematic reconstructions prefer larger  $R$  values at high  $p_t$  and for gluon jets (even  $R \gtrsim 1$ ), because of the increased importance of capturing perturbative emission from the jets.
- Monte Carlo studies of dijet resonances confirm this picture. They also indicate that among the different algorithms,  $k_t$  is worst and SISCone and Cambridge/Aachen with filtering are best. This is in accord with expectations based on their areas, i.e. their sensitivity to the UE, and is most relevant at high scales. Differences between algorithms, expressed as the extra luminosity needed to obtain a given (toy) signal significance, are at the level of a few tens of percent.

Furthermore, it seems that event-dependent choices for the  $R$  value can lead to additional improvements of a similar order of magnitude.

- Pileup is a major issue, and significantly degrades kinematic reconstructions, even at high momentum scales. One can devise tools to measure the amount of pileup event-by-event and to subtract it jet-by-jet. This leads to a noticeable improvement in kinematic reconstruction quality, though it does not quite restore it to the level of the no-pileup case.

- At the LHC’s highest momentum scales, electroweak-scale particles appear to be light. Their decays are collimated into single jets. Sequential-recombination jet algorithms provide a clean way of resolving the consequent substructure, and the most flexible seems to be Cambridge/Aachen, again with filtering to reduce UE contamination.

There are many remaining open questions. Among them: how to reconcile the need for large  $R$  at high  $p_t$  with the task of resolving complex multi-jet events; how this connects with the use of substructure in resolving highly boosted decays; how to calculate the optimal  $R$  analytically, perhaps using the resulting information event-by-event; how to choose the parameters of filtering and how this ties in with possible improvements in pileup subtraction; and how all of this works in full physics studies, including realistic backgrounds and detector effects. It is to be hoped that future work will cast light on these questions.

## 6 Conclusions

This review has covered a range of developments in the practical and theoretical aspects of jet-finding over the past few years. These are steps on the way to a fully developed science of the use of jets, “jetography”.

One important development is that LHC now has access to a range of fast, infrared- and collinear-safe algorithms, together with methods that allow any of the algorithms to be used in a high-luminosity LHC environment. IRC safety is essential if the LHC is to benefit maximally from the huge predictive effort that is ongoing within the QCD theory community. Practicality is a necessary condition for the algorithms to be used in an experimental context.

A number of these advances have been taken up by the LHC experiments. For example both ATLAS and CMS incorporate FastJet within their software frameworks. At the time of writing, it seems that CMS will provide  $k_t$ -algorithm jets and SIScone jets as part of their default jet collections (though for the time being they also maintain a legacy IC-PR type iterative cone). ATLAS is in the process of considering its jet-finding choices, and in particular the anti- $k_t$  algorithm is being investigated as a possible standard choice. These are welcome developments given the importance of IRC safety for straightforward comparisons with perturbative QCD predictions and for the use of perturbative methods in generally thinking about jets.

The second main development is that theoretical work has started on the question of how best to use jets in an LHC type environment. This is an important question because the LHC spans two orders of magnitude in jet energy and has substantial (and variable) pileup, and no single jet-definition will work optimally for the whole range of LHC phenomena.

Progress has been outlined here (section 4) on our analytical understanding of how jets behave, and in section 5 we have seen a handful of examples that benefited significantly from the use of the “right” jet-finding approach. Currently these two aspects of work on jets

are connected qualitatively: the understanding of section 4 helped to interpret the results and inspire some of the methods of section 5. However a rigorous, quantitative link is still missing, and section 5 in any case covered only a small fraction of the possible use-cases for jets. This highlights a clear path for future work: that of bringing our analytical tools to bear on the full range of uses of jets at the LHC, so as to identify optimal jet-finding solutions across the board.

## Acknowledgements

My initial interest in the subject of jet finding owes much to talks, exchanges, arguments, comments, encouragement by/with/from Jon Butterworth, Günther Dissertori, Joey Huston, Mike Seymour, Markus Wobisch, as well as many others. The bulk of my direct involvement in the subject has been in collaboration with Matteo Cacciari and Gregory Soyez and they have done a lot to transform the subject — without their ideas, determination and enthusiasm, the advances that I’ve been involved with would not have happened. Many others have contributed, both as collaborators, Andrea Banfi, Jon Butterworth, Adam Davison, John Ellis, Mrinal Dasgupta, Lorenzo Magnea, Are Raklev, Juan Rojo, Mathieu Rubin, Sebastian Sapeta, Giulia Zanderighi; and in terms of more informal exchanges: Timothy Chan, Olivier Devillers (both from the field of computational geometry) as well as Patrick Aurenche, Siegmund Brandt, Tancredi Carli, Pierre-Antoine Delsart, Yuri Dokshitzer, Steve Ellis, David d’Enterria, Michel Fontannaz, Peter Jacobs, Thomas Kluge, David Kosower, Bruce Knuteson, Peter Loch, Michelangelo Mangano, Arthur Moraes, Andreas Oehler, Klaus Rabbertz, Christof Roland, Philipp Schieferdecker, Torbjörn Sjöstrand, Peter Skands, George Sterman, Brock Tweedie, Monica Vazquez Acosta. I am also grateful to David Kosower for his detailed comments on this manuscript.

## References

- [1] G. Sterman and S. Weinberg, “Jets From Quantum Chromodynamics,” *Phys. Rev. Lett.* **39** (1977) 1436.
- [2] G. Aad *et al.* [The ATLAS Collaboration], “Expected Performance of the ATLAS Experiment - Detector, Trigger and Physics,” arXiv:0901.0512 [hep-ex].
- [3] G. L. Bayatian *et al.* [CMS Collaboration], “CMS physics: Technical design report,” CMS-TDR-008-1.
- [4] J. M. Campbell, J. W. Huston and W. J. Stirling, “Hard interactions of quarks and gluons: A primer for LHC physics,” *Rept. Prog. Phys.* **70** (2007) 89 [arXiv:hep-ph/0611148].
- [5] G. C. Blazey *et al.*, “Run II jet physics,” hep-ex/0005012.

- [6] S. D. Ellis, J. Huston, K. Hatakeyama, P. Loch and M. Tonnesmann, “Jets in Hadron-Hadron Collisions,” *Prog. Part. Nucl. Phys.* **60** (2008) 484 [arXiv:0712.2447 [hep-ph]].
- [7] D. d’Enterria, “Jet quenching in QCD matter: from RHIC to LHC,” arXiv:0902.2488 [nucl-ex].
- [8] S. Salur [STAR Collaboration], “First Direct Measurement of Jets in  $\sqrt{s_{NN}} = 200$  GeV Heavy Ion Collisions by STAR,” arXiv:0809.1609 [nucl-ex].
- [9] J. E. Huth *et al.*, “Toward a standardization of jet definitions,” FNAL-C-90-249-E, published in the proceedings of the 1990 Summer Study on High Energy Physics, Research Directions for the Decade, Snowmass, Colorado, June 25 – July 13, 1990.
- [10] S. D. Ellis, Z. Kunszt and D. E. Soper, “The One Jet Inclusive Cross-Section at Order  $\alpha_s^3$ . 1. Gluons Only,” *Phys. Rev. D* **40** (1989) 2188.
- [11] S. Catani, Y. L. Dokshitzer, M. Olsson, G. Turnock and B. R. Webber, “New clustering algorithm for multi - jet cross-sections in  $e^+ e^-$  annihilation,” *Phys. Lett. B* **269**, 432 (1991);
- [12] S. Catani, Y. L. Dokshitzer, M. H. Seymour and B. R. Webber, “Longitudinally invariant  $K(t)$  clustering algorithms for hadron hadron collisions,” *Nucl. Phys. B* **406**, 187 (1993).
- [13] S. D. Ellis and D. E. Soper, “Successive Combination Jet Algorithm For Hadron Collisions,” *Phys. Rev. D* **48**, 3160 (1993) [hep-ph/9305266].
- [14] Y. L. Dokshitzer, G. D. Leder, S. Moretti and B. R. Webber, “Better jet clustering algorithms,” *JHEP* **9708**, 001 (1997) [hep-ph/9707323];
- [15] M. Wobisch and T. Wengler, “Hadronization corrections to jet cross sections in deep-inelastic arXiv:hep-ph/9907280; M. Wobisch, “Measurement and QCD analysis of jet cross sections in deep-inelastic positron proton collisions at  $\sqrt{s} = 300$ -GeV,” DESY-THESIS-2000-049.
- [16] S.D. Ellis, private communication to the OPAL Collaboration; D.E. Soper and H.-C. Yang, private communication to the OPAL Collaboration; L.A. del Pozo, University of Cambridge PhD thesis, RALT-002, 1993; R. Akers *et al.* [OPAL Collaboration], “QCD studies using a cone based jet finding algorithm for  $e^+ e^-$  collisions at LEP,” *Z. Phys. C* **63**, 197 (1994);
- [17] M. Cacciari, G. P. Salam and G. Soyez, “The anti- $k_t$  jet clustering algorithm,” *JHEP* **0804** (2008) 063 [arXiv:0802.1189 [hep-ph]].
- [18] C. Buttar *et al.*, in “Standard Model Handles and Candles Working Group: Tools and Jets Summary Report,” arXiv:0803.0678 [hep-ph].

- [19] G. Arnison *et al.* [UA1 Collaboration], “Hadronic Jet Production At The Cern Proton - Anti-Proton Collider,” *Phys. Lett. B* **132** (1983) 214.
- [20] F. Abe *et al.* [CDF Collaboration], “The Topology of three jet events in  $\bar{p}p$  collisions at  $\sqrt{s} = 1.8$  TeV,” *Phys. Rev. D* **45** (1992) 1448.
- [21] M. Cacciari, G. P. Salam and G. Soyez, “The Catchment Area of Jets,” *JHEP* **0804** (2008) 005 [arXiv:0802.1188 [hep-ph]].
- [22] M. H. Seymour and C. Tevlin, “A comparison of two different jet algorithms for the top mass reconstruction at the LHC,” *JHEP* **0611** (2006) 052 [arXiv:hep-ph/0609100].
- [23] M. H. Seymour, “Jet shapes in hadron collisions: Higher orders, resummation and hadronization,” *Nucl. Phys. B* **513** (1998) 269 [hep-ph/9707338].
- [24] G. P. Salam and G. Soyez, “A practical Seedless Infrared-Safe Cone jet algorithm,” *JHEP* **0705** (2007) 086 [arXiv:0704.0292 [hep-ph]].
- [25] M. Cacciari, G. P. Salam and G. Soyez, <http://fastjet.fr/>.
- [26] P. A. Delsart, K. Geerlins and J. Huston, <http://www.pa.msu.edu/~huston/SpartyJet/SpartyJet.html>.
- [27] T. Aaltonen *et al.* [CDF Collaboration], “Measurement of the cross section for W-boson production in association with jets in  $p\bar{p}$  collisions at  $\sqrt{s} = 1.96$  TeV,” *Phys. Rev. D* **77** (2008) 011108 [arXiv:0711.4044 [hep-ex]].
- [28] J. Campbell and R. K. Ellis, “Next-to-leading order corrections to  $W + 2\text{jet}$  and  $Z + 2\text{jet}$  production at hadron colliders,” *Phys. Rev. D* **65** (2002) 113007 [hep-ph/0202176].
- [29] Z. Nagy, “Three-jet cross sections in hadron hadron collisions at next-to-leading order,” *Phys. Rev. Lett.* **88** (2002) 122003 [hep-ph/0110315]; “Next-to-leading order calculation of three-jet observables in hadron hadron collision,” *Phys. Rev. D* **68** (2003) 094002 [hep-ph/0307268].
- [30] C. F. Berger *et al.*, “Precise Predictions for  $W + 3$  Jet Production at Hadron Colliders,” arXiv:0902.2760 [hep-ph].
- [31] R. K. Ellis, K. Melnikov and G. Zanderighi, “Generalized unitarity at work: first NLO QCD results for hadronic  $W+3\text{jet}$  production,” arXiv:0901.4101 [hep-ph].
- [32] R. K. Ellis, K. Melnikov and G. Zanderighi, arXiv:0906.1445 [hep-ph].
- [33] S. Frixione and B. R. Webber, “Matching NLO QCD computations and parton shower simulations,” *JHEP* **0206** (2002) 029 [arXiv:hep-ph/0204244].

- [34] P. Nason and G. Ridolfi, “A positive-weight next-to-leading-order Monte Carlo for Z pair hadroproduction,” JHEP **0608**, 077 (2006) [arXiv:hep-ph/0606275].
- [35] S. D. Ellis, J. Huston and M. Tonnesmann, “On building better cone jet algorithms,” in *Proc. of the APS/DPF/DPB Summer Study on the Future of Particle Physics (Snowmass 2001)* ed. N. Graf, p. P513 [hep-ph/0111434].
- [36] M. G. Albrow *et al.* [TeV4LHC QCD Working Group], “Tevatron-for-LHC report of the QCD working group,” [arXiv:hep-ph/0610012].
- [37] S. Moretti, L. Lonnblad and T. Sjostrand, “New and old jet clustering algorithms for electron positron events,” JHEP **9808** (1998) 001 [arXiv:hep-ph/9804296].
- [38] T. Sjostrand, “The Lund Monte Carlo For E+ E- Jet Physics,” Comput. Phys. Commun. **28** (1983) 229.
- [39] J. Dorfan, “A Cluster Algorithm For The Study Of Jets In High-Energy Physics,” Z. Phys. C **7**, 349 (1981).
- [40] H. J. Daum, H. Meyer and J. Burger, “A Cluster Algorithm For Jet Studies,” Z. Phys. C **8**, 167 (1981).
- [41] K. Lanus, H. E. Roloff and H. Schiller, “Selection Of Jets In Multi - Hadron Final States Produced By E+ E- Annihilation,” Z. Phys. C **8**, 251 (1981).
- [42] A. Backer, “Normicity, A General Jet Measure,” Z. Phys. C **12**, 161 (1982).
- [43] W. Bartel *et al.* [JADE Collaboration], “Experimental Studies On Multi - Jet Production In E+ E- Annihilation At Petra Energies,” Z. Phys. C **33** (1986) 23;
- [44] S. Bethke *et al.* [JADE Collaboration], “Experimental Investigation Of The Energy Dependence Of The Strong Coupling Strength,” Phys. Lett. B **213** (1988) 235.
- [45] N. Brown and W. J. Stirling, “Jet Cross-Sections At Leading Double Logarithm In E+ E- Annihilation,” Phys. Lett. B **252**, 657 (1990).
- [46] S. Catani, “Jet topology and new jet counting algorithms,” CERN-TH.6281-91, in Erice 1991, Proceedings, QCD at 200-TeV, p. 21.
- [47] G. Leder, “Jet fractions in e+ e- annihilation,” Nucl. Phys. B **497**, 334 (1997) [hep-ph/9610552].
- [48] A. Banfi, G. P. Salam and G. Zanderighi, “Principles of general final-state resummation and automated implementation,” JHEP **0503** (2005) 073 [arXiv:hep-ph/0407286].
- [49] G. Dissertori and M. Schmelling, “An Improved theoretical prediction for the two jet rate in e+ e- annihilation,” Phys. Lett. B **361** (1995) 167.

- [50] A. Banfi, G. P. Salam and G. Zanderighi, “Semi-numerical resummation of event shapes,” JHEP **0201** (2002) 018 [arXiv:hep-ph/0112156].
- [51] S. Catani, B. R. Webber, Y. L. Dokshitzer and F. Fiorani, “Average Multiplicities In Two And Three Jet E+ E- Annihilation Events,” Nucl. Phys. B **383** (1992) 419.
- [52] S. Catani, F. Krauss, R. Kuhn and B. R. Webber, “QCD Matrix Elements + Parton Showers,” JHEP **0111** (2001) 063 [arXiv:hep-ph/0109231].
- [53] S. Chekanov *et al.* [ZEUS Collaboration], “Substructure dependence of jet cross sections at HERA and determination of  $\alpha(s)$ ,” Nucl. Phys. B **700** (2004) 3 [arXiv:hep-ex/0405065].
- [54] S. Catani, Y. L. Dokshitzer and B. R. Webber, “The K-perpendicular clustering algorithm for jets in deep inelastic scattering and hadron collisions,” Phys. Lett. B **285** (1992) 291.
- [55] M. Seymour, <http://hepwww.rl.ac.uk/theory/seymour/ktclus/>.
- [56] J. M. Butterworth, J. P. Couchman, B. E. Cox and B. M. Waugh, “KtJet: A C++ implementation of the K(T) clustering algorithm,” Comput. Phys. Commun. **153**, 85 (2003) [hep-ph/0210022]; <http://hepforge.cedar.ac.uk/ktjet/>.
- [57] V. M. Abazov *et al.* [D0 Collaboration], “The inclusive jet cross-section in p anti-p collisions at  $\sqrt{s} = 1.8$ -TeV using the k(T) algorithm,” Phys. Lett. B **525**, 211 (2002) [hep-ex/0109041].
- [58] V. M. Abazov *et al.* [D0 Collaboration], “Subjet multiplicity of gluon and quark jets reconstructed with the  $k_T$  algorithm in  $p\bar{p}$  collisions,” Phys. Rev. D **65**, 052008 (2002) [hep-ex/0108054].
- [59] A. Abulencia *et al.* [CDF II Collab.], “Measurement of the inclusive jet cross section using the k(t) algorithm in p anti-p collisions at  $\sqrt{s} = 1.96$ -TeV,” Phys. Rev. Lett. **96**, 122001 (2006)[hep-ex/0512062].
- [60] A. Abulencia *et al.* [CDF - Run II Collaboration], “Measurement of the Inclusive Jet Cross Section using the  $k_T$  algorithm in  $p\bar{p}$  Collisions at  $\sqrt{s} = 1.96$  TeV with the CDF II Detector,” Phys. Rev. D **75** (2007) 092006 [Erratum-ibid. D **75** (2007) 119901] [arXiv:hep-ex/0701051].
- [61] V. S. Fadin, “Double Logarithmic Asymptotics Of The Cross-Sections Of E+ E- Annihilation Into Quarks And Gluons. (In Russian),” Yad. Fiz. **37** (1983) 408; B. I. Ermolaev and V. S. Fadin, “Log - Log Asymptotic Form Of Exclusive Cross-Sections In Quantum Chromodynamics,” JETP Lett. **33** (1981) 269 [Pisma Zh. Eksp. Teor. Fiz. **33** (1981) 285]; A. H. Mueller, “On The Multiplicity Of Hadrons In QCD Jets,” Phys. Lett. B **104**, 161 (1981); Y. L. Dokshitzer, V. S. Fadin and V. A. Khoze,



- “Double Logs Of Perturbative QCD For Parton Jets And Soft Hadron Spectra,” *Z. Phys. C* **15** (1982) 325; A. Bassetto, M. Ciafaloni and G. Marchesini, “Jet Structure And Infrared Sensitive Quantities In Perturbative QCD,” *Phys. Rept.* **100** (1983) 201.
- [62] A. T. Pierce and B. R. Webber, “Comparisons of new jet clustering algorithms for hadron hadron collisions,” *Phys. Rev. D* **59** (1999) 034014 [arXiv:hep-ph/9807532].
  - [63] A. Banfi, G. P. Salam and G. Zanderighi, “Infrared safe definition of jet flavour,” *Eur. Phys. J. C* **47** (2006) 113 [arXiv:hep-ph/0601139].
  - [64] A. Banfi, G. P. Salam and G. Zanderighi, “Accurate QCD predictions for heavy-quark jets at the Tevatron and LHC,” *JHEP* **0707** (2007) 026 [arXiv:0704.2999 [hep-ph]].
  - [65] S. Hoeche, F. Krauss, S. Schumann and F. Siegert, “QCD matrix elements and truncated showers,” arXiv:0903.1219 [hep-ph].
  - [66] D. Krohn, J. Thaler and L. T. Wang, “Jets with Variable R,” arXiv:0903.0392 [hep-ph].
  - [67] J. M. Butterworth, A. R. Davison, M. Rubin and G. P. Salam, “Jet substructure as a new Higgs search channel at the LHC,” *Phys. Rev. Lett.* **100** (2008) 242001 [arXiv:0802.2470 [hep-ph]].
  - [68] M. Cacciari, J. Rojo, G. P. Salam and G. Soyez, “Quantifying the performance of jet definitions for kinematic reconstruction at the LHC,” *JHEP* **0812** (2008) 032 [arXiv:0810.1304 [hep-ph]].
  - [69] S. D. Ellis, C. K. Vermilion and J. R. Walsh, “Techniques for improved heavy particle searches with jet substructure,” arXiv:0903.5081 [hep-ph].
  - [70] L. Lonnblad, “Ariadne Version 4: A Program For Simulation Of QCD Cascades Implementing The Color Dipole Model,” *Comput. Phys. Commun.* **71** (1992) 15.
  - [71] L. Lonnblad, “Arclus: A New Jet Clustering Algorithm Inspired By The Color Dipole Model,” *Z. Phys. C* **58** (1993) 471.
  - [72] S. Chekanov, “A new jet algorithm based on the k-means clustering for the reconstruction of heavy states from jets,” hep-ph/0512027.
  - [73] H. Steinhaus, “Sur la division des corp materiels en parties,” *Bull. Acad. Polon. Sci.* **1** (1956) 801.
  - [74] L. Angelini *et al.*, “Jet analysis by deterministic annealing,” *Phys. Lett. B* **545**, 315 (2002) [hep-ph/0207032]; L. Angelini *et al.*, “Deterministic annealing as a jet clustering algorithm in hadronic collisions,” *Phys. Lett. B* **601**, 56 (2004) [hep-ph/0407214].

- [75] D. Y. Grigoriev, E. Jankowski and F. V. Tkachov, “Towards a standard jet definition,” *Phys. Rev. Lett.* **91**, 061801 (2003) [hep-ph/0301185]; “Optimal jet finder,” *Comput. Phys. Commun.* **155**, 42 (2003) [hep-ph/0301226].
- [76] C. F. Berger *et al.*, “Snowmass 2001: Jet energy flow project,” in *Proc. of the APS/DPF/DPB Summer Study on the Future of Particle Physics (Snowmass 2001)* ed. N. Graf, *In the Proceedings of APS / DPF / DPB Summer Study on the Future of Particle Physics (Snowmass 2001), Snowmass, Colorado, 30 Jun - 21 Jul 2001, pp P512* [arXiv:hep-ph/0202207].
- [77] Y. S. Lai and B. A. Cole, “Jet reconstruction in hadronic collisions by Gaussian filtering,” arXiv:0806.1499 [nucl-ex].
- [78] I. Volobouev, <http://projects.hepforge.org/fftjet/>.
- [79] T. Sjostrand, S. Mrenna and P. Skands, “Pythia 6.4 physics and manual,” *JHEP* **0605** (2006) 026, [arXiv:hep-ph/0603175].
- [80] G. Marchesini, B. R. Webber, G. Abbiendi, I. G. Knowles, M. H. Seymour and L. Stanco, “HERWIG: A Monte Carlo event generator for simulating hadron emission reactions with interfering gluons. Version 5.1 - April 1991,” *Comput. Phys. Commun.* **67** (1992) 465; G. Corcella *et al.*, “HERWIG 6: An event generator for hadron emission reactions with interfering gluons (including supersymmetric processes),” *JHEP* **0101** (2001) 010 [hep-ph/0011363].
- [81] T. Sjostrand, L. Lonnblad, S. Mrenna and P. Skands, “PYTHIA 6.3: Physics and manual,” arXiv:hep-ph/0308153.
- [82] I. P. Lokhtin and A. M. Snigirev, “A model of jet quenching in ultrarelativistic heavy ion collisions and high-p(T) hadron spectra at RHIC,” *Eur. Phys. J. C* **45** (2006) 211 [arXiv:hep-ph/0506189]; “Simulation of jet quenching at RHIC and LHC,” arXiv:hep-ph/0612109.
- [83] C. Adler *et al.* [STAR Collaboration], ‘Multiplicity distribution and spectra of negatively charged hadrons in Au Au collisions at  $\sqrt{s_{NN}} = 130\text{-GeV}$ ,’ *Phys. Rev. Lett.* **87** (2001) 112303 [arXiv:nucl-ex/0106004].
- [84] M. R. Anderberg, “Cluster Analysis for Applications,” (Number 19 in Probability and Mathematical Statistics, Academic Press, New York, 1973).
- [85] D. Eppstein “Fast hierarchical clustering and other applications of dynamic closest pairs,” *J. Experimental Algorithmics* **5** (2000) 1-23 [cs.DS/9912014].
- [86] J. Cardinal and D. Eppstein, “Lazy algorithms for dynamic closest pair with arbitrary distance measures,” Tech. Rep. 502, Univ. Libre de Bruxelles, 2003.

- [87] M. Cacciari and G. P. Salam, “Dispelling the  $N^3$  myth for the  $k(t)$  jet-finder,” *Phys. Lett. B* **641** (2006) 57 [arXiv:hep-ph/0512210].
- [88] G. L. Dirichlet, “Über die Reduktion der positiven quadratischen Formen mit drei unbestimmten ganzen Zahlen,” *J. Reine und Ang. Math.* **40** (1850) 209; G. Voronoi, “Nouvelles applications des paramètres continus à la théorie des formes quadratiques,” *J. Reine und Ang. Math.* **133** (1908) 97; See also: F. Aurenhammer, “Voronoi Diagrams - A Survey of a Fundamental Geometric Data Structure,” *ACM Comp. Surveys* **23** (1991) 345; A. Okabe, B. Boots, K. Sugihara and S. N. Chiu, “Spatial Tessellations — Concepts and Applications of Voronoi Diagrams,” 2nd edition, John Wiley, 2000.
- [89] S. Fortune, “A sweepline algorithm for Voronoi diagrams,” in *Proceedings of the second annual symposium on Computational geometry*, p. 312 (1986).
- [90] O. Devillers, S. Meiser, M. Teillaud, “Fully dynamic Delaunay triangulation in logarithmic expected time per operation,” *Comp. Geom.: Theory and Applications* **2**, 55 (1992); O. Devillers, “On Deletion in Delaunay Triangulation,” arXiv:cs.CG/9907023.
- [91] A. Fabri *et al.*, “On the design of CGAL a computational geometry algorithms library,” *Softw. Pract. Exper.* **30** (2000) 1167.
- [92] J.-D. Boissonnat *et al.*, “Triangulations in CGAL,” *Comp. Geom.* **22** (2001) 5.
- [93] M. Cacciari and G. P. Salam, “Jet clustering in particle physics, via a dynamic nearest neighbour graph implemented with CGAL”, LPTHE-06-02, unpublished note.
- [94] T. M. Chan, “Closest-point problems simplified on the RAM,” In *Proc. 13rd ACM-SIAM Sympos. on Discrete Algorithms* (2002).
- [95] E. D. Demaine, J. S. B. Mitchell, J. O’Rourke, “The Open Problems Project” (problem 63), <http://maven.smith.edu/~orourke/TOPP/P63.html>.
- [96] I. Volobouev, presentation at MC4LHC meeting, CERN, July 2006.
- [97] T. Sjöstrand, private communication, 2009.
- [98] S. Brandt and H. D. Dahmen, “Axes And Scalar Measures Of Two-Jet And Three-Jet Events,” *Z. Phys. C* **1** (1979) 61.
- [99] The CMS Collaboration, “Performance of Jet Algorithms in CMS,” CMS-PAS-JME-07-03 (March 2008), [http://cms.cern.ch/iCMS/jsp/openfile.jsp?tp=draft&files=AN2008\\_002\\_v3.pdf](http://cms.cern.ch/iCMS/jsp/openfile.jsp?tp=draft&files=AN2008_002_v3.pdf).
- [100] B. Abbott, M. Bhattacharjee, D. Elvira, F. Nang and H. Weerts [for the D0 Collaboration], “Fixed cone jet definitions in D0 and R(sep),” FERMILAB-PUB-97-242-E.

- [101] T. Aaltonen *et al.* [CDF Collaboration], “Measurement of the Inclusive Jet Cross Section at the Fermilab Tevatron p-pbar Collider Using a Cone-Based Jet Algorithm,” Phys. Rev. D **78** (2008) 052006 [arXiv:0807.2204 [hep-ex]].
- [102] M. Furman, “Study Of A Nonleading QCD Correction To Hadron Calorimeter Reactions,” Nucl. Phys. B **197** (1982) 413.
- [103] F. Aversa, P. Chiappetta, M. Greco and J. P. Guillet, “QCD Corrections to Parton-Parton Scattering Processes,” Nucl. Phys. B **327** (1989) 105; “Jet production in hadronic collisions to  $O(\alpha_s^3)$ ,” Z. Phys. C **46** (1990) 253.
- [104] J. P. Guillet, “One jet  $O(\alpha_s^3)$  cross-section: Mass dependence,” Z. Phys. C **51** (1991) 587.
- [105] B. Jager, M. Stratmann and W. Vogelsang, “Single-inclusive jet production in polarized p p collisions at  $O(\alpha_s^3)$ ,” Phys. Rev. D **70** (2004) 034010, [arXiv:hep-ph/0404057].
- [106] D. de Florian and W. Vogelsang, “Resummed cross section for jet production at hadron colliders,” Phys. Rev. D **76** (2007) 074031, [arXiv:0704.1677 [hep-ph]].
- [107] N. Kidonakis and G. Sterman, “Resummation for QCD hard scattering,” Nucl. Phys. B **505** (1997) 321, [arXiv:hep-ph/9705234].
- [108] N. Kidonakis, G. Oderda and G. Sterman, “Threshold resummation for dijet cross sections,” Nucl. Phys. B **525** (1998) 299, [arXiv:hep-ph/9801268].
- [109] N. Kidonakis, G. Oderda and G. Sterman, “Evolution of color exchange in QCD hard scattering,” Nucl. Phys. B **531** (1998) 365, [arXiv:hep-ph/9803241].
- [110] N. Kidonakis and J. F. Owens, “Effects of higher-order threshold corrections in high- $E(T)$  jet production,” Phys. Rev. D **63** (2001) 054019, [arXiv:hep-ph/0007268].
- [111] M. Dasgupta, L. Magnea and G. P. Salam, “Non-perturbative QCD effects in jets at hadron colliders,” JHEP **0802** (2008) 055 [arXiv:0712.3014 [hep-ph]].
- [112] L. G. Almeida, S. J. Lee, G. Perez, G. Sterman, I. Sung and J. Virzi, “Substructure of high- $p_T$  Jets at the LHC,” arXiv:0807.0234 [hep-ph]; L. G. Almeida, S. J. Lee, G. Perez, I. Sung and J. Virzi, “Top Jets at the LHC,” arXiv:0810.0934 [hep-ph].
- [113] S. Catani, L. Trentadue, G. Turnock and B. R. Webber, “Resummation of large logarithms in  $e^+ e^-$  event shape distributions,” Nucl. Phys. B **407** (1993) 3.
- [114] S. J. Burby and E. W. N. Glover, “Resumming the Light Hemisphere Mass and Narrow Jet Broadening distributions in  $e^+e^-$  annihilation,” JHEP **0104** (2001) 029 [arXiv:hep-ph/0101226].
- [115] M. Dasgupta and G. P. Salam, “Resummation of non-global QCD observables,” Phys. Lett. B **512** (2001) 323 [arXiv:hep-ph/0104277].

- [116] M. Dasgupta and G. P. Salam, “Resummed event-shape variables in DIS,” JHEP **0208** (2002) 032 [arXiv:hep-ph/0208073].
- [117] G. Oderda and G. Sterman, “Energy and color flow in dijet rapidity gaps,” Phys. Rev. Lett. **81** (1998) 3591 [arXiv:hep-ph/9806530].
- [118] C. F. Berger, T. Kucs and G. Sterman, “Energy flow in interjet radiation,” Phys. Rev. D **65**, 094031 (2002) [arXiv:hep-ph/0110004].
- [119] R. B. Appleby and M. H. Seymour, “Non-global logarithms in inter-jet energy flow with kt clustering requirement,” JHEP **0212** (2002) 063 [arXiv:hep-ph/0211426].
- [120] Y. Delenda, R. Appleby, M. Dasgupta and A. Banfi, “On QCD resummation with  $k(t)$  clustering,” JHEP **0612** (2006) 044 [arXiv:hep-ph/0610242].
- [121] M. Dasgupta and G. P. Salam, “Accounting for coherence in interjet  $E(t)$  flow: A case study,” JHEP **0203** (2002) 017 [arXiv:hep-ph/0203009].
- [122] A. Banfi, G. Marchesini and G. Smye, “Away-from-jet energy flow,” JHEP **0208** (2002) 006 [arXiv:hep-ph/0206076].
- [123] A. Banfi, G. P. Salam and G. Zanderighi, “Semi-numerical resummation of event shapes,” JHEP **0201** (2002) 018 [hep-ph/0112156].
- [124] S. Catani, Y. L. Dokshitzer and B. R. Webber, “Average number of jets in deep inelastic scattering,” Phys. Lett. B **322** (1994) 263.
- [125] J. R. Forshaw and M. H. Seymour, “Subjet rates in hadron collider jets,” JHEP **9909** (1999) 009 [arXiv:hep-ph/9908307].
- [126] W. Ochs and R. P. Ramos, “Particle Multiplicity in Jets and Sub-jets with Jet Axis from Color Current,” Phys. Rev. D **78** (2008) 034010 [arXiv:0807.1082 [hep-ph]].
- [127] G. P. Korchemsky and G. Sterman, “Nonperturbative corrections in resummed cross-sections,” Nucl. Phys. B **437** (1995) 415, [arXiv:hep-ph/9411211].
- [128] Y. L. Dokshitzer and B. R. Webber, “Calculation of power corrections to hadronic event shapes,” Phys. Lett. B **352** (1995) 451, [arXiv:hep-ph/9504219].
- [129] R. Akhoury and V. I. Zakharov, “On The Universality Of The Leading,  $1/Q$  Power Corrections In QCD,” Phys. Lett. B **357** (1995) 646 [arXiv:hep-ph/9504248].
- [130] P. Ball, M. Beneke and V. M. Braun, “Resummation of  $(\beta_0\alpha_s)^n$  corrections in QCD: Techniques and applications to the tau hadronic width and the heavy quark pole mass,” Nucl. Phys. B **452** (1995) 563, [arXiv:hep-ph/9502300].

- [131] Y. L. Dokshitzer, G. Marchesini and B. R. Webber, “Dispersive Approach to Power-Behaved Contributions in QCD Hard Processes,” Nucl. Phys. B **469** (1996) 93, [arXiv:hep-ph/9512336].
- [132] E. Gardi, “Dressed gluon exponentiation,” Nucl. Phys. B **622** (2002) 365, [arXiv:hep-ph/0108222].
- [133] M. Beneke, “Renormalons,” Phys. Rept. **317** (1999) 1, [arXiv:hep-ph/9807443].
- [134] A. Aktas *et al.* [H1 Collaboration], “Measurement of event shape variables in deep-inelastic scattering at HERA,” Eur. Phys. J. C **46** (2006) 343 [arXiv:hep-ex/0512014].
- [135] S. Chekanov *et al.* [ZEUS Collaboration], “Event shapes in deep inelastic scattering at HERA,” Nucl. Phys. B **767** (2007) 1 [arXiv:hep-ex/0604032].
- [136] M. L. Mangano, “Hard scattering in high-energy QCD,” [arXiv:hep-ph/9911256].
- [137] J. M. Butterworth, J. R. Forshaw and M. H. Seymour, “Multiparton interactions in photoproduction at HERA,” Z. Phys. C **72** (1996) 637, [arXiv:hep-ph/9601371].
- [138] M. Dasgupta and G. P. Salam, “Event shapes in  $e^+e^-$  annihilation and deep inelastic scattering,” J. Phys. G **30** (2004) R143 [arXiv:hep-ph/0312283].
- [139] Y. L. Dokshitzer, A. Lucenti, G. Marchesini and G. P. Salam, “Universality of  $1/Q$  corrections to jet-shape observables rescued,” Nucl. Phys. B **511** (1998) 396 [Erratum-ibid. B **593** (2001) 729] [arXiv:hep-ph/9707532].
- [140] Y. L. Dokshitzer, A. Lucenti, G. Marchesini and G. P. Salam, “On the universality of the Milan factor for  $1/Q$  power corrections to jet shapes,” JHEP **9805** (1998) 003 [arXiv:hep-ph/9802381].
- [141] M. Dasgupta and B. R. Webber, “Two-loop enhancement factor for  $1/Q$  corrections to event shapes in deep inelastic scattering,” JHEP **9810** (1998) 001, [arXiv:hep-ph/9809247].
- [142] M. Dasgupta, L. Magnea and G. Smye, “Universality of  $1/Q$  corrections revisited,” JHEP **9911** (1999) 025, [arXiv:hep-ph/9911316].
- [143] G. E. Smye, “On the  $1/Q$  correction to the C-parameter at two loops,” JHEP **0105** (2001) 005, [arXiv:hep-ph/0101323].
- [144] M. Dasgupta and Y. Delenda, “On the universality of hadronisation corrections to QCD jets,” arXiv:0903.2187 [hep-ph].
- [145] M. Campanelli, K. Geerlings, J. Huston, in “Standard Model Handles and Candles Working Group: Tools and Jets Summary Report,” arXiv:0803.0678 [hep-ph].

- [146] D. Benedetti *et al.*, in “Les Houches physics at TeV colliders 2005, standard model, QCD, EW, and Higgs working group: Summary report,” arXiv:hep-ph/0604120.
- [147] M. Cacciari, J. Rojo, G. P. Salam and G. Soyez, in “Standard Model Handles and Candles Working Group: Tools and Jets Summary Report,” arXiv:0803.0678 [hep-ph].
- [148] V. Büge, M. Heinrich, B. Klein, K. Rabbertz, in “Standard Model Handles and Candles Working Group: Tools and Jets Summary Report,” arXiv:0803.0678 [hep-ph].
- [149] M. Cacciari, J. Rojo, G. P. Salam and G. Soyez, <http://quality.fastjet.fr>.
- [150] M. M. Nojiri and M. Takeuchi, JHEP **0810** (2008) 025 [arXiv:0802.4142 [hep-ph]].
- [151] M. Cacciari and G. P. Salam, “Pileup subtraction using jet areas,” Phys. Lett. B **659** (2008) 119 [arXiv:0707.1378 [hep-ph]].
- [152] A. Abulencia *et al.* [CDF Run II Collaboration], “Measurement of the inclusive jet cross section in  $p\bar{p}$  interactions at  $\sqrt{s} = 1.96$ -TeV using a cone-based jet algorithm,” Phys. Rev. D **74** (2006) 071103 [arXiv:hep-ex/0512020].
- [153] O.L. Kodolova *et al.*, “Study of  $\gamma$ +Jet Channel in Heavy ion Collisions with CMS,” CMS NOTE-1998/063. V. Gavrilov, A. Oulianov, O. Kodolova and I. Vardanian, “Jet Reconstruction with Pileup Subtraction,” CMS RN 2003/004.
- [154] S. L. Blyth *et al.*, “A cone jet-finding algorithm for heavy-ion collisions at LHC energies,” J. Phys. G **34** (2007) 271 [arXiv:nucl-ex/0609023].
- [155] A. L. Fitzpatrick, J. Kaplan, L. Randall and L. T. Wang, “Searching for the Kaluza-Klein Graviton in Bulk RS Models,” JHEP **0709** (2007) 013 [arXiv:hep-ph/0701150].
- [156] W. Skiba and D. Tucker-Smith, “Using jet mass to discover vector quarks at the LHC,” Phys. Rev. D **75** (2007) 115010 [arXiv:hep-ph/0701247].
- [157] B. Holdom, “ $t$  at the LHC: The physics of discovery,” JHEP **0703** (2007) 063 [arXiv:hep-ph/0702037].
- [158] B. Holdom, “The heavy quark search at the LHC,” JHEP **0708** (2007) 069 [arXiv:0705.1736 [hep-ph]].
- [159] K. Agashe *et al.*, “LHC Signals for Warped Electroweak Neutral Gauge Bosons,” Phys. Rev. D **76** (2007) 115015 [arXiv:0709.0007 [hep-ph]].
- [160] M. H. Seymour, “Searches for new particles using cone and cluster jet algorithms: A Comparative study,” Z. Phys. C **62** (1994) 127.

- [161] J. M. Butterworth, B. E. Cox and J. R. Forshaw, “W W scattering at the LHC,” *Phys. Rev. D* **65** (2002) 096014 [arXiv:hep-ph/0201098].
- [162] J. M. Butterworth, J. R. Ellis and A. R. Raklev, “Reconstructing sparticle mass spectra using hadronic decays,” *JHEP* **0705** (2007) 033 [arXiv:hep-ph/0702150].
- [163] J. M. Butterworth, J. R. Ellis, A. R. Raklev and G. P. Salam, “Discovering baryon-number violating neutralino decays at the LHC,” arXiv:0906.0728 [hep-ph].
- [164] K. Agashe, A. Belyaev, T. Krupovnickas, G. Perez and J. Virzi, “LHC signals from warped extra dimensions,” *Phys. Rev. D* **77** (2008) 015003 [arXiv:hep-ph/0612015].
- [165] B. Lillie, L. Randall and L. T. Wang, “The Bulk RS KK-gluon at the LHC,” *JHEP* **0709** (2007) 074 [arXiv:hep-ph/0701166].
- [166] R. Frederix and F. Maltoni, “Top pair invariant mass distribution: a window on new physics,” *JHEP* **0901** (2009) 047 [arXiv:0712.2355 [hep-ph]].
- [167] U. Baur and L. H. Orr, “Searching for t-bar t Resonances at the Large Hadron Collider,” *Phys. Rev. D* **77** (2008) 114001 [arXiv:0803.1160 [hep-ph]].
- [168] J. Thaler and L. T. Wang, “Strategies to Identify Boosted Tops,” *JHEP* **0807** (2008) 092 [arXiv:0806.0023 [hep-ph]].
- [169] G. Brooijmans, “High pT Hadronic Top Quark Identification, Part I: Jet Mass and YSplitter,” ATLAS note, ATL-COM-PHYS-2008-001.
- [170] D. E. Kaplan, K. Rehermann, M. D. Schwartz and B. Tweedie, “Top Tagging: A Method for Identifying Boosted Hadronically Decaying Top Quarks,” *Phys. Rev. Lett.* **101** (2008) 142001 [arXiv:0806.0848 [hep-ph]].